ISSN1000-9620

Marine Science Bulletin

Volume 1 • Number 2 1999

LIBRARY
Pacific Islands Fisheries Science Center
NOAA Fisheries
Honolulu, Hawai'i

LIBRARY
Pacific Islands Fisheries Science Center
NOAA Fisheries
Honolulu, Hawai'i

ISSN 1000-9620
02>
771000 962001

NATIONAL MARINE DATA AND
INFORMATION SERVICE OF CHINA

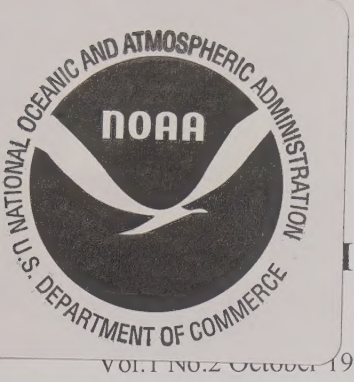

IENCE BULLETIN

Vol.1 No.2 October 1999

CONTENTS

Assessment of Effects of Qinshan Nuclear Power Station on the Ecological Environment and Water Quality of its Adjacent Waters after its Running
……*Yang Guanming*（杨关铭）and *He Dehua*（何德华）et al. (1)

The Characteristics of Dynamics and Sedimentation in the Mouth Area of Xiashimen Strait Channel, Zhejiang, China
…… … *Jiang Guojun*（蒋国俊） and *Yao Yanming*（姚炎明） (9)

Study on Coastal Profile Changes of the Caofeidian Area in the Bohai Sea Since 1983
…… …… …… …… …… …… …… …… … *Wang Yan*（王 艳） (19)

Study on the Role of Tidal Currents in the Process of Formation and Development of the Changjiang River Delta … …… …… … … *Zhu Yurong*（朱玉荣）(25)

Wind-Driven Slanting Profile Wave Derived from the Unified Variational Principle of Water Gravity Wave …… *Fu Yuhua*（付昱华）(36)

Comparison of Some Features of the Subtropical Countercurrent, the North Equatorial Current and the North Equatorial Countercurrent in the Northwest Pacific Ocean
…… *Sun Xiangping*（孙湘平）(45)

The Basic Features of Sea Surface Wind of each Season in the Shore and Offshore Area of Qingdao… …… …… … …… … … … … … …… *Diao Xuexian*（刁学贤）(59)

Analysis on Features of Temperature and Salinity in the Northern Taiwan Straits During February-March, 1998
…… *Hu Jianyu*（胡建宇）and *Hong Huasheng*（洪华生）et al. (69)

Analysis on Causes for Yearly Increment of Content of the Inorganic Phosphorus in the Nearshore Sea Area of Yantai
… …… … …… *Ji Ling*（纪 灵）and *Ren Rongzhu*（任荣珠）et al. (76)

Study on Sediment Transport in the Qianjiang Bay of Guang'ao, Shantou City by Using the Element Geochemistry Method
…… …… ……*Liu Shao*（刘 韶）and *Zhao Huanting*（赵焕庭）et al. (84)

A Regime of Inequality Requires Compensation …… …… ……*Li Linghua*（李令华）(96)

Assessment of Effects of Qinshan Nuclear Power Station on the Ecological Environment and Water Quality of its Adjacent Waters after its Running

LIBRARY
APR 23 2002
National Atmospheric
U.S. Dept

Yang Guanming, He Dehua, Wang Zhengfang, Wang Chunsheng, Chen Yongshou, Hu Xigang
(*Second Institute of Oceanography, SOA*)

Abstract On the basis of the data of biological and nonbiological factors collected respectively from 1989 to 1990 and from 1995 to 1996 in the waters nearby the Qinshan Nuclear Power Station, the ecological environment and water quality of the waters are analyzed and assessed in the paper. The results show: (a) the surveyed area has the typical ecological characteristics of high tidal range estuary, rich nutrients and low biological productivity, (b) tide, runoff and offshore seawater intrusion are the key factors which result in seasonal and annual changes of various biological and non-biological factors, (c) the risking of seawater eutrophication index is resulted from enormous amount of the discharges of industrial and domestic sewage, (d) because the survey area is located in a high tidal-range estuary, thermal effluent from cooling system does not induce significant temperature changes, (e) the first stage project of Qinshan nuclear power station has no notable impacts on the ecological environment in the waters since its running.

Keywords nuclear power station, waters, ecological environment, water quality assessment

The Qinshan nuclear power station is the first nuclear project that was designed and built by China itself. It is located in Haiyan County of Zhejiang province and near the north side of the bottom of Hangzhou Bay. The installed capacity of the first stage project of the station is 30×10^4kw and the project went into operation in 1992. The second stage project ($4\times60\times10^4$kw) and the third stage project ($2\times70\times10^4$kw) are under construction at present. In order to make out the impacts on the water ecological environment caused by discharging into Hangzhou Bay of the cooling water carrying after-heat that is produced in the nuclear reactor operation process of the huge thermal energy transforming into the electrical energy, the Second Institute of Oceanography of SOA made a baseline ecological environmental investigation from 1989 to 1990 (stage I investigation) and a comparison investigation from

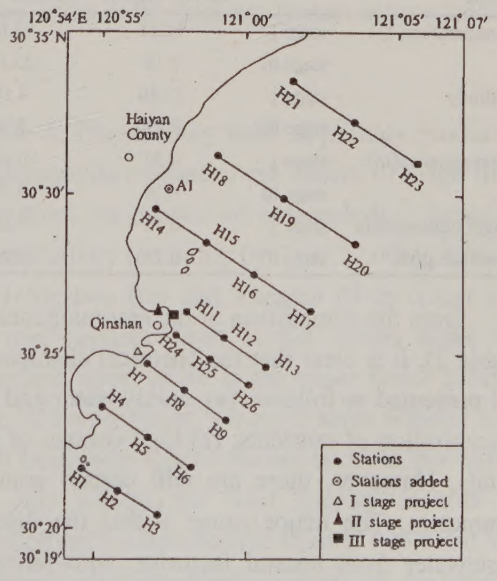

Fig.1 Location of sampling stations

1995 to 1996 (stage III investigation) in the waters nearby the nuclear power station (see Fig.1). According to the analysis results of the two investigations, the authors analyze and assess the variations of ecological environment and water quality in the waters after running of the first stage nuclear project in the paper.

1 Characteristics of environment and ecology

1.1 Physical and chemical environment

The tide of the surveyed area is an irregular shallow semidiurnal tide. The mean tidal range is 531cm and the maximum possible tidal range is 985cm. Influenced by the sub-tropical monsoon and marine wind currents, the rainfall in the area is plenty and is concentrated mainly between April and September, in which the rainfall is about 69% of the total of a year. The perennial mean rainfall is between 1200 and 1500mm. The seawater in the area is turbid and the content of suspended sediment is high. The main composition of the sea bottom sediment is silty sand. Because of the scour of the tide, the sedimentary environment in the area is extremely unstable and most of the sediment is solid sand (Xu*et al.*, 1991).

The comparison of the hydrographic parameters between Stage I and III investigations is listed in Table 1. The results show that the characteristics of high concentration of suspended sediment, low water color and low transparency are unchanged and the light transmission feature of sea water is also very similar between the two stage investigations.

Table.1 Comparison of average of hydrographic parameters

Items		Spring (April)	Summer (July)	Autumn (Oct.)	Winter (Jan.)	Annual average
Temperature(℃)	stage I	12.11	23.62	20.64	7.78	16.04
	stage III	9.10	25.10	21.00	7.50	15.04
Salinity	stage I	12.30	4.18	5.69	9.07	7.84
	stage III	9.09	7.76	13.31	15.15	11.34
Transparency(m)	stage I	0.32	0.40	0.80	0.21	0.16
	stage III	0.14	0.20	0.15	0.14	0.28
Light transmission	stage I	0.21	0.28	0.24	0.14	0.22
coefficient(m)	stage III	0.25	0.29	0.20	0.15	0.22

From the comparison of the environmental chemical parameters between the two investigations (Table 2), it is clear that the chemical characteristics in the high tidal-range estuary are unchanged and presented as follows: (a) muddy water and high concentration of suspended particulate; (b) high concentration of nutrients; (c) high content of dissolved oxygen and (4) low concentration of trace metals. However, there are still certain annual differences among the environmental chemical parameters. The major cause is that the discharging into the sea waters of a great amount of wastewater from coastal factories, aqua-farms and residential areas make the concentrations of nutrient salts (except for Si) increase and the content of dissolved oxygen decrease. In addition, the little rainfall and rainoff during 1995 to 1996 are another influencing factor that causes the differences.

Table 2 Comparison of environmental chemical parameters

Time	PO_4^{3-}-P (μ g/dm^3)	NO_2^--N (μ g/dr	NO_3^--N (μ g/dm^3)	NH_4^+-N (μ g/dm^3)	SiO_3^{2-}-Si (μ g/dm^3)	TDM (mg/dm^3)	SPM (mg/dm^3)	DO (mg/dm^3)
1995-1996 (stage III)	49.0	26.0	1476.5	56.8	2366.0	12.63	942.5	8.63
1989-1990 (stage I)	47.0	12.4	1125.0	31.5	2896.5	8.95	747.0	9.11

1.2 Marine organisms

1.2.1 Species diversity and community characters

A total of 322 and 284 species of organisms are identified in the samples of the two investigations respectively. Among them, the species number of phytoplankton is more than half of the total number and the diatom occupies an absolute position. Due to the environment of sea-river mixing estuary, fresh water species, brackish water species, a few offshore eurychoric species and benthic single-celled algae floating with the tidal current compose a diverse community structure of phytoplankton. To adapt the physical environment of the violent movement of tidal current, most species of phytoplankton were minute and tiny. The species of fouling organism on hanging plates and benthos in sediment are scarce.

The comparison of species number and dominant species between the two investigations is shown in Table 3. Although the species numbers of most of groups except for phytoplankton are slightly higher in Stage III than in Stage I , the dominant species of all the groups are basically the same. The community of plankton is dominated by brackish water estuary species and coastal low saline species, and the community of benthos still maintains an *Exopalaemon-Palaemon* structure which is constant for years in the area (Lin*et al.*, 1986). In a word, the results of the two investigations suggest that the pattern of about 99% of organisms belonging to brackish water and coastal low saline species is unchanged and the communities in the area are typical estuary-coastal low saline ecological communities.

1.2.2 Basic biomass

The comparison of basic biomass is listed in Table 4. The standing stock of primary producers in the area is low, and the seasonal mean value of chlorophyll*a* content of the waters in Stage III is 0.257mg/m^3. Compared with that in Stage I investigation, the content of chlorophyll*a* decreases about 70% in Stage III. The mean value of primary productivity (counting by C) is 27.00mg C/m^2 • d, which is lower than those in the mouth areas of Hangzhou Bay and Yangtze River (Liu*et al.*, 1991). The high suspended-sediment content and thin euphotic layer in the waters make the phytoplankton take photosynthesis only in shallow surface layer, which is the major factor causing the low primary productivity in the area. During Stage III investigation, owing to some reasons such as low rainfall, weak rainoff and so on, more than 60 freshwater species do not occur in the waters compared with Stage I investigation. This not only affects the total species number of phytoplankton, but also makes the cell concentration of phytoplankton decline from 8 020.5 ind./dm^3 in Stage I to 2742.1 ind./dm^3, resulting in the decrease of chlorophyll*a* content in the waters. Compared with Sanmen Bay, Xiangshan Inlet and Hangzhou Bay (ECRCE, 1992) the zooplankton biomass is higher, which is related to the hydrographic condition of mixing in the surveyed area of the south and north flows at the time of flood.

Table 3 Comparison of biological species number and deminant species

Projects		1995-1996 (stage III)	1989-1990 (stage I)
Phytoplankton	Species number Dominant species	*168* *Skeletonema costatum*、*Coscinodiscus jonesianus*、*C. oculus-iridis*、*Thalassionema nitzschioides*	*228* *Skeletonema costatum*、*Coscinodiscus jonesianus*、*C. argus*、*C. asteromphalus*
Zooplankton	Species number Dominant species	*49* *Labidocera euchaeta*、*Tortanus vermivulus*	*44* *Tortanus vermivulus*、*Labidocera euchaeta*
Fish larvae	Species number Dominant species	*13* *Coilia mystus*	*12* *Coilia mystus*、*Salanx acuticeps*
Benthos	Species number in sediment Species number of draw net Dominant species of draw net	*16* *42* *Exopalaemon annandalei*、*Collichthys lucidus*、*Palaemon gravieri*	*2* *33* *Collichthys lucidus*、*Exopalaemon annandalei*、*Palaemon gravieri*
Fouling organism (on hanging plates)	Species number Species	*2* *Diatom*、*Entermorpha clathrata*	*2* *Hydrozoa*、*Bryozoa*
Total species number		284	322

Table 4 Comparison of basic biomass

Time	Chlorophyll a (mg/m^3)	Abundance of phytoplankton ($ind./dm^3$)	Zooplankton	
			Biomass(mg/m^3)	Abundance($ind./m^3$)
1995-1996 (stage III))	0.257	2742.1	91.7	108.5
1989-1990 (stage I)	0.930	8020.5	145.3	318.8

1.2.3 Biomass of benthos and fouling organisms (on hanging plates)

The benthos and fouling organisms in the area are obviously less than those in other estuaries and inlets and the disparity is very great. Their biomass is extremely poor in the area. The biomass of benthos in sediment in Stages I and III are 0.03 and 0.06g/m^2 respectively, and the inhabited densities 2.0 and 4.28 ind./m^2 respectively. The species on hanging plates are also scarce. The phenomenon is resulted from the poor living environment in which the bottom sediment is extremely unstable and the content of organic substance in sediment is very low because of strong scour of tidal current in the area.

1.3 Characteristics of ecological environment and its effects

The surveyed area has typical ecological characteristics of a high tidal range estuary. The physical and chemical features such as rapid tidal current, high tidal range, high content of suspended sediment, low content of organic substance in sediment, low transparency of water, low salinity, high concentration of nutrient salts, high content of dissolved oxygen and so on directly

affect the species composition and abundance variations of all organism groups. Because of the extremely unstable sedimentary environment, most of benthos and epiorganism can not inhabit or live there, which result in poor resources and simple species composition. In consideration of the water environment in which there are plenty of sunshine, dissolved oxygen and rich nutrient salts carried with runoff that are completely enough to satisfy the needs of growth and reproduction of primary producer-phytoplankton, it should be reasonable that there are rich phytoplankton, high chlorophyll *a* content and great primary productivity. However, because of the muddy water, low transparency, thin euphotic layer and the scour of strong tidal current in the area, the potentialities of the most essential trophic level in the ecosystem are limited and then the primary productivity and the chlorophyll*a* content display a low level. Though there are many species of phytoplankton, the individual sizes of them are all smaller. As a secondary producer, the zooplankton does not present the distribution of bloom of shrimp seed called by local fishermen, which is an important set net fishery resources for the local people, but occurs in some neighboring estuaries such as Xiangshan Inlet, Sanmen Bay and so on (He *et al.*, 1988), though the standing stock of the zooplankton in the surveyed area is not too low. From the above analysis, it can be seen that in the waters with very rich nutrient-salts nearby Qinshan, the productivity is not high because there are simultaneously many environmental factors preventing the growth and eproduction of plankton. When the nutrients in the water can not be completely utilized by organisms and become excess, there is potentially a crisis of eutrophication, which would influence the recycling of matter. Thus it can be seen that a high productivity ecosystem should be a more perfect system, and every link of its energy transmission and material cycle must be closely related to each other. If an obstacle occurs in one link of an ecosystem, the ecosystem will be affected and even destroyed. The ecosystem of the waters nearby Qinshan located at the bottom of Hangzhou Bay, a typical high tidal range estuary, has some defects and its productivity is in a low level.

The surveyed area is in the mouth of Qiantang River, and the flood and ebb tides make the runoff from Qiantang River and the water from outside of Hangzhou Bay mix in the area completely. The seasonal and annual changes of the intensity of two different water bodies directly affect the physical and chemical features of the waters and the distributions of organisms. Generally, the salinity of the waters is usually in a low level. During Stage III investigation, the rainfall declines and correspondingly the runoff of Yangtze River and Qiantang River decreases sharply and the salinity of water increases obviously compared with that in Stage I investigation. The variations of the marine hydrographic environment directly influence the composition and distribution of marine organisms. The percentage of freshwater species declines clearly in Stage III, while the number of warm water offshore species increases to a degree. In addition, because the entry of higher salinity water changes the living environment of most of estuary single-cell algae, and at the same time the growth rate of some offshore pelagic algae that are distributed in the surveyed waters with the invading of offshore seawater is prevented owing to the increase of suspended sediment content and the decrease of transmittancy, the cell concentration of phytoplankton declines obviously and the content of chlorophyll*a* that is originally not high decreases about 70% compared with Stage I . However, during the seven year period from 1989 to 1996, the benthos community structure of *Exop alaemon-Palaemon* basically didn't change, and the diversity indexes of zooplankton had also no

obvious variation (Wang*et al.*, 1999). The marine organism community structure of estuary coastal low saline species was relatively stable.

2 Assessment of water quality (including obnoxious species)

2.1 Assessment of water quality

The criteria of water quality assessment are the Criteria of Seawater Quality (SOA, 1982) and the pollution index - the E value of eutrophication index ($E = \frac{\Sigma P \times \Sigma N \times COD}{4500} \times 10^6$). On the basis of the results of Stages I and III eclogical environment investigations, the assessment of water pollution degree has been made by calculating the ratio of actual parameter to the criterion value.

Table 5 is the comparison between the water quality criteria and various parameters. The surveyed waters belong to a high nutrient water, and all of the mean values of N and P contents in both Stage I and III investigations exceed class III of CSQ. Meanwhile, it is a high organic matter water. The averages of COD exceed class I of CSQ. Although the oil concentration has a declining trend from Stages I to III, it still exceeds class I of CSQ and the water presents slight oil pollution condition. The contents of SPM exceed greatly Class III of CSQ. Relatively, the concentrations of dissolved trace metals are obviously low and has a decreasing tendency. Only do the concentrations of trace metals accord with class I of CSQ. The E values of eutrophication index far exceed the criterion and it is higher in Stage III than Stage I . The above results show that the waters nearby Qinshan belong to a rich eutrophication water and the eutrophication degree is continuously rising.

Table 5 Comparison of water quality criteria and various parameters

Projects		Nutrient salts		Organic matter			Dissolved trace metals						Eutrophication index (E)
		P	N	COD*	SPM*	Oil*	Hg	Cu	Pb	Zn	Cd	As	
Criteria	Class I	15	100	>3	10	0.05	0.5	10	50	100	5	50	<1
	Class II	30	200	>4	50	0.10	1.0	100	100	1000	10	100	
	Class III	45	300	>5	150	0.50	1.0	100	100	1000	10	100	
1995-1996 (Stage III)		49.0	1476.5	3.42	393.45	0.0885	0.0038	1.98	0.460	2.8575	0.117	2.25	59.6
1989-1990 (Stage I)		47.5	1125.8	3.27	747.00	0.1545	0.0275	1.50	0.470	4.0875	0.183	3.58	40.0

Note: *unit is mg/dm^3, unit is μg/dm^3。

2.2 Obnoxious species

2.2.1 Red tide and its species

There were no occurrence of red tide during the two investigations, and neither were there reports about taking place of red tide in the waters. In the samples, there are two red tide species that have been already recorded in other sea waters: (a) *Protoperidinium micans*. It was identified only in samples of a few stations in July of 1989. Its cell concentration was low (240 ind./dm^3) and its occurrence frequency was also very low. (b) *Skeletonema costatum*. Although it was the main dominant species and the nutrient salts did also reach a degree of rich eutrophication, red tide couldn'

t take place because the muddy water and strong hydrodynamic factors were extremely unfavourable for the growth and reproduction of red tide species, namely the waters had no conditions for blooming of red tide species.

Noctilucas cintillans, which is the main red tide species in most of estuaries and coastal waters of China, was not identified during both of the two stage investigations.

2.2.2 Contamination microbe

E.coli and fecalcoliform are the main indicators of monitoring the contamination degree of domestic sewage. Both of the two bacteria are identified in the waters. The numbers of E. coli in the two stages didn't exceed the value of CSQ (10^4cell/dm^3). The monitoring for petroleum-degrading bacteria in water is necessary to evaluate the oil polluting degree and self-purification capability of the waters. The annual variation range of petroleum-degrading bacteria in the waters was 0.4×10^3 ~ 110×10^3 cell/dm^3. The quantity was close to the value in the coastal area of Ningbo, but was lower about 10^2 ~ 10^3 cell/dm^3 than that in other sea waters such as Bohai Sea, Dalian Bay, Xiamen Harbour, Jiaozhou Bay and so on. The low bacterium quantity was in correspondence with the low oil concentration (0.001~ 0.138mg/dm^3) in the waters.

From Table 6, it's suggested that the quantities of bacteria in Stage III investigation increased somewhat compared with Stage Ⅰ. The situation was related to some factors such as the increase of domestic sewage, the aggrevation of organic polluting and so on.

Table 6 Comparison of pollution bacteria

Time	E. coli in surface water (cell/dm^3)	Fecalcoliform in surface water (cell/dm^3)	Petroleum-degrading bacteria in surface water ($\times10^3$cell/dm^3)
1995-1996 (stage III)	748.3	1080.5	31.2
1989-1990 (stage Ⅰ)	191.8	1323.0	16.7

3 Conclusion

Influenced by geographic location, sea bottom topography and tidal current, the surveyed waters has the typical ecological characteristics of a high tidal range estuary--low salinity, low water colour, low transparency, high suspended sediment concentration, high nutrient salt concentration and low biological productivity. The main factors contributing to the seasonal and annual changes of these parameters are rainfall, runoff and intrusion of seawater from out of the Bay. Although the chief factor influencing the ecological environment of the waters is the discharge of the cooling water carrying after-heat produced in the nuclear reactor operation process, the thermal rising effect occuring in the waters around the discharging point is not obvious because of the special environmental characteristics in the strange tide estuary. During the investigations, it was not found that the thermal rising phenomenon and its unfavourable impact on the ecological environment and water quality took place in the waters. However, it was found from the investigation results that in recent years a great amount of industrial and domestic sewages discharged into the sea has had an obvious effect on the ecological environment, which has seriously aggravated the rich eutrophication

degree of water quality. Though the red tide couldn't take place in the surveyed area owing to the presence of above hydrodynamic factors, the eutrophication water would be a trouble water causing blooming of red tide when it was transported outward. This should be paid great attention to by the departments concerned. For this reason, the emphasis should be laid on strengthening administration of land-originated pollutant, controlling strictly the setting up blindly of sewage discharge points, building wastewater treatment plants and strengthening regular monitoring of the seawater quality. There is no doubt that with the gradual expansion of nuclear energy projects, the superposed influence of warming effect from the cooling water carrying after heat should be paid enough attention to.

References

Editorial Committee of Records of Chinese Estuaries, (1992) Records of Chinese Estuaries, Part 5. China Ocean Press

He Dehuam *et al.*, (1988) A Preliminary Analysis of Bait in Zhejiang Coastal Shallow Waters I. Zooplankton and Fishery, In:*Proceedings of International Symposium on the Coastal Zone.*China Ocean Press, 482488

Liu Ruiyu *et al.*, (1986) Ecological Characteristics of Benthos in Yellow Sea and East China Sea.*Studia Marina Sinica,* 27:153174

Liu Ziling *et al.*, Distribution Features of Chlorophyll*a* and Primary Productivity in the Waters around the Qinshan Nuclear Power Station.*Donghai Marine Science,* 9(2):153174

State Oceanic Administration, (1982) Criteria of Sea Water Quality (GB-3097-82). China Ocean Press

Wang Chunsheng *et al.*, (1999) Community Structure and Annual Variation of Zooplankton in the Waters around the Qinshan Nuclear Power Station.*Donghai Marine Science,* 17(1):3747

Xu Jianping *et al.*, (1991) Basical Hydrographic Characteristics of the Waters near the Qinshan Nuclear Power Station. *Donghai Marine Science*, 9(2):115

The Characteristics of Dynamics and Sedimentation in the Mouth Area of Xiashimen Strait Channel, Zhejiang , China

Jiang Guojun Yao Yanming
(*Department of Resources & Oceanic Engineering, Zhejiang University*)

Abstract According to the hydrographic and sediment data, the dynamic sedimentation characteristics are dealt with based on the analyses of the hydra-dynamics and the suspended and bottom sediment characters in Xiashimen (XSM) strait channel mouth area in the eastern part of Zhoushan Islands. It is pointed out that both of the changes of the hydra-dynamics and the fine sediment supply from Changjiang estuary result in the sedimentation mechanism of mainly the fine sediments flocculating deposition and secondly the coarser sediment deposition in single grain. The dynamic sedimentation characteristics are developed under the action of the deposition mechanism and reworking differences in different bedform areas.

Keywords fine sediment, flocculation in flowing water, sedimentation, single grain deposit, Xiashimen mouth area

Introduction

The Xiashimen strait channel is the major waterway through which large ships go into and out of Zhoushan and Ningbo harbors. However, there is a shallower segment about 7 km in length and less 20 m in depth which has affected the going of super-large ships (larger than 150 000 tons) in and out of the harbors. In order to suit the development tendency of the international transport ships becoming larger and give full play to the role of the Ningbo-Zhoushan deep harbor and promote the establishment and development of the Shanghai International Shipping Center, the shallower segment of Xiashimen strait channel must be dredged. The study of the dynamical sedimentation of Xiashimen strait channel mouth area is of great importance to understanding the development of the shallow segment and drawing up the dredging plan. At the same time, the study is also important to recognizing the sedimentation of the strait channel mouth area under the influence of strait channel effect.

In this paper, based on the measured data of hydro-sediments of 9 station during June of 1994 and September of 1995 in the Xiashimen strait channel mouth area, the dynamical characteristics, the dynamical deposition processes and the sedimentation mechanism are discussed.

1 Hydrodynamic characteristics

The Xiashimen strait channel mouth area faces the East Sea with Taohuadao Island, Xiashidao Island and Xuanshandao Island of the Zhoushan Islands behind. Affected by the landforms, the

hydrodynamics shows distinct characteristics, which are mainly depicted as follows:

1.1 Distinct change in tidal current directions

In the open area beyond the 20m isobath, the tidal current direction shows the character of a rotary curent, with the maximum flood current direction of about 300° and the maximum ebb current direction of about 100° . In the Xiashimen strait channel, restricted by the island landform, the current direction presents the strict character of a reversing current, with the flood current direction of about 300° and the ebb current direction of about 120° . Between the 20m-isobath and the Xiashimen strait channel, the current directions change from revolving current to a reversing current.

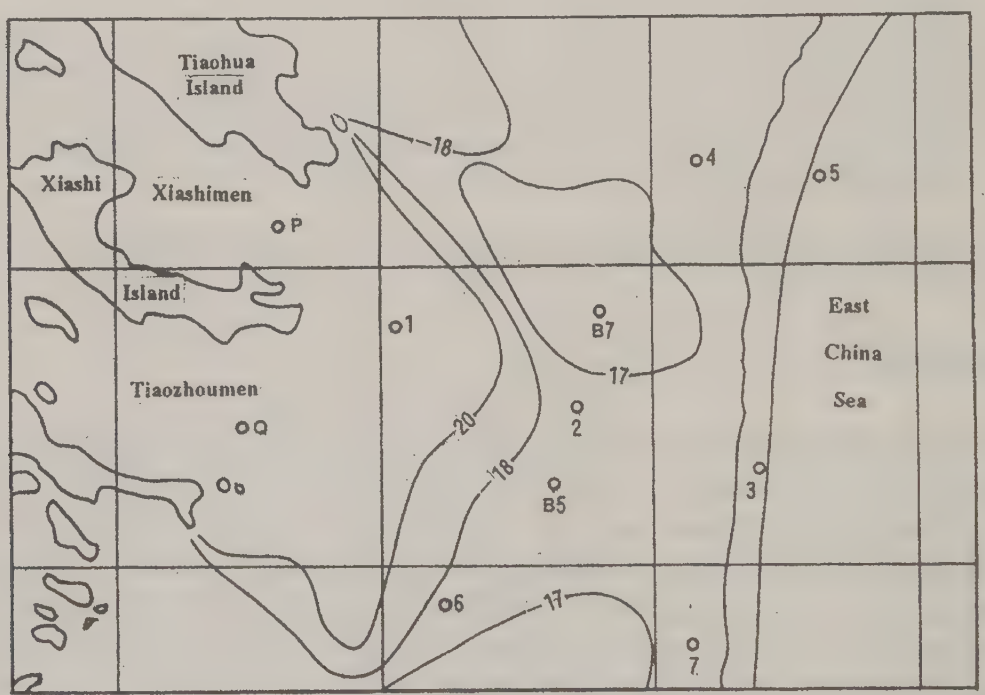

Fig. 1 The situation and hydrographic stations in the Xiashimen mouth area

1.2 Large differences in tidal current velocity

Within the distance of 10km from the open continental to the Xiashimen strait channel, the tidal current velocities change greatly because the water passing sections change greatly. The measured data have shown that the maximum flood velocity and the mean velocity are respectively 146cm/s and 76.1cm/s(Station P) during the spring flood in the Xiashimen strait channel but respectively 73. 0cm/s and 56.6cm/s (3# station) near the 20m isobath during the same time, which means the former velocities are 100% and 34.5% larger than the later ones respectively; the maximum ebb velocity is 138.0cm/s and the mean velocity is 80.8cm/s in the strait channel and the maximum ebb velocity and the mean velocity are respectively 108.0cm/s and 76.7cm/s near the 20m isobath line during the spring ebb, which have only reduced 21.7% and 5.1% respectively comparing the strait channel with the open sea. The result demonstrates that the flood currents increase clearly with the water flowing from the open sea to the strait channel, and the larger the velocity is, the more the

velocity increases. However, the ebb currents change slightly, and the velocity is maintained along the jet axis in the open sea area under the action of the strait channel effect.

1.3 Strong wave action

The 12 month's measured wave data from 1994 to 1995 show that the wave action is strong. The mean wave heights are 0.7～1.2m and the maximum wave height is above 2.0m and the mean periods are 3.6～4.1s and the longest period is 8s, in which the swell action is about 52% and mainly from the open direction ENE～SSE.The waves are able to rebuild the shallow segment sediments in the strait channel mouth area because the waves, with long wave length, long wave period and high wave height, can act directly on deeper water.

1.4 Large differences in slack time

Under the influences of the landforms and the tidal current characters, there are marked differences in the flood and ebb slack time in the Xiashimen strait channel mouth area. The slack time during which the velocity is less than 5cm/s reaches 30~60min due to reversing current character in the strait channel (P station) . But in the open sea area near the 20m isobath, the least velocity is above 15cm/s under the action of the rotary current, so that the slack time almost does not occur. However the lower velocity time during which the velocity is smaller than 21cm/s is over 30min. Between the strait channel and the 20m isobath, the slack time gradually decreases from the strait channel towards the 20m isobath.

2 Sedimentary characteristics

2.1 The change characteristics of sediment concentration

There are at least four time scales of sediment concentration changes.

(a) The changes with season: under the influence of the seasonal changes of waves, there are marked in seasonal changes sediment concentration. Compared with that in summer, the winter sediment concentration is two times that in summer (Table 1).

Table 1 The sediment concentration and their changes in the Xiashimen mouth area* Unit: g / m^3

Season	Tide type	Tide term	Within XSM		Mouth area of XSM				Open sea near 20m isobath line		
			XSMP	XSMQ	XSM1	XSM2	XSM6	XSM4	XSM5	XSM3	XSM7
Summer	S	F	84.7	159.7	124.3	47.5	69.1	24.8	17.5	33.4	33.5
		E	131.1	198.3	151.9	53.3	45.7	29.4	17.1	34.5	52.0
	N	F	97.5	67.8	50.6	26.6	70.4	16 5	18.2	22.7	22.5
		E	100.5	56.9	67.0	32.2	57.2	21.5	14.3	16.3	27.2
Winter	S	F	386.3	266.0	299.9	111.3	80.4	52.3	92.0	106.1	46.3
		E	333.7	313.1	356.7	133.8	90.1	46.4	77.3	91.3	44.6
	N	F	218.3	164.8	220.1	168.2	121.4	43.4	91.9	73.1	38.9
		E	221.6	179.0	254.2	150.3	156.1	63.6	122.9	84.7	44.1

* XSM mean Xiashimen strait channel, S means Spring tide, N means Neap tide, F means Flood tide, E mean Ebb tide

(b) The changes with the spring and neap tides: the sediment concentration during the spring tide is larger than that during the neap tide, usually the former is about 30%～50% larger than the later, which demonstrates that the stronger dynamic action results in the higher sediment

concentration. However, reverse cases may occur in the open sea near the 20m isobath(Table 1). The reasons are that the wave action is much stronger than the velocity action so that the higher sediment concentration may occur during the neap tide when the wave action is stronger than the spring tide. The change of the sediment concentration also proves that the wave action is able to effectively rebuild the XSM mouth area sediment. But in the strait channel, the sediment concentration is controlled mainly by the tidal current strength since the wave is unable to propagate into the strait channel under the shelter of the islands. Additionally the large depth in the strait channel will result in the wave is unable to act on the bottom of the channel that also reduce the wave action on the sediment concentration and relatively strengthen the effect of the tidal currents.

(c) The changes with the flood and ebb tide terms: Compared with the flood term, the sediment concentration is relatively high during the ebb tide term (Table 1). One of the reasons is that the ebb tidal current is stronger than the flood tidal current, which results in the higher ebb tidal sediment concentration. Another reason is the influence of the ebb water with high sediment concentration from the Hangzhou Bay, which results in the higher sediment concentration near the XSM mouth area during the ebb tide. However, there are no regular changes of sediment concentration with the tidal term change under the wave action in the open area near the 20m-isobath (Table 1)。

(d) The changes with the tidal period: Figure 2 shows the change process of sediment concentration with the tidal velocity. It is shown that the sediment concentration is relatively higher under the high velocity action. This kind of change is especially clear in the XSM strait channel. However, the sediment concentration is able to drop rapidly under the action of low velocity, which demonstrates that the suspended sediment is able to deposit swiftly. This process is certainly not the result of the single grain settlement of the grains less than 32 μ m in size under the action of gravity during the short slack time.

2.2 The grain size characters of suspended sediments

Analysis of the suspended sediments' grain size shows that the main part of the suspended sediments is silt (Table 2). The fine grains of less than 32 μ m in size account for over 95% of the suspended sediment, whose grain settlement velocity is less than 0.06cm/s (Qian, N. & Wan Z., 1984), so that most of the suspended grains are not deposited during the slack time except the near bottom ones. Therefore, the suspended sediments in the salty water environment are able to flocculate and deposit in the form of floc.

Although the sampling positions are distributed in the Xiashimen waterway, Tiaozhoumen waterway and the open area where the water depth, hydrodynamics and the distance from the strait channel mouth are completely different, except the clay content is highest in the strait channel and decrease with the increasing of the distances from the strait channel mouth, and other sizes of the suspended sediments do not change regularly (Table 2). These demonstrate that the clay content in the strait channel is high due to the sheltering action of the islands and the waves can not enter the channel and the deposited sediments are unable to rebuild, while others are deposited and re-suspended in mass forms.

2.3 Sediments' characters

Analyses of the deposited sediments show that the content of the fine grain sediment less than 32 μ m is almost the same as that of the suspended sediment and the content of those greater than 32

μ m size increases slightly (Table 3), indicating that the bottom sediments are deposited from the suspended ones.

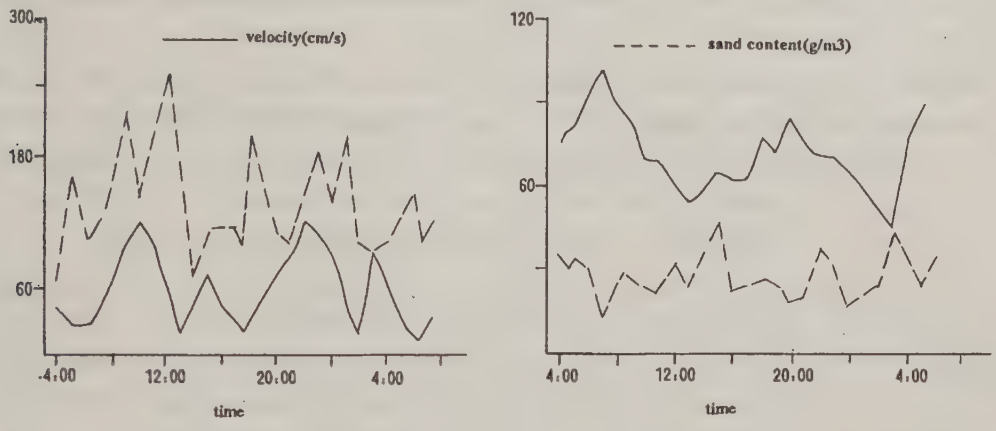

a. Inside the Xiashimen Strait Channel b.Outside the Xiashimen Strait Channel

Fig.2 Process Curves of Velocity and Sand Content in the XSM Mouth Area

Table 2 Suspended sediment grain size distribution in XSM mouth area (%)

Area	Station	Clay	Very fine silt	Fine silt	Middle silt	Coarse silt	Sand
Tiaozhoumen waterway	XSM Q#	3.25	16.26	23.45	30.44	21.38	5.22
Xiashimen waterway	XSM P#	5.08	39.33	39.53	14.48	1.08	0.50
The open sea area outside XSM	XSM 1#	4.23	20.90	31.07	33.53	9.64	0.59
	XSM 2#	2.79	16.43	27.29	33.27	19.62	0.60
	XSM 3#	0.57	22.33	38.98	25.45	10.69	1.99
Mean outside XSM	XSM	3.18	23.05	32.06	27.44	12.49	1.78
Hengsha of Changjiang estuary	H46	7.90	27.20	32.60	21.90	9.90	0.30
Jiuduansha Changjiang estuary	H24	7.70	28.60	33.70	18.90	10.10	1.45
South trough of Changjiang estuary	H11	8.40	28.60	33.75	19.50	8.25	1.20

Table 3 Bottom sediment grain size distribution in XSM mouth area(%)

Sediment types		Clay	Very fine silt	Fine silt	Middle silt	Coarse silt	Sand
In XSM waterway (XSMP)		5.1	39.3	39.5	14.5	1.1	0.5
Near waterway mouth	XSM1	4.2	20.9	31.1	33.5	9.6	0.6
	XSM2	2.8	16.4	27.3	33.3	19.6	0.6
	XSM4	2.9	14.7	29.6	28.2	17.1	7.5
	XSM6	4.2	22.0	31.2	31.9	9.8	0.8
Near 20m-isobath	XSM3	0.6	22.3	39.0	25.5	10.7	2.0
	XSM5	2.0	16.1	25.0	29.7	21.7	5.5
	XSM7	3.5	23.5	31.5	25.4	14.9	1.3
South trough of Changjiang Estuary		16.2	5.2	8.3	11.1	16.7	42.5

From the mouth of XSM strait channel to the vicinity of the 20m-isobath, the content of clay gradually decreases, and the content of grains coarser than the coarse silt increases from 1.1%

through 19.6% at the top of the mouth shallow to 10.7% near the 20m-isobath (Table 3). Others change irregularly. This change tendency in the space is similar to that of the suspended sediments, which also proves that the bottom sediments in XSM mouth area are deposited from the suspended sediment in floc form.

The sediment probability curve in XSM mouth area is composed of a four-section curve (Fig.3), the part of bed-load is about 4.0%～22.0%, the part of suspended load is above 80%, the turning grain size between the bed-load and the suspended load is between 5.0～5.6 ϕ. Judging from the spatial change of the probability curve, the content of bed-load is about 4% in XSM strait channel and it increases to 7% at the top of the mouth shallow bar and reaches 15% near the 20m-isobath, where it even may reach 22%. With this change, the turning grain size between the bed-load and the suspended load also increases from 4.6～5.0 ϕ in the XSM strait channel to 5.3～5.6 ϕ near the 20m-isobath, which shows that part of the suspended load settles and transforms into bed-load with the velocity decreasing out of the strait channel and the more it moves towards the sea, the more active the bed-load is. However, the bed-load in XSM mouth area rarely exceeds 20%, and the sediments move mainly in suspended form.

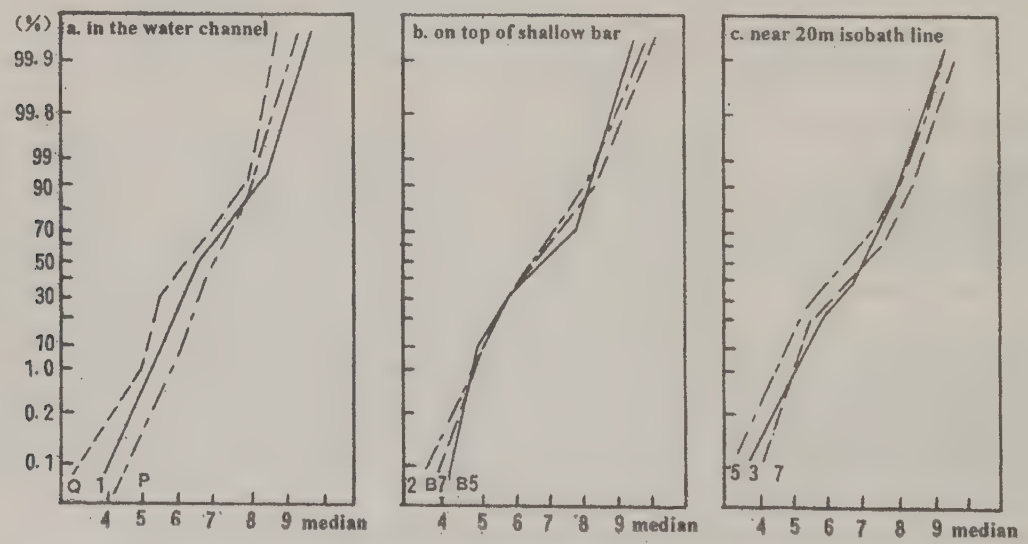

Fig.3 The sediment probability curves in the XSM mouth area

The calculation of the sediment grain size parameters shows that the mean size is between 6.6～7.6 ϕ, the sorting coefficient is about 1.0 in XSM mouth area, which demonstrates that the sediments are mainly good sorting fine sediments. The kurtosis coefficient is less than 3.0 and the skewness coefficient is about 0.0, which shows that the sediment distribution is a kind of low-flat normal frequency distribution curve (Table 4).

The sediment median shows a change character of coarse-fine-coarse, the sorting coefficient demonstrates the regularity of good-bad-good, the skewness changes in a pattern negative-positive-negative, and the kurtosis high-low-high (Table 4).

The shallow strata drilling data show that the thickness of the Holocene strata is over 5.0m in the mouth area, in which the top layer is gray saturation flow-mold mud, and the soil is uniform,

nipping thin layer fine silt, and mass mud occasionally occurs , containing a small amount of organisms with odor and the fragments of shell, showing a thick bed structure.

Analysis of the clay minerals shows that the clay minerals consist of Illite, Chlorite, Kaoline, Montmorillonite in the XSM mouth area. Their content characters are the same as those in the south trough of the Changjiang estuary (Table 5). It can thus be seen that the sediments of the XSM mouth area come mainly from the Changjiang estuary. They are the southward transported sediments from the Changjiang estuary and the main content is the fine sediment with grain size less than 32 μm.

Table 4 The bottom sediment grain size parameters in XSM mouth area

Station	Position	Mean size	Median size	Sorting	Skewness	Kurtosis
XSMP	In the strait channel deep water area	7.648	7.575	0.782	-0.314	2.536
XSMQ		6.639	6.541	1.185	-0.081	2.221
XSMM		6.942	6.833	1.101	-0.132	2.259
XSM2	Top of Mouth shallow bar	6.786	6.814	1.043	0.196	2.184
XSMB5	South vane of the mouth shallow bar	6.855	6.921	1.095	0.152	2.203
XSMB7	North vane of the mouth shallow bar	6.813	6.898	1.087	0.057	2.301
XSM3	Near 20m-isobath outside the strait channel	7.021	6.827	0.980	-0.404	2.703
XSM5		7.023	7.001	1.169	-0.007	2.227
XSM7		7.029	6.956	1.087	-0.184	2.180
Mean of different positions	Deep water area in the strait channel	7.076	6.983	1.023	-0.122	2.339
	Mouth shallow bar area	6.818	6.878	1.054	0.034	2.229
	Near 20m-isobath outside strait channel	7.024	6.938	1.079	-0.194	2.370

3 The mechanism of dynamic sedimentation

3.1 Depositional conditions of sediment

The sediment characters are developed under the special hydrodynamic and water environment conditions in the mouth area of XSM.

Table 5 Comparison of clay minerals between XSM mouth area and Changjiang estuary

Position	Mineral type			
	Illite	Chlorite	Kaoline	Montmorillonite
Outside XSM mouth	66.40	20.30	8.90	4.40
In XSM strait channel	68.70	21.70	6.20	3.40
Hengsha of Changjiang estuary	65.40	15.60	6.80	12.30
Jiuduansha of Changjiang estuary	68.50	15.70	7.40	8.50
South trough of Changjiang estuary	68.10	16.50	7.10	3.30

The ebb water comes from Changjiang estuary and Hangzhou Bay, and the measured salinity is

1) Jiang Guojun, the study of strait channel effects with special reference to Zhoushan islands. (the doctoral thesis of the East China Normal University), 1996

between 17～23 which is within the best range of the fine sediments' flocculation(Zhang, Z., Ruan, W. and Jiang, G., 1995, Jiang G. & Zhang, Z., 1995) so that the fine sediments have the water environment condition for flocculation in the mouth area of XSM.

It is fund from the laboratory test and field measurement that the fine grain less than 32 μ m in size are flocculated and deposited when the velocity is less than 21cm/s. Before that time, the grains coarser than 32 μm are deposited singly under the action of gravity (Jiang, G., 1993). In XSM strait channel, the periodic change characters of the currents make the time of the velocity with less than 5cm/s be between 30～60min. In the mouth area, the time with flow velocity less than 21cm/s is also over 30min(Fig 2). This shows that there exist conditions for the fine sediments flocculating deposition and the singgular coarse grain deposition in XSM mouth area.

From the field measurement (Kranck, K., 1973; Guan, X., 1992) we find that the fine sediments less than 32 μm in size are flocculated and deposited under the suitable water environment and hydrodynamic conditions. The fine grains less than 32 μm in size in XSM mouth area account for over 95%, which provides the material condition for flocculation and deposition.

3.2 The deposition processes and mechanism of sediments

When the ebb current flows out of the XSM mouth, the velocity gradually decreases with the flow diffusing and the discharge area increasing. Especially after the maximum velocity of ebb, the connection of the periodic reducing of the tidal current with the discharge area increasing results in the velocity rapidly decreasing. When the velocity is less than the critical settlement velocity of the coarse silt, the coarse silt and sand deposit singly under the action of gravity. With the velocity further decreasing, as the velocity is less than the critical flocculating velocity of the fine grains, the fine grains cohere with each other and form flocs which make the settlement velocity double and redouble or even increase tens of times and the fine sediments deposit in large amounts. The results are that the mixed and bad sorting sediments develop in XSM mouth area. After the reversing of the flow, the flood current flow towards the mouth of XSM, the discharge area gradually decrease, which causes the water to rise locally near the mouth area, and combined with the periodic changes of flood currents, results in the flood velocity reducing relatively. When the flood velocity is also reduced to less than the critical settlement velocity of coarse silt and the critical flocculating velocity respectively, the coarse single grain deposition and the fine grain flocculating deposition occur respectively, which results in the mixed sediments again.

The field measurements of the suspended sediment settlement shows that all fine grains less than 32 μm in size are flocculated while the flow velocity is less than 21cm/s in the water with salinity less than 30 but larger than 5 (Guan, X. Et al, 1992, Krone, R.B., 1972). This kind of water environment and hydrodynamic conditions are provided in the XSM mouth area. In fact, if the suspended grains were deposited in single grain under the action of gravity in the flowing water, the differences in the critical settlement velocities for different grains would cause the suspended sediment sorting along the transported road and result in the grain size divided into different belts. This has been proved by much tidal flat deposition (Ren, M., et al, 1983). The mixed sediments in XSM mouth area prove that the deposits are just formed by the coarse single grain gravity deposition and the fine grain flocculating deposition. The changes in grain size distribution of suspended sediments with the change of velocity also prove that the coarse silts are deposited in single grain

under the gravity action and the fine sediments are deposited by flocculation[1]. The process line of sediment concentration which shows a lower sediment concentration near the slack time also proves that the fine grains are deposited by flocculation.

The changes of the flow direction and the marked difference in the velocity result in the development of the circular flow, which causes the suspended sediments to concentrate on the strait mouth area and the suspended sediment front to develop(Jiang, G., et al 1997), thus accelerating flocculation deposition. As the suspended sediment front is basically stable near the strait channel mouth area, the sediments deposition position is also stable. It is thus clear that the development of the shallow bar near the XSM strait channel is the result of the combination of the stable deposition position with the suspended flocculating deposition.

3.3 The sediments sorting and rebuilding

The flocculation deposition forms the mixed sediments in the XSM mouth area. The east direction waves have a mean wave height of 1.0~1.2m, a mean period of 4.0~4.5s and a wavelength of 32m. This kind of wave has an action depth of 16m. On the the mouth shallow bar with a depth of 17m, about 50% waves are able to act directly on the shallow bar and rebuild the sediments. Under the wave action, the sediments on the shallow bar are re-suspended and carried away by the tidal currents. The fact that the change of sediment concentration with the change of spring and neap is not marked proves that the wave has a certain ability to rebuild the sediments on the XSM shallow bar.

However, laboratory tests show that the fine sediments do not flocculate and the coarse silt deposits singly under gravity action when the flow velocity is greater than the critical flocculating velocity for fine sediments but smaller than the critical velocity for coarse silts. Under the wave action the fine sediments are re-suspended and carried away but the coarse silt deposits on the shallow bar. The results are that the sediments are coarse, well sorted and show a positive skewness distribution which is near the normal distribution. Towards the sea, the sediments are not rebuilt with the depth gradually increasing. The distribution is similar to the suspended sediment distribution. In the strait channel where the wave is not able to enter, the sediments are rarely rebuilt by the wave the clay content is relatively high and the sediments distribution is a negative skewness one which is also near the normal distribution.

It should be pointed out that when the wave action is small (usually the wave height is smaller than the mean wave height), the waves are unable to act directly on the shallow bar and rebuild the sediments. Along with the periodic changes of tidal flow , the fine sediments are deposited in floc and the coarse sediments are deposited singly and still form the mixed sediments when the velocity is slack. So the sediments at the top of the shallow bar is slightly coarser than that in the inner strait channel and the open area. The sediments are weakly rebuilt since the water in the XSM mouth area is generally deep. The stable sediment front results in the stable position of the deposition forming a thick sedimentary structure (Jiang, G., et al 1997).

4 Conclusions

Based on the above analyses the following results are obtained:

(1) The hydrodynamics is complex in the XSM mouth area under the action of tidal currents and waves. In the strait channel, the currents show a to-and-fro character and the slack time is about 30~60min. In the open area the currents are revolving currents and the velocity is relativly small, but the slack time is short or even does not occur. The wave action is strong and is able to rebuild the deposited sediments at the top of shallow bar.

(b) The sediments in the XSM mouth area mainly come from the Changjiang estuary. Under the influence of the diluted water from Changjiang River, Qiantang River and Yongjiang River, the fine sediments are deposited in floc and the coarse sediments are deposited singly when the velocity is slow. The sediments in the XSM mouth area form mixed deposits. Under the influence of the stable sediment front, the deposition is also stable and forms a thick structure.

(c) The wave action makes the sediments re-suspend in the XSM mouth area. The coarse silt is deposited when the velocity is smaller than the critical settlement velocity. The fine sediments are deposited in floc when the velocity is less than the critical flocculating velocity (less 21cm/s). The waves rebuild make the sediment in the top of mouth shallow bar relatively coarse and the sorting well, the skewness is positive. But in the strait channel and the open deep area the wave is unable to act on the bottom and the sediments are rarely rebuilt. The deposited sediments are similar to the suspended sediments forming mixed deposits.

Reference

Zhang Zhizhong, Ruan Wenjie and Jiang Guojun, 1995, The relationship between the mouth bar deposition and the flocculating settlements in flowing water in Changjiang estuary.*Oceanoligia et Limnologia Sinica*, 26(6):632～638.(In Chinese)

Jiang Guojun, 1993, the dynamical sedimentation of different grain size in Taizhou bay tidal flat, Zhejiang province. *Marine Science Bulletin.*12(5):51～55. (In Chinese)

Kranck, K., 1973, Flocculation of Suspended Sedimentation in the sea.*Nature*, Vol.246, 348~350.

Jiang Guojun et al, 1997, the development mechanism of the mouth shallow bar out of the Xiashimen waterway.*Proce edings of the 8th whole china coastal engineering symposiumthe 1997 harbor and coast development symposium for both coast of Taiwan Strait*, ocean press, 154～163. (In Chinese)

Qian Ning and Wan Zhaohui, 1984.*Sediment kinetics.* Science press, 35-78.

Jiang Guojun and Zhang Zhizhong, 1995, the fine sediment flocculating deposition and the cation concentration in Changjiang estuary. A*acta Oceanologica Sinica*, 17 (1) : 76～83. (In Chinese)

Guan Xuwei et al, 1992, the field micro-observation of sediment flocculation in Changjiang estuary.*Sediment research* , (3) : 54～59 (in Chinese)

Krone, R. B., 1972, A field study of flocculation as a factor in estuaries shearing processes.*Tech. Bull.* , No. 19.

Ren Meie et al, 1983, Sedimentation on tidal mud flat of China with special reference to Wanggang area, Jiangsu Province; Sedimentation *on the Continental Shelf, with Special Reference to the East China Sea*, Ocean Press Vol. 1, p.1~19 The first author synopsis

Study on Coastal Profile Changes of the Caofeidian Area in the Bohai Sea Since 1983

Wang Yan
(*Research Institute of Marine Resources, Liaoning Normal University, Dalian*)

Introduction

The Caofeidian sandbar-lagoon system is situated along the northwest coast of the Bohai Sea. The system has evolved from the abandoned delta, which came into being by Suhe River and Xiaoqinghe River in the middle Holocene. At the moment, the system has almost lost the supply of river sediments. (Fig.1)

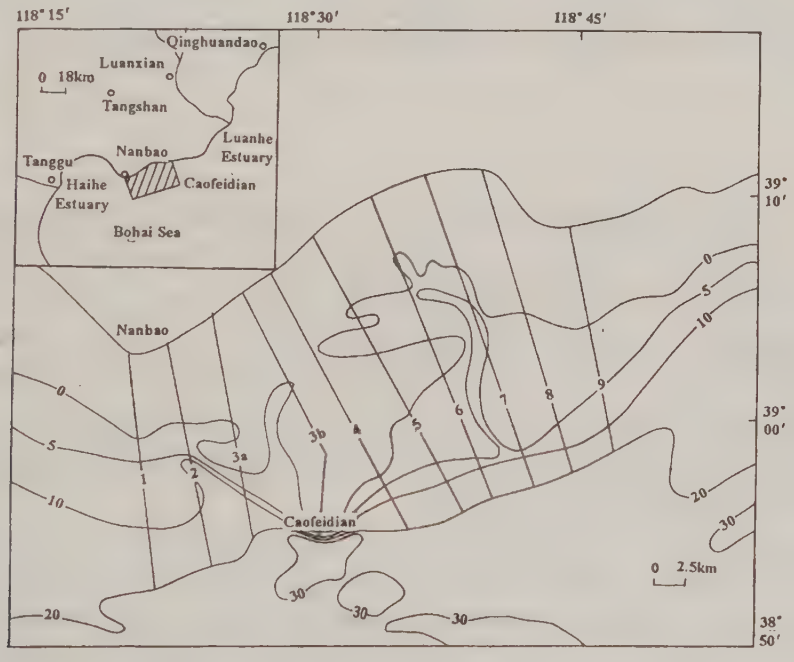

Fig.1 Research area and profiles position

It is almost the broadest silt flat which is 20km wide along the northwest coast of the Bohai Sea in the Caofeidian area. There are successive land forms toward sea--old and new barriers、beach and lagoons. The barrier in the Caofeidian area is the biggest one (8km wide) which is spreading in northwest direction. It is submerged in high tide and comes out in low tide. In the Caofeidian area,

the tide difference is below 2m and the stormy wave is the main hydrologic motive power. The strongest power of wind is in spring (March to May) and winter (December to February).

Method

There are ten coastal profiles in 1983、1996 and 1997 in the Caofeidian area. Among them, the profile in 1983 is obtained from the marine chart measured in 1983 with a 1:50000 scale; the profiles in 1996 and 1997 were measured by the First Navigational Engineering、Prospecting & Designing Institute of the Ministry of Communications in Nov.1996 (winter) and May1997 (spring).

Put the data which was gained from the ten profiles into the computer, and work respectively out the average altitudes of the shallow and the underwater slope that form the coastal profile and the changes of the coastal erosion from 1983 to 1996 and from 1996 to 1997. So we can obtain the yearly and seasonal law of coastal accumulation and erosion and the coastal sedimentary characteristics.

There is no tidal station in the Caofeidian area. As the Qinhuangdao Station (145km northward) and the Tanggu Station (57km westward) have longer histories of observation, we can use the tidal records of thses two stations to show the changes of sea level in the Caofeidian area.

Results

From the contrast of nine coastal profiles in 1983 & 1996 (Table 1,Fig2), there are six profiles (2、3a、4、5、7、8) showing that there are accumulations on the shallow in the mass. In this case, the shallow on the seaward side of the sandbar (about 5km wide) is mostly subjected to erosion, and there are accumulations on the shallow on the landward side of the sandbar. Meanwhile there are seven profiles in the nine (1、2、3a、4、5、6、7) showing that the underwater slope is subjected to erosion. So the coastal changes are accumulations on the shallow and erosions on the underwater slope in the Caofeidian area for 13 years from 1983 to 1996, and the matter is conveyed from the seaward side to the landward side of the sandbar.

From the contrast of nine coastal profiles in 1996 & 1997, there are seven profiles (1、2、3a、4、5、6、8) showing that the shallow is mostly subjected to erosion, and there are seven profiles (1、2、3a、4、5、6、7) showing that there are accumulations on the underwater slope. The coastal changes from 1996 to 1997 are seasonal coastal changes of the Caofeidian sandbar and lagoon system. So the seasonal changes are just opposite to the yearly changes, in other words, there are erosions on the shallow and accumulations on the underwater slope. It's alternates with accumulations and erosions on the shallow, generally the raised parts are subjected to erosion, and the accumulations always occur on the caved parts. These seasonal coastal changes are correlated closely with the seasonal hydraulic dynamical characteristics. In the Caofeidian area, the stormy waves are strongest in winter and spring. The two measurements of coastal profiles from 1996 to 1997 are just through a winter and a spring (Nov. 1996 ~ May 1997). So the shallow suffers from erosion under the strong stormy waves, and the sediments are conveyed to the underwater slope.

The average accumulative speed is 3.2cm/a on the shallow of the Caofeidian sandbar and lagoon

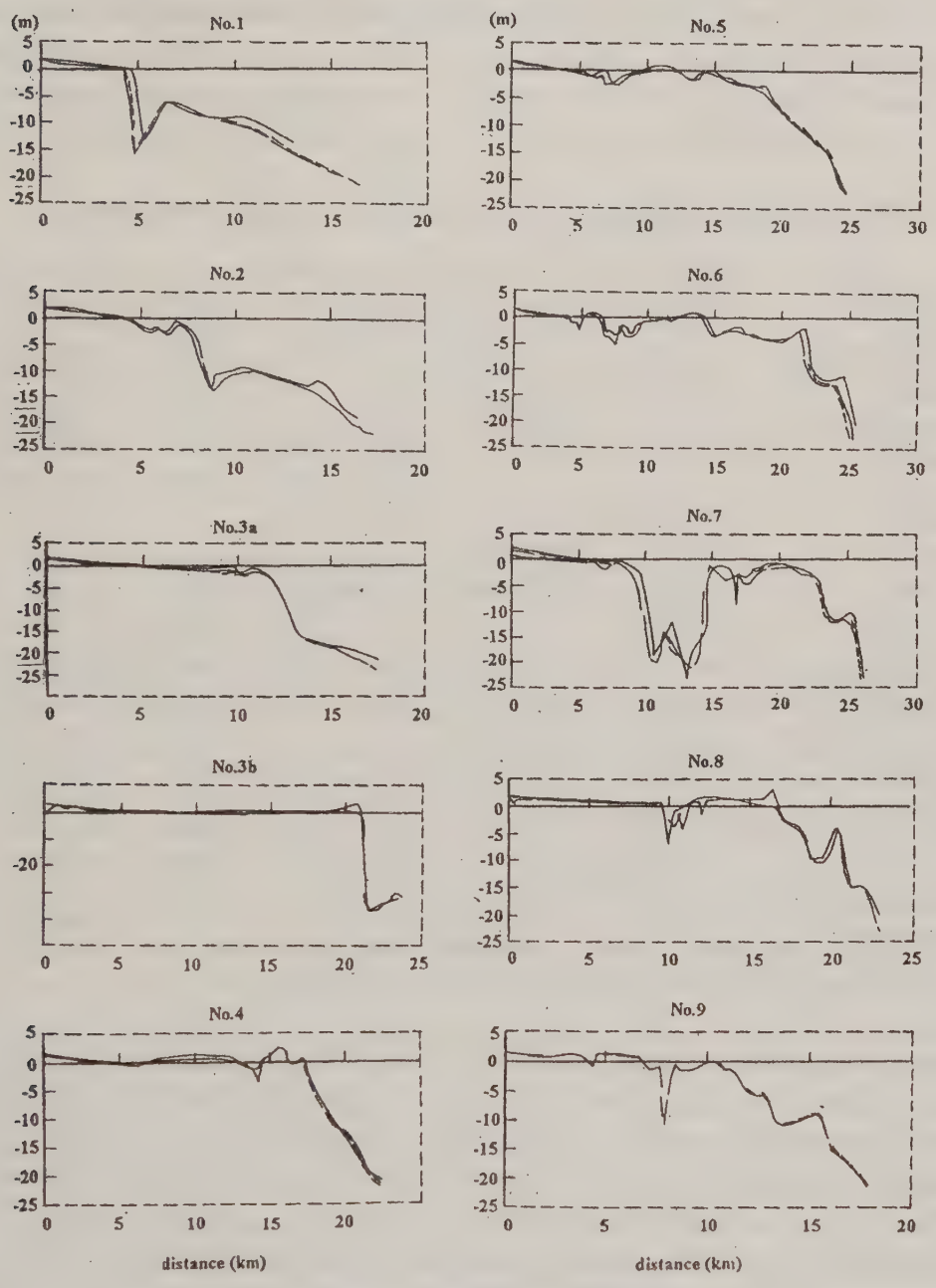

Fig.2 Coastal profiles in the Caofeidian area

system from 1983 to 1996, and the average erosive speed is 7.2cm/a for these 13 years on the underwater slope. From 1996 to 1997, the seasonal (winter to spring) erosive speed on the shallow is 11.4cm/a, and the accumulative speed on the underwater slope is 33.9cm/a. So the seasonal intensity of coastal changes is much stronger than the yearly one. And the intensity of coastal hydrologic motive power in winter and spring is also much stronger than the yearly average hydrologic motive power.

Based upon the accumulative and erosive distributing rule from the contrast of ten coastal

profiles in the Caofeidian area, combining marine condition of physiognomy in this area, we could have some knowledge as follows. In the Caofeidian area, the shallow on the seaward side of sandbar has suffered from by erosion and at the same time, there are accumulations on the shallow on the landward side of sandbar since 1983. The underwater slope in front of the sandbar has also been subjected to erosion since 1983 in the mass, but on some parts there are also accumulations. (Fig.3)

Table 1 Deep(m)、Changes of accumulation and erosion(m) & Velocity(m/a)

Profile number		D_{1983}	D_{1996}	D_{1997}	$C_{(1983\sim1996)}$	$C_{(1996\sim1997)}$	$V_{(1983\sim1996)}$	$V_{(1996\sim1997)}$
1	Shallow	1.19	0.717	0.628	-0.473	-0.089	-0.036	-0.089
	Underwater slope	-8.77	-9.94	-10.3	-1.17	-0.36	-0.09	-0.36
2	Shallow	-0.603	-0.198	-0.401	+0.405	-0.203	+0.031	-0.203
	Underwater slope	-11.54	-11.92	-11.97	-0.38	-0.05	-0.029	-0.05
3a	Shallow	-0.365	0.376	-0.169	+0.741	-0.545	+0.057	-0.545
	Underwater slope	-13.19	-15.75	-15.6	-2.56	+0.15	-0.197	+0.15
3b	Shallow	0.348	0.334	*	-0.014	*	-0.001	*
	Underwater slope	-27.17	-24.25	*	+2.92	*	+0.225	*
4	Shallow	-0.062	0.197	0.134	+0.259	-0.063	+0.02	-0.063
	Underwater slope	-12.16	-13.53	-12.62	-1.37	+0.91	-0.105	+0.91
5	shallow	-0.709	-0.474	-0.572	+0.235	-0.098	+0.018	-0.098
	Underwater slope	-7	-11.69	-10.68	-4.69	+1.01	-0.361	+1.01
6	Shallow	-1.1	-1.491	-1.552	-0.391	-0.061	-0.03	-0.061
	Underwater slope	-11.23	-11.99	-11.75	-0.76	+0.24	-0.058	+0.24
7	Shallow	-6.421	-4.977	-4.654	+1.444	+0.323	+0.111	+0.323
	Underwater slope	-10.26	-12.24	-11.22	-1.98	+1.02	-0.152	+1.02
8	Shallow	-1.227	0.341	0.054	+1.568	-0.287	+0.121	-0.287
	Underwater slope	-10.07	-8.56	-8.48	+1.51	+0.08	+0.116	+0.08
9	Shallow	*	-2.3	-2.3	*	0	*	0
	Underwater slope	*	-13.65	-13.6	*	+0.05	*	+0.05

In**C&V** column, +show accumulation, -show erosion, 0show balance; *show no data

Several main factors in making the sedimentary pattern in the Caofeidian area are the location、 marine condition of physiognomy, climate, hydrology and short supply of sand. The Caofeidian sandbar and lagoon system is protruding on the northwest coast of the Bohai Sea. The water area out of the sandbar is very broad, and the underwater slope is very steep. The distance between 0m~10m fathom lines is 200m~800m wide, and the one between 10m~20m is 800m~1000m wide. Because the Bohai Bay is a semi-enclosed bay, the blowing distance of wind is short, and the ground swell is not common. So the forming of the ocean wave is closely related to wind. As the wind direction is usually SW (spring) and NW (winter), the waves in SW (spring) and NW (winter) directions are very strong. In spring and winter, the stormy waves directly act on the sandbar and underwater slope, and the working area is only 500m wide. When stormy waves reach the sandbar, the seaward side of sandbar suffers from scouring. The violent current with sediments crosses the sandbar and forms accumulations on the landward side. Meanwhile the current develops from the lagoon rushes on the tide flat and erodes sediments on the top of it. The sediments which are eroded from the top of the tide flat form accumulations in the base of the lagoon and the tide flat.

So the erosion on the sandbar and the underwater slope is very serious. In summer and autumn, the waves in this area aren't strong, so the sedimentary pattern formed in spring and winter could be preserved.

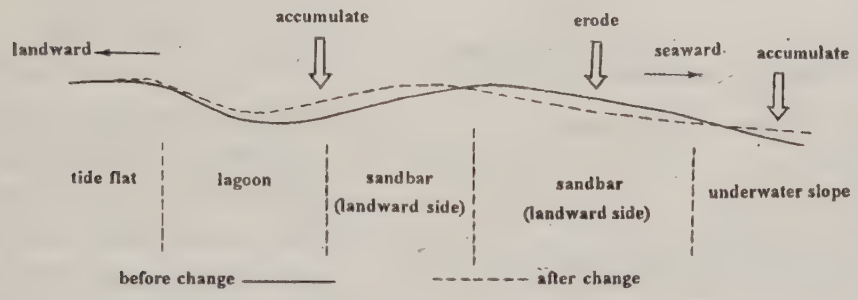

Fig.3 Changes of accumulation and erosion of coastal profiles

In addition, because reservoirs have been built in the upper reacher of the rivers nearby the research area, the quantity of sediment transport is dropping from 20.10 million tons in the 1960s to 0.79 million tons in the 1980s. The sand supply from the Luanhe River delta to the Caofeidian area is also reduced. So it is lacking massive sand supply along the coast of the Caofeidian area. It makes the Caofeidian sandbar and lagoon system always in the state of erosion. And the sedimentary pattern in this area is more obvious because of lack of sand supplies.

Although the erosion by stormy waves and lack of sand supplies are the main factors comtributing to the coastal changes in the Caofeidian sandbar and lagoon system, the effects of the global sea level change, the ground subsidence and the powerful storm tide should be considered synthetically. Based upon the hydrological data of Qinhuangdao station and Tanggu station, the northwest coastal area of the Bohai Sea has risen continuously since the 1980s. This phenomenon results in the fact that it is a slowly sinking region around the research area. At the same time, the course of quick sinking is owing to earthquake and over-drawing of groundwater. So the phenomenon of sea level going up in the northwest coast of the Bohai Sea is a reflection together with the global sea level rise and the ground subsidence. In addition, the modeling action on the coast by storm surges is also important. Once strong storm surge can destroy the sediments being accumulated for a long time. The storm surge along the northwest coast of the Bohai Sea usually occurs in July and August every year. It promotes the conveying and the distributing of sediments and adjusts the partial relief. So it is also an important factor in changing the coastal sedimentary pattern in the Caofeidian area. Based upon the statistic data of the storm surge affecting the northwest coast of the Bohai Sea and the contrast of the average sea level in Qinhuangdao and Tanggu, we could see that the storm surge and the short-term sea level rise have a corresponding connection. (Fig.4)

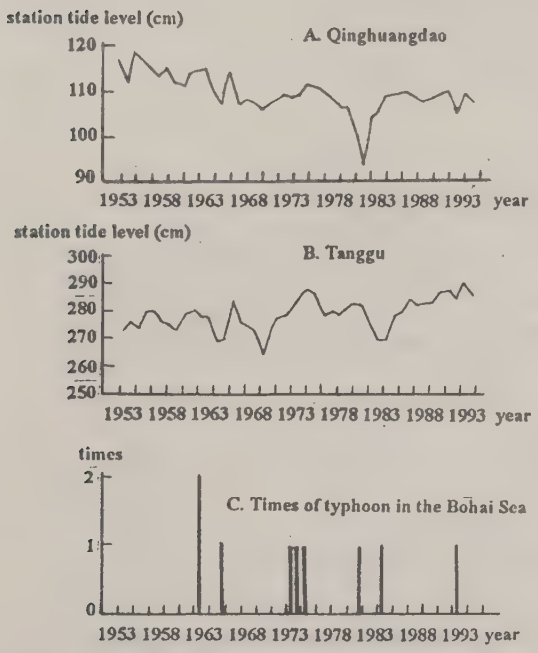

Fig.4 Average sea level in Qinhuangdao and Tanggn (Tian et al., 1997) & times of typhoon in the Bohai Sea from 1950 to 1995

Conclusions

(1) The average accumulative speed is 3.2cm/a on the shallow of Caofeidian sandbar and lagoon system from 1983 to 1996, and the average erosive speed is 7. 2cm/a for 13 years on the underwater slope. The shallow on the seaward side of the sandbar (about 5km wide) mostly suffers from erosion, and there are accumulations on the shallow on the landward side of the sandbar. From 1996 to 1997 the seasonal (winter to spring) erosive speed on the shallow is 11.4cm/a, and the accumulative speed on the underwater slope is 33.9cm/a. The shallow is subjected to erosion under the strong stormy waves, and the sediments are conveyed to the underwater slope.

(2) The stormy waves in winter and spring play a the decisive role in modeling the coastal sedimentary pattern. Besides, the global sea level rise、 ground subsidence and the powerful storm surge are also important contributing factors.

Reference

Tian, S., Xin, Y.X. and Yang, G.S., Study on relation between average sea level change and earthquake along the Bohai Sea, *Marine Science Bulletin*, 1997, 16 (5): 48~54 (in Chinese with English abstract).

Study on the Role of Tidal Currents in the Process of Formation and Development of the Changjiang River Delta

Zhu Yurong
(*Institute of Oceanology, Chinese Academy of Sciences, Qingdao*)

Abstract The Changjiang River Delta is a delta of tremendous scale which is formed under the control of tide and tidal currents. The study on the role of tide and tidal currents in the process of formation and development of the Changjiang River Delta can provide a typical example for the ocean-continent interaction process in the east area of our country. The tide and tidal currents in the Bohai Sea, Yellow Sea and East China Sea at the post-glacial transgression maximum are simulated, the sediment transport field in the Paleo-Changjiang River Estuary(PCRE) and its peripheral area at that time is calculated, and the seabed erosion/accretion pattern is obtained according to the divergence of sediment transport rate. The results show that a distinctive wave belly of standing tidal wave existed at the post-glacial transgression maximum and the wave belly lines protruded seawards from the wave belly point in the mouth of the PCRE. Under the wave belly control tidal currents converge to or diverge from the wave belly point. After a single tidal cycle, sediments started by tidal currents are mainly netly transported into the PCRE in the southeast and east directions, while there is a small amount of sediment to be netly transported to the northeast-southwest area off northern Jiangsu coast. The above sediment transport certainly results in deposition within the PYRE, in the area to the northeast of PCRE, and in the nearshore area between the south bank of the PCRE and the northern one of the Qiantangjiang River Estuary, while erosion occurs in the areas to the east and southeast of PCRE. The seabed erosion/accretion pattern is consistent with the situation of convergence or divergence of sediment transport rate. The Changjiang River Delta developed under the condition that the Changjiang River supplies a large amount of sediment, and the tide and tidal currents in the open sea impel this sediment to deposit as much as possible within the PCRE and its peripheral area. The tide and tidal currents in the open sea provide necessary and favorable dynamic conditions for the development of the Changjiang River Delta. When the Changjiang River Delta developed, it was very possible to form small scale sand bodies, which might be the embryonic of the Radial Sand Ridges in the southern Yellow Sea, in the area to the northeast of PCRE. The stretch seawards of the Changjiang River Delta is gradually enlarging the Hangzhou Bay.

Keywords the Changjiang River Delta; tide; tidal currents; sediment transport; formation and development

1 Introduction

The Changjiang River is the first longest of China's rivers, its runoff is abundant and its sediment discharge per year is only next to that of the Yellow River. The modern Changjiang River mouth has evolved from a trumpet estuary (Chen et al., 1988a), and the process of the trumpet

estuary becoming the modern Changjiang River mouth was the same as the formation and development of the Changjiang River Delta. At the post-glacial transgression maximum, i.e., 7000aB.P., in the modern Changjiang River Delta area was a huge trumpet estuary, and its bayhead was located roushly in Zhenjiang and Yangzhou (Chen et al., 1988a; Zhu et al., 1996) (Fig.1). Since then, this huge estuary was gradually filled up and transformed into a delta. At the same time, the Changjiang River mouth gradually moved eastwards, and shifted to south under the Coriolis force. At present there are runoff, wave, tide, tidal current and ocean current in the modern Changjiang River mouth area, among which the runoff and tidal current are the dominant hydrodynamics, and the tide is regular semidiurnal one with middle-strength (Shen et al., 1988). The Changjiang River Delta is a typical tide-controlling delta (Li et al., 1979) in the world.

Chen Jiyu et al.(1988a) thought that a large quantity of sediment provided by the abundant runoff of the Changjiang River supplied necessary material for the formation and development of the Changjiang River Delta, waves was the main destroying factor in the process of the development of the Changjiang River Delta, and ocean current, which transported sediment to other areas, also took part in the sedimentary process of the Changjiang River Delta. However, up to now, it is unclear what is the role of tide and tidal current, which are the dominant hydrodynamics besides runoff in the Changjiang River mouth area, in the process of the formation and development of the Changjang River Delta, although many authors have studied the formation and development of the Changjiang River Delta from the aspects of geology, morphology, sedimentology and paleo-geography (Li et al., 1979; Chen, 1988; Chen et al., 1988b; Wang et al., 1981; Sun, 1981; Zhao, 1984). What is the actual role of the tide and tidal current in the process of the formation and development of the Changjiang River Delta, since it is a typical tidal-controlling delta in the world? In geological history, how do the tide and tidal current in the open sea interact with the plentiful sediment supplied by the runoff of the Changjiang River to form the present modern Changjiang River Delta tremendous scale? In order to study the role of tide and tidal current in the process of the development of the Changjiang River Delta from the point of view of sediment dynamics, the M_2 tide and tidal current in the Bohai Sea, Yellow Sea and East China Sea at 7000a B.P. will be simulated, and the sediment transport field as well as the seabed erosion/accretion pattern in the Paleo-Changjiang River Estuary(PCRE) and its adjoining area will also be calculated.

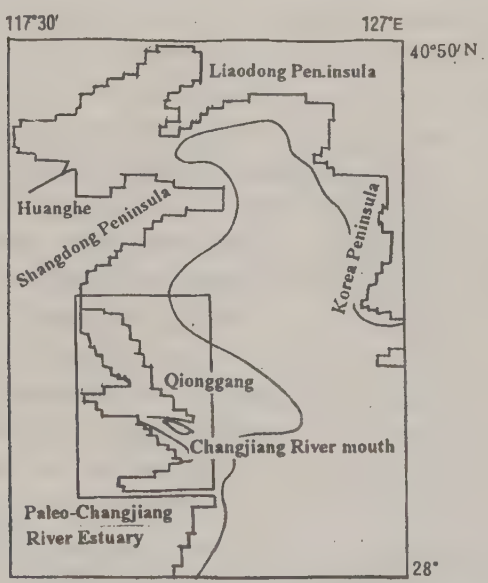

Fig.1 The locations of the Paleo-Changjiang River Estuary and the present Changjiang River mouth (after Zhu Chen et al., 1996)

2 Method

2.1 Calculating tide and tidal current

With a 2-D tidal model including the terms of bottom friction force and Coriolis force, the M_2 tide and tidal current in the Bohai Sea, Yellow Sea and East China Sea at the post-glacial transgression maximum are simulated with ADI method. The tidal model, the numerical method, and the determination of the paleo-coastal line, the paleo-water depth and the paleo-harmonic constants at the two water boundaries are referred to in Zhu (1998). When calculating the paleo-tidal current at 7000a B.P., the present annual average velocities instead of those at 7000aB.P., which are not known, are given at the boundaries in which the Changjiang River and the Qiantangjiang River flew into their estuaries, respectively. Thus, the influence of runoff on the paleo-tidal current field is considered.

2.2 Calculating sediment transport field

2.2.1 Sediment transport formulae

The net bedload transport rate per width within a single tidal cycle is calculated with the Hardisty's modified formula (1983) derived from the Bagnold's formula(1963), and the net suspended load transport rate per width within a single tidal cycle is computed with the Bagnold's formula (1966) from Qianning et al.(1991). The above Badnolds formulae are applicable to non-cohesive sediment.

Emphasis is laid on the study of sediment transport direction in this paper so as to qualitatively analyse the mechanism of the seabed sedimentation and submarine morphology. The absolute magnitude of bedload/suspended-load transport rate is not considered, but their relative magnitudes are needed in order to compare with each other in different areas. The divergence of sediment transport rate is calculated for dividing the seabed erosion/accretion areas.

2.2.2 The disposal of the sediment transport mode

The sediment transport mode must be defined firstly before calculating the sediment transport rate. If sediment is transported in a mode of suspension, the formula of suspended load transport rate will be used, whilst, if sediment is transported in a mode of bedload, the formula of bed load transport rate will be used. The problem is how to determine the sediment transport mode. When the grain size of seabed sediment is known in a specific site, McCave (1971) suggested that the sediment transport mode be determined based upon the ratio of the seabed shear velocity to the sediment settling velocity. But in a vast shelf sea area, e.g., the whole East China Sea area, it is impossible to determine the transport mode for some grain size, because in this area, the tidal current velocity and sediment grain size in different sites are quite different even at the same time. In addition, to determine sediment transport mode, neither the method of dividing a whole large area into many small areas nor that of determining sediment transport mode one by one in every calculating point can work.

To simplify the problem, and in view of the sediment transport direction being mainly considered in this paper, the sediment transport mode is dealt with as follows. The 9 kinds of grain size, i.e., 0.016mm, 0.032mm, 0.063mm, 0.105mm, 0.125mm, 0.18mm, 0.25mm, 0.375mm, 0.

45mm, for non-cohesive sediment, are selected based upon the grain size range of the sedimentary body revealed by drilling core within the Paleo-Changjiang River Estuary (Wang et a., 1981), and of the bottom sediment in the adjoining area of the PCRE(Liu, 1992). For each grain size, both the bedload transport rate and the suspended load transport rate are calculated. And then, the sediment transport direction and the relative magnitude of sediment transport rate, especially the sediment transport direction, are compared with each other in order to qualitatively explain the formation mechanism of seabed sedimentation and submarine morphology. To understand the general picture of sediment transport in a vast area, the method to determine sediment transport mode as above is more reasonable than that which dictates that the sediment with grain size being less/greater than some certain grain size will transport in a mode of suspension/bedload.

The sediment source is not considered when calculating the suspended load or bedload transport rate per width within a single tidal cycle for 9 kinds of grain size. Thus, if only there are sediments, which come from rivers, seabed, open sea or eroded coast, and enter the tidal currents, the sediment transport pattern given in this paper will be obtained. The more grain sizes are selected, the more sediment transport law will be found although only 9 kinds of grain size are selected in this paper.

2.3 Calculating the divergence of sediment transport rate

The divergence of suspended load or bedload transport rate per width in a single tidal cycle is calculated in terms of the definition of divergence in higher mathematics. The seabed will erode if the symbol of divergence is plus, whereas, the seabed will deposit if the symbol is minus. The aim to calculate divergence is to divide seabed erosion/accretion area, and to obtain the erosion/accretion pattern in seabed.

3 Results

3.1 The calculated results of tide and tidal current

At the post-glacial transgression maximum, i.e., 7000aB.P., in the modern Changjiang River Delta area was a large estuary with its bayhead located in the Zhenjiang and Yangzhou area. Its north bank extended from Yangzhou through Taizhou to Haian, and was connected with the northern Jiangsu coastline, which had a concave shape (Zhu et al., 1996). As a whole, at 7000aB.P the number of the amphidromic points and the distribution trend of the cotidal and isoamplitude lines are similar to those at present, but the amount of the isoamplitude lines in the whole calculating domain was lower by 20~30cm than that of the present because of the expansion of water area. The location of the amphidromic point south of the Shandong Peninsula was about 20km southwestward of its present position, but the other three generally did not change. The progressive tidal waves in the Yellow Sea from the East China Sea meet their corresponding reflective tidal waves. Such a superimposition leads to the formation of the distinctive wave loop of standing tidal wave with its antionode located in the central point of the PCRE, and the wave loop lines protruding seawards. The scale of the distinctive tidal wave is larger than the present one in the Qianggang area.

At the flood half tide level, tidal currents converge to the mouth of the Paleo-Changjiang River Estuary (PCRE), and meet the ebb ones, which move seaward from the bayhead, at the mouth. At the

ebb half tide level, the tidal currents diverge from the mouth to sea, while the flood tidal currents inside the PCRE move towards bayhead from the mouth. And the current velocities reach the maximum at the flood and ebb half tide levels, respectively. Hence, the above distinctive tidal wave area off the mouth of the PCRE has the characteristics of a wave loop of standing tidal wave, and its scale is very large. The antinode of the standing tidal wave was generally located in the central point of the mouth of the PCRE, and its node was the amphidromic point south of the Shandong Peninsular. In short, the antinode, i.e., the central point of the mouth of the PCRE, is the converging point of tidal currents in open sea. Noticeably, the movement regime of the tidal currents north to the central axis line of the PCRE is similar to that at present, but the converging degree of tidal currents is not so strong as the present one. At 7000aB.P., the radial tidal current field with its apex being the antinode point in the mouth of the PCRE is determined by the characteristics of the wave loop of the standing tidal wave.

At the flood/ebb half tidal levels, tidal currents at the mouth of the PCRE move exactly in opposite directions. This phenomenon can be explained by the fact that the tidal currents within the PCRE was delayed by bottom friction and the phase of the tidal currents within the PCRE is not consistent with the one in the shelf. Thus, the tidal currents in the open sea flood/ebb while the tidal currents within the PCRE ebb/flood. The co-tidal chart and the tidal current field at the flood/ebb half tidal level at 7000aB.P. as well as the verification of the paleo-tidal current field are referred to in Zhu (1998).

3.2 The calculated results of sediment transport rate and the seabed erosion/accretion pattern

3.2.1 The net sediment transport direction within a single tidal cycle

In the PCRE and its adjoining area, the bedload transport rates per width within a single tidal cycle for 9 kinds of grain size are calculated with the Hardisty's modified formula. The results show that under the action of M_2 tidal currents the net transport directions within a single tidal cycle for 9 kinds of grain size are the same. The sediment was netly transported into the PCRE from the southeast and east directions. When the grain size is relatively small, there was a small amount of sediment netly transported to the wide-belt blank area, which extended in the northeast direction, off the northern Jiangsu coast (Fig.2b, Fig.3b).

The suspended load transport rates per width within a single tidal cycle for 9 kinds of grain size are calculated with the Bagnolds suspended load transport formula (Qian, 1991). The results show that under the action of M_2 tidal currents the net transport directions within a single tidal cycle for 9 kinds of grain size are the same. The sediment was netly transported into the PCRE from the southeast and east directions. When the grain size is relatively small, there was a small amount of sediment netly transported to the wide-belt blank area, which extended in the northeast direction, off the northern Jiangsu coast (Fig.2a, Fig.3a).

To sum up, at 7000aB.P., in a site if only sediment was started by tidal currents whether in a mode of suspension or in a mode of bedload, the net transport directions within a single tidal cycle for different kinds of grain size were the same. In short, within a single tidal cycle, all sediments started by tidal currents had the same net transport direction. All sediments were netly transported into the PCRE from the southeast and east directions, whereas there was a small amount of sediment netly transported to the wide-belt blank area off the northern Jiangsu coast.

3.2.2 The relative magnitude of suspended load or bedload transport rate per width within a single tidal cycle

The suspended load and bedload transport rates per width within a single tidal cycle for each grain size are calculated, respectively. The results show that under the action of paleo-tidal currents, for each grain size, the magnitude of suspended load transport rate was always greater than that of its bedload transport rate. The suspended load transport rate and the bedload transport rate become small and small with the grain size becoming larger and larger. The ratio of the suspended load transport rate to the bedload transport rate also becomes small and small with the grain size becoming larger and larger. On the contrary, the ratio of the bedload transport rate to the suspended load transport rate becomes greater and greater with the grain size becoming smaller and smaller. It infers that the sediment with a small grain size is easy to be transported in a mode of suspension, whereas, the sediment with a large grain size is easy to be transported in a mode of bedload.

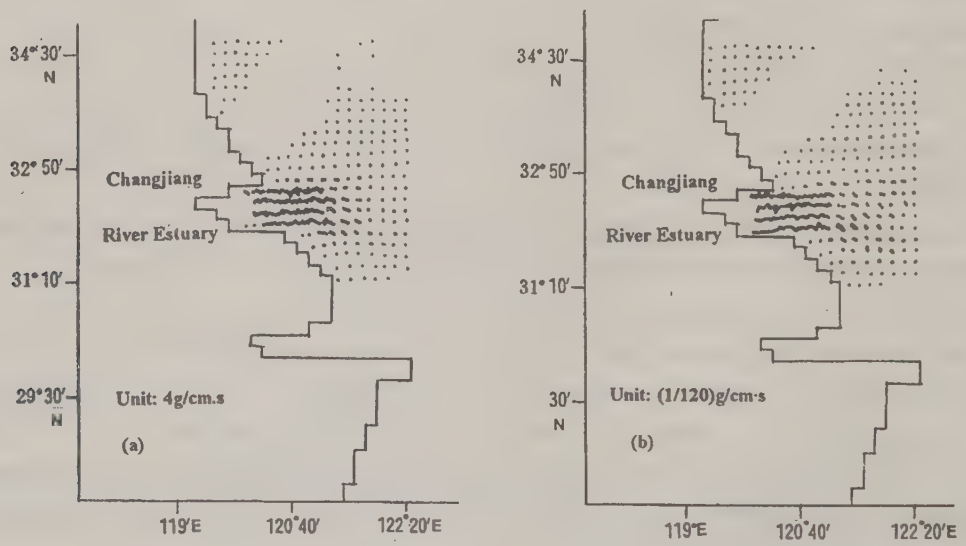

Fig.2 The sediment transport patterns for the 0.016mm grain size under the action of M_2 tidal currents in 7000aB.P. (a: suspended load; b: bedload)

3.2.3 The seabed erosion/accretion pattern

The seabed erosion and accretion areas are divided based upon the symbols (+/-) of divergence of the suspended load and bedload transport rates per width within a single tidal cycle. The seabed erosion/accretion pattern shows that all sediments with different grain sizes, whether transported in a mode of suspension or in a mode of bedload, generally deposit within the PCRE and its adjoining area, especially in the area to the northeast of PCRE, and the nearshore area between the south bank of the PCRE and the northern one of the Qiantangjiang River Estuary, while erosion occurs in the areas to the east and southeast of PCRE (Fig.4, Fig.5). The erosion/accretion pattern becomes complicated locally with the grain size becoming larger and larger, but the whole erosion/accretion pattern does not change, and is consistent with the situation of convergence or divergence of

sediment transport rate.

3.2.4 The development of the Changjiang River Delta, the occurrence of the embryonic form of the radial sand ridges and the enlargement of the Hangzhou Bay

The sediment transport and deposition as the above certainly results in the gradual filling of the PCRE so that the PCRE became smaller and smaller, the Changjiang River mouth gradually shifted southwards under the Coriolis force, and the Changjiang River Delta gradually developed. It is no doubt that the sediment used to fill the PCRE was mainly from the Changjiang River, whose

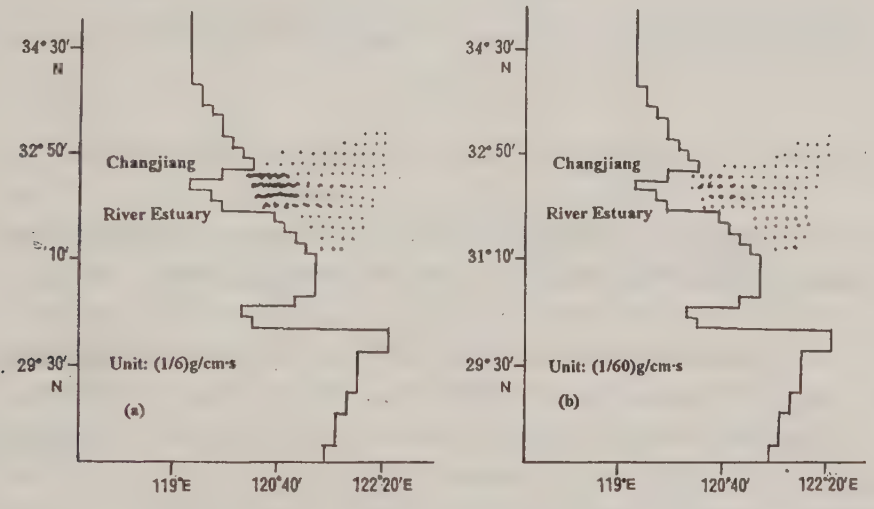

Fig.3 The sediment transport patterns for the 0.25mm grain size under the action of M_2 tidal currents in 7000aB.P. (a: suspended load; b: bedload)

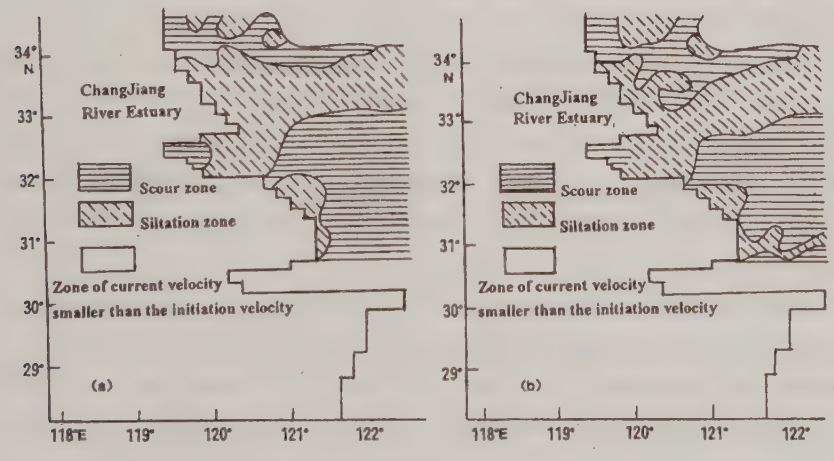

Fig.4. The erosion/accretion patterns for the 0.016mm grain size caused by sediment transport under the action of M_2 tidal currents in 7000aB.P. (a: suspended load; b: bedload)

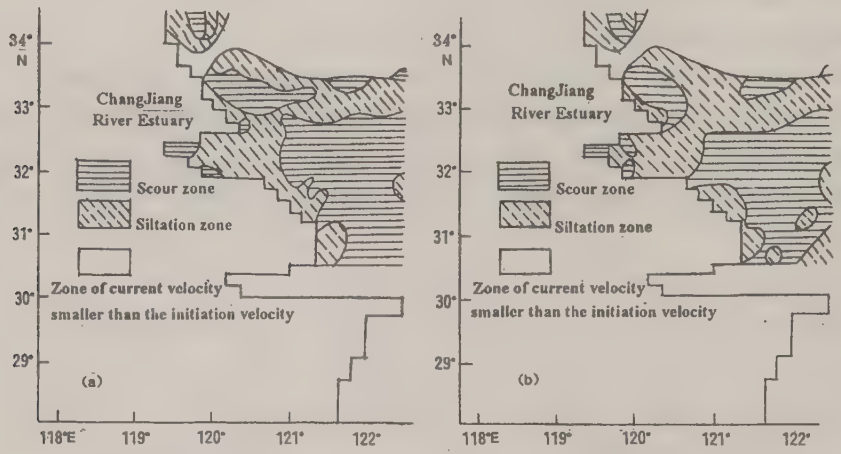

Fig.5. The erosion/accretion patterns for the 0.25mm grain size caused by sediment transport under the action of *M*$_2$tidal currents in 7000aB.P. (a: suspended load; b: bedload)

abundant runoff carried enormous sediment into the PCRE. The role of tide and tidal current lies in that they netly transported sediment into the PCRE from open sea. Thus, the enormous sediment provided by the Changjiang River was impelled to deposit as much as possible within the PCRE and its adjoining area to fill the PCRE and to construct the Changjiang River Delta. The tide and tidal current in open sea provided necessary and favorable hydrodynamic conditions for the filling of the PCRE and the formation and development of the Changjiang River Delta. In short, abundant sediment and favorable hydrodynamics netly transported sediment to land from sea are the two essential conditions for the development of a huge or large delta.

Is the sediment transport direction calculated above correct? The development, the construction, and the existence of the huge tidal-controlling Changjiang River Delta are the best evidence for the correctness of the sediment transport direction calculated in this paper. At the post-glacial transgression maximum, if the sediment provided by the Changjiang River were transported to open sea form the PCRE other than the situation in this paper, the PCRE would not be filled, and the PCRE might possibly be enlarged. Even though the amount of this sediment deposited in the PCRE were greater than that to be transported by tidal currents to open sea so that the PCRE might not be enlarged, it would be impossible to develop the modern Changjiang River Delta with such a tremendous scale. Under such conditions, the most possible is to form a small delta within the PCRE, and the occurrence in the Ganges-Brahmaputa.Estuary (Dilip, et al., 1994) is the case. Although the Ganges and Brahmaputa Rivers provide a large amount of sediment into their common estuary area, the delta developed within the estuary has not almost prograded during the past two centuries. The survey results show that the strong tidal currents, which are the dominant hydrodynamics in the estuary area, netly transport sediment provided by the two rivers to open sea from the estuary area so that the deposition within the estuary is hindered. Hence, to form a large delta in an estuary area, it must meet two conditions at the same time, i.e., abundant sediment source and favorable hydrodynamic conditions. The progressive tidal wave system in the East China Sea

from the northeast Pacific Ocean netly transported sediment into the PCRE from open sea and impelled sediment to deposit within the PCRE as much as possible. Therefore, in a sense, if the progressive tidal wave system in the East China Sea did not exist, it would not be impossible to develop the Changjiang River Delta with such a tremendous scale, even though the sediment brought by the Changjiang River was abundant.

In a word, at the post-glacial transgression maximum the sediment brought by the Changjiang River mainly filled the PCRE and developed the Changjiang River Delta under action of the tide and tidal currents. When the Changjiang River Delta developed, it was very possible to form a little scale sand bodies, in the area to the northeast of PCRE because there was a small amount of sediment to be transported to this area. And this sand bodies may be the embryonic of the Radial Sand Ridges now in the southern Yellow Sea. Only when the PCRE was almost filled up, did it become possible to form the radial sand ridges with a certain scale through the radial tidal current field controlling the directly dispersed sediment from the Changjiang River or reforming the submarine Changjiang River delta formed when the PCRE existed. In the process of the PCRE being filled, deposition also occurred in the nearshore area between the southern bank of the PCRE and the northern one of the Qiantangjiang River Estuary. The progradation of this nearshore area led to the enlargement of the Hangzhou Bay and the Qiantangjiang River Estuary. Hence, the final formation of the Hangzhou Bay was closely related to the seaward stretch of the Changjiang River Delta.

4 Discussion

4.1 The change of the characteristics of the tidal wave in the Changjiang River mouth

The course curves of tidal level and tidal current velocity during a single tidal cycle for 18 points in the PCRE and its adjoining area are calculated. The results show that the tidal wave within the PCRE at the post-glacial transgression maximum was neither typical progressive wave nor typical standing wave, and in fact, it had both at the same time because of the reflection and friction effects within the PCRE. Off the PCRE was a noticeable wave loop of standing tidal wave with its antinode generally located in the central point of the mouth, thus, the maximum tidal range within the scope of the wave loop occurs in the mouth of the PCRE. When the tidal waves propagated into the PCRE from its mouth, it was very possible that the tidal range continually increased due to the narrowing effect of the PCRE. Therefore, tidal bore might occur within the PCRE, and the tide and tidal currents within the PCRE have strong-tide characteristics. Chen et al.(1988b) also concluded that there had been tidal bore phenomenon in the PCRE. The iso-amplitude lines in the PCRE are not given in this paper because relative coarse mesh is used here. The detailed study on the characteristics of tide and tidal currents in the PCRE is needed under the condition that fine mesh is used.

Now the M_2 tide waves both within and off the modern Changjiang River mouth are progressive ones because the modern Changjiang River mouth has shifted out of the influence scope of the wave loop of the standing wave, and entered the area occupied by the progressive wave in the East China Sea. Now the antinode of standing wave is located in the Qianggang area off northern Jiangsu coast instead of in the modern Changjiang River mouth. Therefore, the tide in the modern

Changjiang River mouth area has become weaker than before, and it belongs to middle-strength type. The main marine dynamics in the PCRE and its adjoining area at the post-glacial transgression maximum was dominated by tide and tidal currents, whereas, now the main hydrodynamics in the modern Changjiang River mouth is prevailed by both runoff and tide and tidal currents.

4.2 The process of the formation and development of the Changjiang River Delta

At the post-glacial transgression maximum, the Changjiang River mouth was a large estuary with strong tide and tidal current. And the tide and tidal current impelled sediment to be netly transported to land from open sea, and the large amount of sediment brought by the Changjiang River to deposit within the estuary to form sand bodies. With the estuary being filled, the Changjiang River mouth gradually narrowed and the sediment provided by the Changjiang River started to form sand islands similar to the present Chongming Island. When the Changjiang River mouth shifted southeastwards greatly, the early sand islands arranged like goose-line might combine to land so that the Changjiang River Delta gradually developed. Since the post-glacial transgression maximum, the development of the Changjiang River Delta has undergone the following process, i.e., from the delta within the PCRE through the one more and more protruding the mouth of the PCRE, up to the modern Changjiang River Delta with a tremendous scale.

5 Conclusion

(1) At the post-glacial transgression maximum, the progressive tidal waves in the Yellow Sea from the East China Sea met their corresponding reflective tidal waves. Such a superimposition led to the formation of the distinctive wave loop of standing tidal wave with its antionode located in the central point of the PCRE, and the wave loop lines protruding seawards. Under the control of the wave loop, tidal currents converge to or diverge from the antinode in the mouth of the PCRE. The tidal current field north to the central axis line of the PCRE was similar to the present one in the southern Yellow Sea. The radial tidal current field at 7000a B.P. and the present one provided necessary and favorable conditions for the formation and development of the Changjiang River Delta and the formation and the maintainment of the radial sand ridges in the southern Yellow Sea, respectively.

(2) At the post-glacial transgression maximum, all sediment started by tidal currents was mainly transported into the PCRE from the southeast and east directions, while there was a small amount of sediment to be netly transported to the wide-belt blank area, which extended in the northeast direction, off the northern Jiangsu coast.

(3) All sediments started by tidal currents, which were transported whether in a mode of suspension or in a mode of bedload, generally deposit within the PCRE and its adjoining area, especially in the area to the northeast of PCRE, and the nearshore area between the southern bank of the PCRE and the northern one of the Qiantangjiang River Estuary. The erosion/accretion pattern is consistent with the situation of convergence or divergence of sediment transport rate.

(4) The Changjiang River Delta has developed under the condition that the Changjiang River supplied a large amount of sediment, and the tide and tidal currents in open sea impelled this sediment to deposit as much as possible within the PCRE and its peripheral area. The tide and tidal

currents in open sea provided necessary and favorable dynamic conditions for the development of the Changjiang River Delta. When the Changjiang River Delta developed, it was very possible to form small scale sand bodies, which might be the embryonic of the Radial Sand Ridges in the southern Yellow Sea, in the area to the northeast of PCRE. The stretch seawards of the Changjiang River Delta enlarged the Hangzhou Bay.

(5) The characteristics of the tidal wave in the Changjiang River mouth changed from a mixed type of standing tidal wave and progressive tidal wave at 7000a B.P. to the present progressive tidal wave. The dominant hydrodynamics in the Changjiang River mouth changed from the strong-tide type at 7000a B.P. to the present mixed one of runoff and middle-strength tide. The early Changjiang River Delta was composed of sand bodies within the PCRE, whereas in the late period, it was formed through sand islands combining to land.

References

Chen Jiyu, Shen Huanting, Yun Caixing, (1988a) The dynamic process and the morphology evolution in the Changjiang River mouth.*Shanghai Science and Technology Press*, 1～5

Chen Jiyu, (1988) The development of the morphology in the part of the Changjiang River mouth. In: Chen Jiyu, Shen Huanting, Yun Caixing,(editors) (1988) The dynamic process and the morphology evolution in the Changjiang River mouth.*Shanghai Science and Technology Press*, 38～47

Chen Jiyu, Yun Caixing, Xu Haigen, (1988b) The development model of the Changjiang River mouth since 2000aBP. In: Chen Jiyu, Shen Huanting, Yun Caixing (editors) (1988) The dynamic process and the morphology evolution in the Changjiang River mouth.*Shanghai Science and Technology Press*, 31～37

Dilip K B, Steven A K, Richard L M, Williard S M, (1994) Suspended sediment distribution and residual transport in the coastal ocean off the Ganges-Brahmaputra river mouth.*Marine Geology*, 120, 41～61

Hadisty J, (1983) An assessment and calibration of formulation for Bagnolds bedload equation.*Sedimentary Petrology*, 53(3)1007～1010

Li Congxian, Wang Jingtai, Li Ping, (1979) The preliminary study on the sedimentary facies in the Changjiang River Delta area. *Journal of Tongji University*, 2(Marine Geology Edition) 1～14

Liu Xiqing, (1992) The up-to-date map of the bottom sediment type in the shelf. of China. *Marine Geology and Quaternary Geology*, 12(4), 11～20

McCave I N, (1971) Sand waves in the North Sea off the coast of Holland.*Marine Geology*, 10, 199～225

Qian ning, Wan Zhaohui, (1991) The mechanics of the sediment movement.*China Science Press*, 1, 1～414

Shen Huanting, Gu Guochuan, Li Jiufa, (1988) The characteristics of tidal waves in the Changjiang River mouth and its influence on the evolution of the river gutter. In: Chen Jiyu, Shen Huanting, Yun Caixing (Editors) (1988)The dynamic process and the morphology evolution in the Changjiang River mouth.*Shanghai Science and Technology Press*, 73～79

Sun Shuncai, (1981) The sedimentary features of the Changjiang River Delta in Holocene.*Acta Oceanologic Sinic*, 3 (1)97～113

Wang Jingtai, Guo Xumin, Xu Shiyuan (1981) The development of the Changjiang River Delta in Holocene.*Geology Science*, 1, 67～80

Zhao Songling, (1984) The geological problem in the Changjiang River Delta area in Quaternary.*Marine Science*, 5, 15～21

Zhu Cheng, Cheng Pen, Lu Chuncheng et al. (1996) The analysis on the coastline evolution law in the Changjiang River Delta and the northern Jiangsu nearshore area since 7000aB.P..*Geography Science*, 16(3)207～213

Zhu Yurong (1998) The numerical simulation and the verification of the Paleo-tidal current field in the northern Jiangsu littoral plain area.*Marine Science Bulletin*. 17(3)1～7

Wind-Driven Slanting Profile Wave Derived from the Unified Variational Principle of Water Gravity Wave

Fu Yuhua
(*China Offshore Oil Production Research Center*)

Abstract Considering that at present the regular waves in common use have the profile symmetrized to a vertical axis, which are different from actual wind-driven sea waves, and based on deriving linear wave, solitary wave, fifth order Stokes wave and stream function wave by using Unified Variational Principle of Water Gravity Wave (UVPWGW), this paper derives wind-driven slanting profile wave by using UVPWGW. Its feature is that under the action of wind pressure, the wave profile is not symmetrized to a vertical axis, but that it is in the forward slanting form.

Keywords unified variational principle of water gravity wave; wind-driven wave; slanting profile

Introduction

The sea wave research and various regular waves, such as linear wave, solitary wave, fifth order Stokes wave and stream function wave have been extensively used in ocean engineering and the like (Mei,1984). There is a blemish in an otherwise perfect thing, i.e., at present the regular waves in common use have the profile symmetrized to a vertical axis, which are different from actual wind-driven sea waves. In order to overcome this disadvantage, based on deriving linear wave (Fu,1992a) , solitary wave (1989a), fifth order Stokes wave (1989b) and stream function wave (Fu,1998) by using Unified Variational Principle of Water Gravity Wave (UVPWGW) (Fu, 1992a), this paper derives wind-driven slanting profile wave by using UVPWGW. Its feature is that under the action of wind pressure, the wave profile is not symmetrized to a vertical axis, but that it is in the forward slanting form.

1 A Unified Variational Principle of Water Gravity Wave

By using optimization method of weighted residuals (OMWR) (Fu,1992b,1995a,1995b), besides a unified variational principle of fluid mechanics (Fu,1994a) and a unified variational principle of elasticity theory(Fu,1994b), a UVPWGW was also established. The brief introduction to UVPWGW can be found in Reference (Fu,1992a), therefore it will not be stated in this paper.

2 Unified Variational Principle for Deriving Wind-Driven Slanting Profile Wave

When deriving Wind-Driven Slanting Profile Wave, the mathematical equations for deriving fifth order Stokes wave are used, which mainly contain four equations:

Continuity equation, i.e., Laplace equation

$$\Delta^2 \phi = 0 \quad (1)$$

Bottom boundary condition

$$v \mid_{S=0} = 0 \quad (2)$$

Kinematic free surface boundary condition

$$\partial y/\partial x + v/(C - u) = 0 \quad S=D+y \quad (3)$$

Dynamic free surface boundary condition

$$(C-u)^2 + v^2 - C^2 + 2[P/\rho + g(Q+y)] = 0 \quad S=D+y \quad (4)$$

where: ϕ- potential function; S - vertical coordinate; x - abscissa (mudline); y - wave profile; C - wave celerity; D-average water depth; Q- a constant; u-horizonta lvelocity; v - vertical velocity; P/ρ - wind pressure on profile.

For handling the boundary conditions directly, we will assume

$$R_1 = \partial y/\partial x + v/(C - u) \quad (3')$$

$$R_2 = (C-u)^2 + v^2 - C^2 + 2[P/\rho + g(Q+y)] \quad (4')$$

It should be noted that when deriving the existing regular waves, the above mentioned wind pressure P/ρ is omitted, while in this paper it must be considered.

For deriving wind-driven slanting profile wave, based on the existing linear wave and taking some modify term, the form of potential function reads

$$\phi = \cosh \beta S(X_1 \sin \beta x + X_2 \cos \beta x) \quad (5)$$

where: X_i constants to be determined

According to Eq. (5), we can obtain

$$u = \beta \cosh \beta S (X_1 \cos \beta x - X_2 \sin \beta x) \quad (5')$$

$$v = \beta \sinh \beta S(X_1 \sin \beta x + X_2 \cos \beta x) \quad (5'')$$

Since the Laplace equation and bottom boundary condition have been satisfied in advance by the above-mentioned equations, therefore the variational principle $\Pi = \Pi_0 + \Pi_{00} + \Pi_1 + \Pi_2 = \min$ will be simplified as follows

$$\Pi = \Pi_1 + \Pi_2 = \min \quad (6)$$

where

$$\Pi_1 = \int R_1^2 \, dx$$

$$\Pi_2 = \int R_2^2 \, dx$$

The integral interval is $[-L/2, L/2]$, L is the wave length. The values of integral can be obtained through numerical integration, with which the interval is divided into 36 parts and the Simpson formula is used.

3 Application Examples of UVPWGW

Example 1. Assume: wave height $H = 5.6896$m, period $T = 7.72sec$, water depth $D = 9.144$m, try to derive the wind-driven slanting profile wave for the case of $P/\rho \neq 0$.

For the existing linear wave ($P/\rho = 0$), we can get the related results as follows:

wave length $L = 65.54$m (7)

The results for wave profile y, horizontal velocity u and vertical velocity v at profile are shown

in Tables 1~3.

For deriving the profile, based on the existing linear wave and taking some modify term, the form of potential function reads

$$y = G_1 \cos \beta x + G_2 \sin \beta x \qquad (8)$$

Table 1. Results of wave profile y

β x(°)	Existing solution	Present solution Eq. (21)	Present solution Eq.(25)	Present solution Eq.(29)
-180	-2.8448	-2.8448	-2.8448	-2.8448
-160	-2.6732	-2.7550	-2.7122	-2.6902
-140	-2.1792	-2.3329	-2.2524	-2.2111
-120	-1.4224	-1.6295	-1.5210	-1.4653
-100	-0.4940	-0.7294	-0.6061	-0.5427
-80	0.4940	0.2585	0.3819	0.4452
-60	1.4224	1.2153	1.3238	1.3795
-40	2.1792	2.0256	2.1061	2.1474
-20	2.6732	2.5915	2.6343	2.6563
0	2.8448	2.8448	2.8448	2.8448
20	2.6732	2.7550	2.7122	2.6902
40	2.1792	2.3329	2.2524	2.2111
60	1.4224	1.6295	1.5210	1.4653
80	0.4940	0.7294	0.6061	0.5427
100	-0.4940	-0.2585	-0.3819	-0.4452
120	-1.4224	-1.2153	-1.3238	-1.3795
140	-2.1792	-2.0256	-2.1061	-2.1474
160	-2.6732	-2.5915	-2.6343	-2.6563
180	-2.8448	-2.8448	-2.8448	-2.8448

Table 2. Results of u at profile

β x(°)	Existing solution	Present solution Eq. (21)	Present solution Eq.(25)	Present solution Eq.(29)
-180	-2.769	-2.463	-2.451	-2.448
-160	-2.626	-2.318	-2.311	-2.310
-140	-2.199	-1.917	-1.914	-1.914
-120	-1.500	-1.283	-1.282	-1.283
-100	-0.552	-0.456	-0.457	-0.456
-80	0.590	0.501	0.501	0.503
-60	1.816	1.492	1.492	1.496
-40	2.945	2.381	2.378	2.381
-20	3.753	3.011	3.000	3.001
0	4.048	3.247	3.227	3.224
20	3.753	3.031	3.005	2.997
40	2.945	2.407	2.381	2.372
60	1.816	1.505	1.487	1.480
80	0.590	0.490	0.484	0.481
100	-0.552	-0.488	-0.483	-0.482
120	-1.500	-1.324	-1.311	-1.308
140	-2.199	-1.954	-1.938	-1.933
160	-2.626	-2.339	-2.325	-2.320
180	-2.769	-2.463	-2.451	-2.448

For the method presented in this paper, the constant Q in Eq.(4) of DFSBC and wave length L ar e unknowns also, and for the sake of convenience we will take β as an unknown instead of L, the value of L will be calculated by using the following formula

$$L = 2\pi / \beta \qquad (9)$$

Now, when solving wind-driven slanting profile wave according to variational principle Eq.(6), there are 6 unknowns all together: X_1 and X_2 in Eq.(5') and (5"), G_1, G_2, Q and β in Eq.(8). For the sake of convenience, let $X_1 \sim X_6$ denote them ($G_1 = X_3, \cdots \beta = X_6$), for the reason that we will modify the profile of linear wave, therefore the value of G_1 is fixed as follows

$$G_1 = H/2 \qquad (10)$$

Then there are 5 unknowns all together to be determined: X_1, X_2, G_2, Q and β.

How to decide these 5 unknowns according to variational principle Eq.(6) ? Now there are many computerized methods for solving extreme value problems, for example, we can use the extreme value condition equations as follows

$$\partial \Pi / \partial X = 0 \qquad (11)$$

However, by using this method not only the minimum solution can be obtained, but also the maximum solution and some other solutions instead of minimum solution can be obtained, so this paper will not use this method. For other optimum seeking methods, in general they can be divided into two kinds: one's program is complicated, but it doesn't require the condition of initial value strictly; another's program is simple, but it requires the condition of initial value strictly, i.e., the initial value and the final solution must be close enough. This paper will use the searching method (Fu, 1989c), which program is the simplest, and take the existing linear wave solution as the initial value. This method means that the existing linear wave solution will be improved into the wind-driven slanting profile wave solution. The solving procedure can be stated briefly as follows: firstly within the initial value, a certain variate is relaxed, while other variates are fixed, then search the relaxed variate and make Π minimum, the rest may be reduced by analogy, after several searching cycles, we can stop searching and get the minimum.

Table 3. Results of ν at profile

β x(°)	Existing solution	Present solution Eq. (21)	Present solution Eq.(25)	Present solution Eq.(29)
-180	0	-0.005	-0.005	-0.005
-160	-0.527	-0.399	-0.399	-0.401
-140	-1.076	-0.799	-0.804	-0.808
-120	-1.635	-1.197	-1.208	-1.216
-100	-2.129	-1.544	-1.559	-1.570
-80	-2.436	-1.754	-1.768	-1.780
-60	-2.413	-1.730	-1.738	-1.747
-40	-1.965	-1.405	-1.407	-1.411
-20	-1.109	-0.791	-0.788	-0.788
0	0	0.010	0.010	0.011
20	1.109	0.823	0.813	0.811
40	1.965	1.468	1.443	1.436
60	2.413	1.823	1.787	1.774
80	2.436	1.862	1.820	1.804
100	2.129	1.642	1.604	1.588
120	1.635	1.266	1.237	1.225
140	1.076	0.831	0.815	0.808
160	0.527	0.401	0.395	0.393
180	0	-0.005	-0.005	-0.005

According to the existing linear wave, the initial values are as follows

$$G_{1,0} = 2.8448, \quad G_{2,0} = 0,$$
$$X_{1,0} = 24.31565, \quad X_{2,0} = 0, \qquad (12)$$
$$Q_0 = -0.1670304, \quad \beta_0 = 0.09586614$$

It should be noted that the existing linear wave is not related with the value of Q, and we will decide the value of Q_0 according to the principle of making the value of Π (actually it is the value of $\Pi_{2,0}$) minimum. When $P/\rho = 0$, the values of $\Pi_{1,0}$ and $\Pi_{2,0}$ are as follows

$$\Pi_{1,0} = 0.6064667 \qquad (13)$$
$$\Pi_{2,0} = 402.4574 \qquad (14)$$

Firstly we analyze the Eqs.(13) and (14). Because the value of $\Pi_{1,0}$ is far smaller than the $\Pi_{2,0}$. When the value of weighted number W_2 equals 1, by using searching method, it is vary difficult to make the values of Π, Π_1, Π_2 all smaller than the values of Π_0, $\Pi_{1,0}$, $\Pi_{2,0}$ given by the existing linear wave solution, while in order to make the values of Π, Π_1, Π_2 all smaller than the values of Π_0, $\Pi_{1,0}$, $\Pi_{2,0}$ given by the existing solution, we can refer to the method presented in (Fu, 1995b), i.e., to adjust the weighted number W_2. For example, the value of W_2 can be chosen

according to the method presented in (Fu, 1990). It should be

$$\Pi_{1,0} = W_2 \Pi_{2,0} \tag{15}$$

$$W_2 = \Pi_{1,0} / \Pi_{2,0} = 1/663.6101 \tag{16}$$

Variational principle Eq.(6) will be changed into

$$\Pi = \Pi_1 + W_2 \Pi_2 = \min \tag{17}$$

Then the value of Π_0 given by the existing solution for the case of $P/\rho = 0$ reads

$$\Pi_0 = \Pi_{1,0} + W_2 \Pi_{2,0} = 1.212933 \tag{18}$$

Now we consider how to handle the wind pressure. Supposing that when there is no wave, the wind pressure is equal to P^*, the abscissa of wave peak is equal to X^*. For the sake of convenience, we suppose that along the wave profile the wind pressure distribution reads

$$P/\rho = \begin{cases} P^* & -L/2 \leqslant x \leqslant X^* \\ -P^* & X^* < x \leqslant L/2 \end{cases} \tag{19}$$

It should be noted that, for other forms of wind pressure distribution, the method of this paper is also applicable.

Firstly considering the case of wind pressure $P^* = 2.0\ m^2/s^2$, taking Eq.(12) as the initial values, instead of the results of Eqs.(14) and (18), the values of $\Pi_{1,0}$, $\Pi_{2,0}$ and Π_0 are as follows

$$\begin{cases} \Pi_{1,0} = 0.6064667 \\ \Pi_{2,0} = 1449.243 \\ \Pi_0 = \Pi_{1,0} + W_2 \Pi_{2,0} = 2.790344 \end{cases} \tag{20}$$

Now, taking Eq.(12) as initial values, by using the searching method with several cycles, the optimum solution will be given as follows

$$G_1 = 2.8448, \quad G_2 = 0.239085,$$

$$X_1 = 27.56843, \quad X_2 = 0.1103166, \tag{21}$$

$$Q = -0.08498359, \ \beta = 0.07924549$$

Substituting the optimum solution into Eq.(17) gives

$$\begin{cases} \Pi_1 = 0.2420313 \\ \Pi_2 = 309.2692 \\ \Pi = \Pi_1 + W_2 \Pi_2 = 0.7080718 \end{cases} \tag{22}$$

For the case of $P^*=2$, the comparison of profile between wind-driven slanting profile wave and existing linear wave is shown in Fig.1.

A comparison with Eq.(22) and Eq.(20) shows that the values of Π, Π_1 and Π_2 given by unified variational principle are only 25.4%, 39.9% and 21.3% respectively of Π_0, $\Pi_{1,0}$ and $\Pi_{2,0}$ given by the existing linear wave.

The results of wave profile y, horizontal velocity u and vertical velocity v at the profile give by the optimum solution Eq.(21) are also shown in Tables 1~3. The coordinates of peak are as follows

$$X^* = 1.058051, \quad Y^* = 2.854829 \tag{23}$$

It should be noted that according to Eq.(23), the wave height of the wind-driven slanting profile wave is equal to 5.709658. For the given value of 5.6896, there exists a error of 0.35%, but it is very small and can be omitted. For the case that the wave height has to be equal to the given value, then

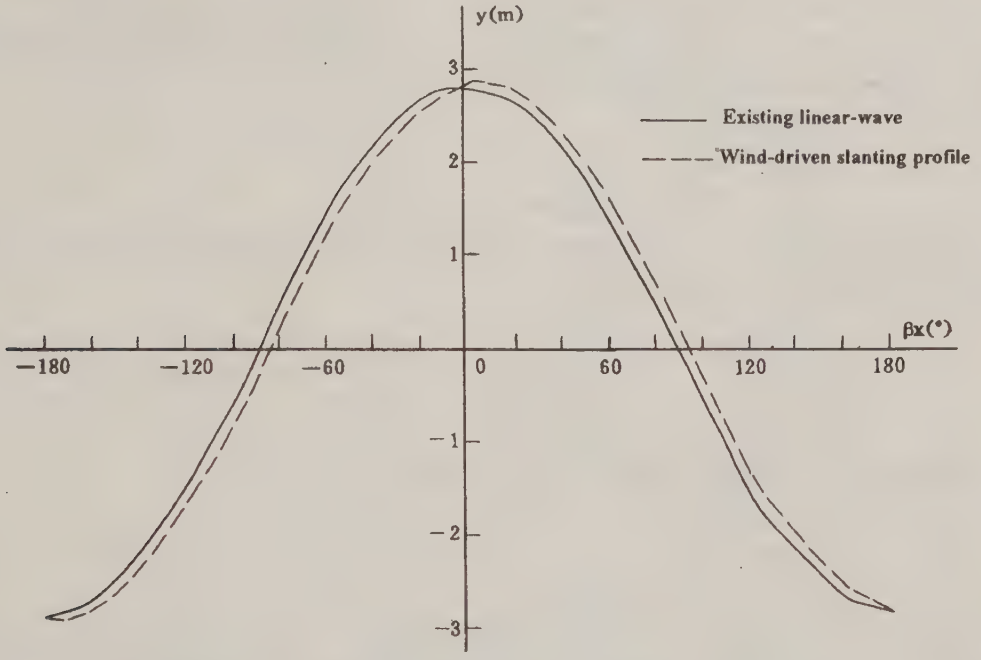

Fig.1 For P*=2 the comparison of profile between wind-driven slanting profile wave and existing linear wave

the method given in Reference (Fu, 1995c) can be used, i.e., changing the constraint condition Eq.(10) into the constraint condition of wave height.

Now considering the case of wind pressure $P^* = 1.0\ m^2/s^2$, taking Eq.(12) as the initial values, the values of $\Pi_{1,0}, \Pi_{2,0}$ and Π_0 are as follows

$$\begin{cases} \Pi_{1,0} = 0.6064667 \\ \Pi_{2,0} = 663.6852 \\ \Pi_0 = \Pi_{1,0} + W_2 \Pi_{2,0} = 1.60658 \end{cases} \quad (24)$$

Now, taking Eq.(12) as initial values, by using the searching method with several cycles, the optimum solution will be given as follows

$$G_1 = 2.8448, \quad G_2 = 0.11385,$$
$$X_1 = 27.54089, \quad X_2 = 0.110427, \quad (25)$$
$$Q = -0.08250834, \quad \beta = 0.07900846$$

Substituting the optimum solution into Eq.(17) gives

$$\begin{cases} \Pi_1 = 0.2300443 \\ \Pi_2 = 130.7515 \\ \Pi = \Pi_1 + W_2 \Pi_2 = 0.4270749 \end{cases} \quad (26)$$

A comparison with Eq.(26) and Eq.(24) shows that the values of Π, Π_1 and Π_2 given by unified variational principle are only 26.6%, 37.9% and 19.7% respectively of Π_0, $\Pi_{1,0}$ and $\Pi_{2,0}$ given by the existing linear wave.

The results of wave profile y, horizontal velocity u and vertical velocity v at the profile give by the optimum solution Eq.(25) are also shown in Tables 1~3. The coordinates of peak are as follows

$$X^* = 0.5062628\,, \quad Y^* = 2.847077 \tag{27}$$

Finally considering the case of wind pressure $P^* = 0.5\ m^2/s^2$, taking Eq.(12) as the initial values, the values of $\Pi_{1,0}, \Pi_{2,0}$ and Π_0 are as follows

$$\begin{cases} \Pi_{1,0} = 0.6064667 \\ \Pi_{2,0} = 467.5301 \\ \Pi_0 = \Pi_{1,0} + W_2 \Pi_{2,0} = 1.310992 \end{cases} \tag{28}$$

Now, taking Eq.(12) as initial values, by using the searching method with several cycles, the optimum solution will be given as follows

$$G_1 = 2.8448\,, \quad G_2 = 0.0495\,,$$

$$X_1 = 27.51337\,, \quad X_2 = 0.1226967, \tag{29}$$

$$Q = -0.08169143\,, \beta = 0.07900056$$

Substituting the optimum solution into Eq.(17) gives

$$\begin{cases} \Pi_1 = 0.2271152 \\ \Pi_2 = 88.78297 \\ \Pi = \Pi_1 + W_2 \Pi_2 = 0.360903 \end{cases} \tag{30}$$

A comparison with Eq.(30) and Eq.(28) shows that the values of Π, Π_1 and Π_2 given by unified variational principle are only 27.5%, 37.4% and 19.0% respectively of Π_0, $\Pi_{1,0}$ and $\Pi_{2,0}$ given by the existing linear wave.

The results of wave profile y, horizontal velocity u and vertical velocity v at the profile give by the optimum solution Eq.(29) are also shown in Table 1~3. The coordinates of peak are as follows

$$X^* = 0.2202315\,, \quad Y^* = 2.845231 \tag{31}$$

From the above-mentioned results we can see that the wind-driven slanting profile waves derived by UVPWGW are better than the original linear wave in the sense of the minimum error squares of the value of Π to satisfy KFSBC and DFSBC.

4 The level of satisfying boundary conditions

The values of R_1 and R_2 defined by Eqs.(9) and (10) really represent the level of satisfying boundary conditions and their accurate values should be equal to zero.

In the case of P^*=2, the values of R_1 and R_2 calculated by the existing linear wave and the wind-driven slanting profile wave given by united variational principle are shown in Table 4 and 5.

From Tables 4 and 5 we can see that the maximum error of this paper for satisfying the boundary condition is far less than the existing solution.

5 Conclusion

This paper discusses the method for deriving the wind-driven slanting profile waves by using UVPWGW based on the linear wave. The examples given in this paper show that the wind-driven slanting profile waves derived by UVPWGW are better than the original linear wave in the sense of the minimum error squares to satisfy kinematic free surface boundary condition and dynamic free

Table 4 Results of the values of R_1

β x(°)	accurate value	existing solution for P*=2	present solution Eq.(21) for P*=2
-180	0	0	-0.019
-160	0	0.046	0.028
-140	0	0.075	0.065
-120	0	0.073	0.082
-100	0	0.033	0.075
-80	0	-0.040	0.046
-60	0	-0.125	0.008
-40	0	-0.179	-0.019
-20	0	-0.141	-0.014
0	0	0	0.020
20	0	0.141	0.054
40	0	0.179	0.056
60	0	0.125	0.022
80	0	0.040	-0.028
100	0	-0.033	-0.073
120	0	-0.073	-0.096
140	0	-0.075	-0.091
160	0	-0.046	-0.063
180	0	0	-0.019

Table 5 Results of the values of R_2

β x(°)	accurate value	existing solution for P*=2	present solution Eq.(21) for P*=2
-180	0	-0.405	3.165
-160	0	0.027	1.434
-140	0	1.293	0.247
-120	0	3.201	-0.207
-100	0	5.245	-0.013
-80	0	6.676	0.448
-60	0	6.911	0.751
-40	0	6.008	0.809
-20	0	4.763	1.021
0	0	-3.807	1.993
20	0	-3.238	-4.007
40	0	-1.992	-1.384
60	0	-1.089	0.982
80	0	-1.324	2.283
100	0	-2.755	2.223
120	0	-4.799	1.044
140	0	-6.707	-0.776
160	0	-7.973	-2.826
180	0	-8.405	-4.835

surface boundary condition. Therefore this method is promising in solving the problems of wave theory.

References

Fu Yuhua, 1989a,A new way for deriving solitary wave,*China Ocean Engineering,* Vol.3, No.3

Fu Yuhua, 1989b,A new way for deriving high order Stokes Waves, *China Ocean Engineering,* Vol.3, No.1

Fu Yuhua,1989c, New solution for problem advance of Mercurys perihelion, Acta Astronomica Sinica, 30(4).(in Chinese)

Fu Yuhua,1990, A new way for solving boundary-layer equations,*China Offshore Oil and Gas(Engineering)*,2(6).(in Chinese)

Fu Yuhua, 1992a,Unified water gravity wave theory and improved linear wave,*China Ocean Engineering*, Vol.6, No. 1

Fu Yuhua, 1992b,The application of optimum MWR in mechanics, physics and astronomy, in:*The advance and engineering application of the method of weighted residuals.* Wuhan University of Technology Press.(in Chinese)

Fu Yuhua, 1994a,A unified variational principle of fluid mechanics and application on solitary subdomain or point,*China Ocean Engineering,*Vol.8, No.2

Fu Yuhua, 1994b,Single point method for solving thin plate problem, 94 international meeting on petroleum and petrochemistry,Beijing (in Chinese)

Fu Yuhua, 1995a, The application of MWR in oceanology and astronomy, The fourth national conference on the method of weighted residuals, Guangzhou (in Chinese)

Fu Yuhua, 1995b, Analyzed and fractal single point method for solving hydraulic problems in ocean engineering, International meeting on petroleum engineering, SPE 29986, Nov., Beijing

Fu Yuhua, 1995c, Optimum fifth order Stokes wave theory,*Acta Oceanologica Sinica,* Vol.14, No.1

Fu Yuhua, 1998, Stream function wave derived from unified variational principle of water gravity wave, *Marine Science Bulletin,*Vol.17, No.2 (in Chinese)

Mei Jiangzhong, 1984, Water wave dynamics, Science Press, Beijing (in Chinese)

Comparison of Some Features of the Subtropical Countercurrent, the North Equatorial Current and the North Equatorial Countercurrent in the Northwest Pacific Ocean

Sun Xiangping
(*First Institute of Oceanography, SOA, Qingdao*)

Abstract Based on the data of temperature and salinity of the 137° E section in the winters and summers from 1967 to 1995, the geo-strophic current of the section is calculated and analyzed, and the drifting tracks of the satellite tracking drift buoy distributed on the 144° E section are also analyzed. In light of the surface dynamic height distribution in the CSK atlas, this paper compares some features of the Subtropical Countercurrent, the North Equatorial Current and the North Equatorial Countercurrent. The main results are as follows:

1. The Subtropical Countercurrent, the North Equatorial Current and the North Equatorial Countercurrent are not simple single currents, but have two branches or more. One of the common features of the three currents mentioned above is "multi-branching" of the current.

2. The zonal distribution of the flow velocity structure, the alternate and intermittent occurrence of the eastward and westward flows, with a shallower flow layer and belonging to the surface flow or subsurface flow are another common feature of these three currents.

3. On multi-year mean, for the flow velocity of the three currents, the strongest is the North Equatorial Countercurrent, the second is the North Equatorial Current and the weakest is the Subtropical Countercurrent. The flow capacity, however, is different, the North Equatorial Current having the maximum flow capacity, the Subtropical Countercurrent the minimum, and the North Equatorial Countercurrent the medium. From the two seasons of winter and summer, the flow velocities of the three currents in summer are all faster than those in winter. But the flow capacity is somewhat different, both the Subtropical Countercurrent and the North Equatorial Current are characterized by strong flow capacity in summer and weak flow capacity in winter while the situation of the North Equatorial Countercurrent turns out contrary to that of the former two.

4. In winter, "the source" of the Subtropical Countercurrent seems to be in the sea area near a "warm ridge" center of "the Subtropical Ridge" to the east of the Bass Strait and Taiwan.

5. In winter, the drifting tracks of the satellite tracking drift buoy basically reflect the paths of the North Equatorial Current and the North Equatorial Countercurrent. Since the subtropical countercurrent zone is an area with frequent vortex, it is difficult for the drifting buoy tracks to reflect the path of the Subtropical Countercurrent.

Keywords the Subtropical Countercurrent, the North Equatorial Current, the North Equatorial Countercurrent, multi-branching, zonal structure

The monitoring of the 137° E section in the northwest Pacific Ocean, made by Japanese eteorological Department, has been going on for 30 years. The section is from 34° N in the north to

1° S in the south, traversing the six main latitudinal currents of Kuroshio, the Kuroshio Countercurrent, the Subtropical Countercurrent, the North Equatorial Current, the North Equatorial Countercurrent and the South Equatorial Current. Fig.1 shows the geographic location of the 137° E section and the sketch model and the example of the six latitudinal currents.

There has been so much discussion about the Subtropical Countercurrent, the North Equatorial Current and the North Equatorial Countercurrent, and extensive study and great progress have been made for the characteristics, forming mechanism and cause of the currents. However, there has been no report about comparing the generality and individuality of the above-mentioned three currents on a fixed section by using the data of the same period, the same method and the dynamic reference surface, nor results of the dynamic height of the partial sea level proved by drifting buoy tracks. This paper will attempt to study this aspect.

Taking the Tropic of Cancer in the northwest Pacific Ocean (23° 27′ N) as a boundary, extending 5.5 latitudes to north and south respectively, the latitudinal area from 18° N to 29° N is regarded as the Subtropical Countercurrent area. On the 137° E section the eastward flow whose velocity is $\geqslant$10cm/s[1] is thought to be Subtropical Countercurrent in this area. The North Equatorial Current is between 5° and 25° N and the North Equatorial Countercurrent between 3° and 10° N. Considering the calculating error of the Geostrophic Current, it is not suitable for the flow velocity to be taken too small, so the westward and eastward flows with flow velocity of $\geqslant$ 10cm/s are tentatively regarded as the flow velocity of the North Equatorial Current and the North Equatorial Countercurrent.

On the basis of the data of temperature and salinity of the 137° E section, the Geostrophic Current is calculated and analyzed, taking 1 000m as the dynamic reference surface. The number of years set for the data: the winter (referring to Jan. in those years) ranges from 1967 to 1995 and the summer (referring to July in those years, individually June) is from 1972 to 1995. (Surveying was not made in 1994). The source of the data is from The Results of Marine Meteorological and Oceanographic Observation, No.41～86, Japan Meteorological Agency. In addition. the following data is cited: (1) Data Report of Hydrographic Observations, Series of WESTPAC, Japan Hydrographic Department[2];(2) WESTPAC Atlas, Japan Hydrographic Department[3];(3) CSR Atlas, Japan Oceanographic Data Center[4]; (4) US-PRC Joint Cruises plots of drifting buoy tracks. It is something rare that the features of the three currents through the 137° E section are analyzed by using the data of such long time series. As the data observed is confined to the two seasons of winter and summer, this paper only analyzes the variations of the three currents and their average status in winter and summer.

1 Flow path

Having limited space, we here take 6 continuous years as an example (Fig.2). The most obvious feature in Fig.2 is that the Subtropical Countercurrent, the North Equatorial Current and the North Equatorial Countercurrent are in some years one current respectively and 2～3 branches, or even 4～5 branches in some other years. Each of them is never a simple single current, but with two and more branches.

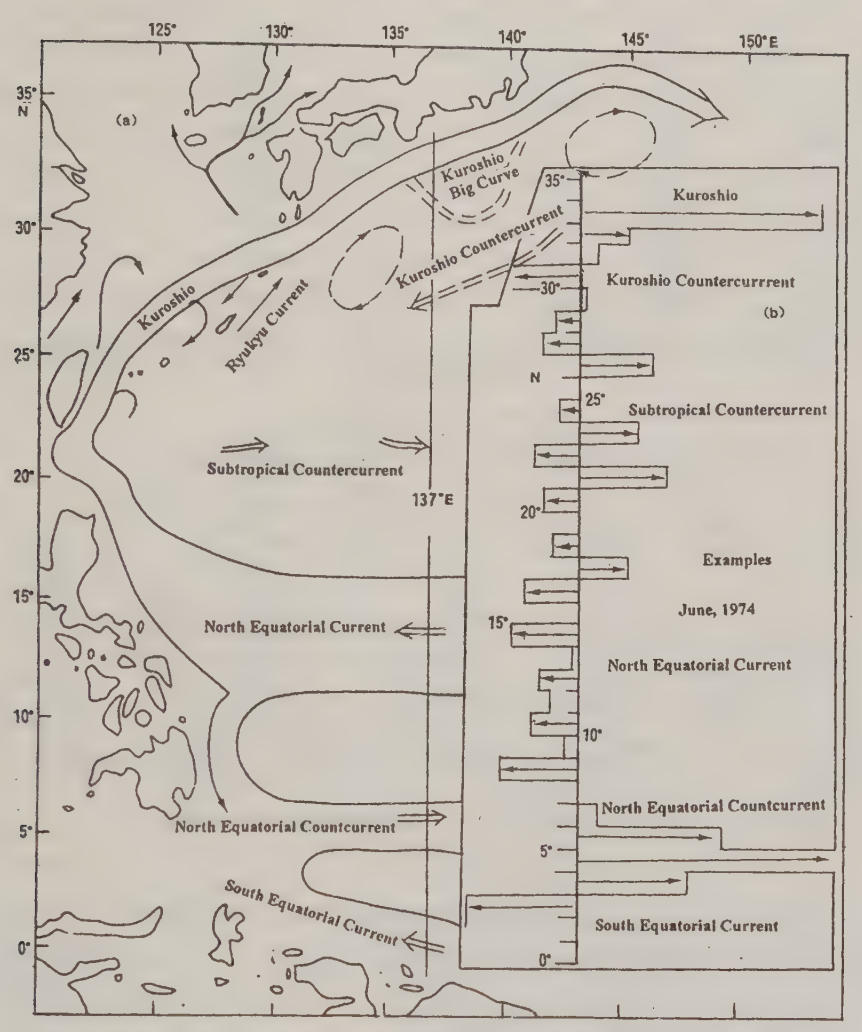

Fig.1 The geographic location and the sketch model(a) and the example(b) of the six latitudinal currents, from reference[5]

Through analyzing the flow velocity structure of the section and zonal distribution of the currents each year, it is known that the three currents occur on this section at the same time every year, but the zonal range where they occur is not fixed each year. The statistical results (Table 1) show that in winter there are four forms of 1, 2, 3 and 4 branches for the Subtropical Countercurrent, five forms of 1, 2, 3, 4 and 5 branches for the North Equatorial Current and 3 forms of 1, 2 and 3 branches for the North Equatorial Countercurrent. In summer there are two forms of 2 and 3 branches for the Subtropical Countercurrent, five forms of 2, 3 ,4, 5 and 6 branches for the North Equatorial Current and three forms of 1, 2 and 3 branches for the North Equatorial Countercurrent. The occurrence year, number and frequency of different forms of the three currents are respectively listed in Table 1. In

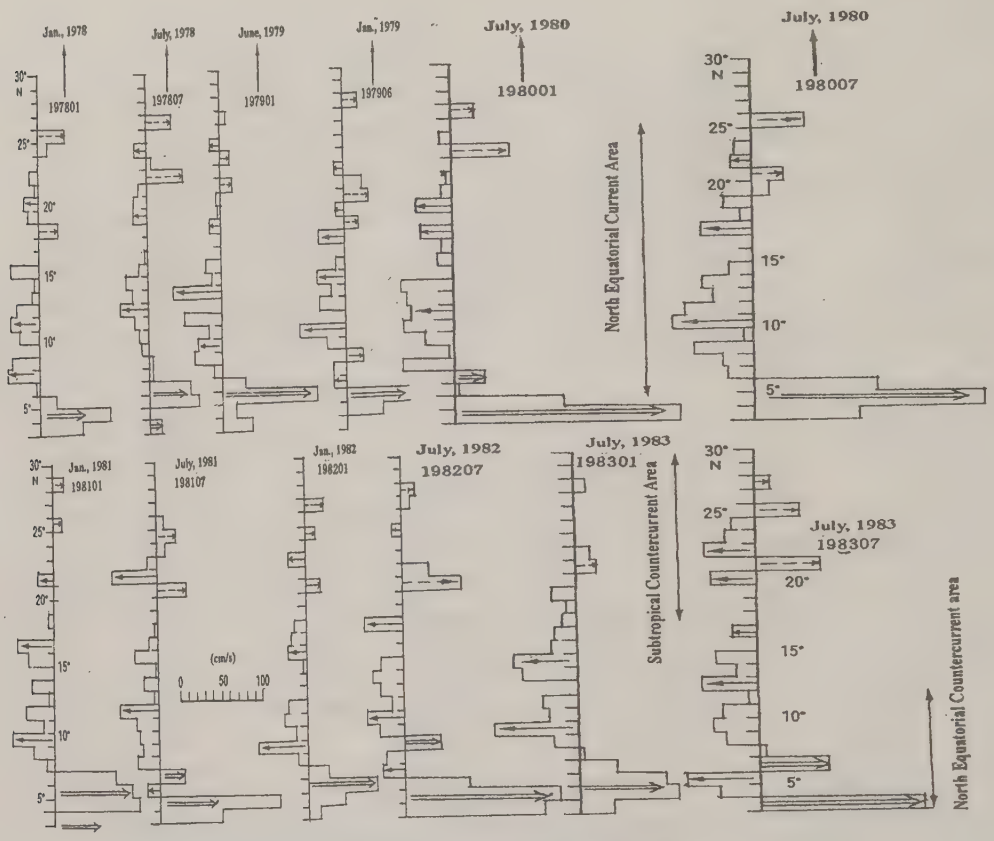

Fig.2 Three zonal currents on the 137° E section from 1978 to 1983

Table 1 the occurrence rates in winter and summer respectively refer to the percentage of occurrence number (once a year) of some form during 29 and 23 years. The table indicates that in winter the most frequent occurrence for the Subtropical Countercurrent is the form of 2 branches, taking up 55. 2%; the 3 branch form for the North Equatorial Current, 41.4% and the single branch for the North Equatorial Countercurrent, 69.0%. In summer it is still dominated by the 2 branch form for the Subtropical Countercurrent, about 60.9%. The North Equatorial Current is somewhat different, with a more scattered occurrence rate, relatively it is dominated by 2 forms of 5 and 4 branches and the sum of these two takes up 60.9%. For the North Equatorial Countercurrent the 2 branch form is a little more, taking up 52.2%. The statistical results in Table 1 reflect an important fact that the multi-branching is a common feature of the Subtropical Countercurrent, the North Equatorial Current and the North Equatorial Countercurrent, i. e, the generality of the three currents. The difference lies in that the branching forms for the three currents are not the same, nor are the occurrence years and rates of the branching forms.

Are the Subtropical Countercurrent, the North Equatorial Current and the North Equatorial Countercurrent evenly distributed or concentrated in some range on latitude? For this reason, statistics have been made of the occurrence of the three currents on each latitude of this section (Fig. 3). In Fig.3, the two areas where the occurrence number is most and sub-most are taken as the zonal

area of occurrence of the Subtropical Countercurrent, and ≥66.6% and ≥ 50% of occurrence rate as those of the North Equatorial Current and the North Equatorial Countercurrent. The figure shows that in winter the Subtropical Countercurrent mostly occurs in the two zones of 22° ~23° N and 26° ~27° N, the North Equatorial Current is mostly between 8° and 15° N and the North Equatorial Countercurrent between 3° and 7° N. In summer the Subtropical Countercurrent mostly appears in the two zones of 21° ~22° N and 24° ~27° N, the North Equatorial Current mostly occurs between 7° ~15° N and 22° ~23° N and the North Equatorial Countercurrent mostly between 3° and 6° N. The general trend is that the zonal area of the Subtropical Countercurrent occurrence in winter is narrower and that in summer is wider, and for the southern boundary of the Subtropical Countercurrent and the North Equatorial Current as well as the northern boundary of the North Equatorial Countercurrent, that in summer moves one latitude southward comparing with that in winter.

Table 1 Statistics of occurrence status of the three currents on the 137° E section

Name	Branch Number	Year Number of times	Year	Occurrence rate(%)
Winter(Jan.)				
Subtropical Countercurrent	1	2	1983,1995	6.9
	2	16	1968,1969,1971,1971,1972,1973,1978,1979,1980,	55.2
	3	10	1967,1975,1976,1977,1982,1984,1986,1989,1992,	34.5
	4	1	1974	3.4
North Equatorial Current	1	1	1975	3.4
	2	3	1983,1988,1992	
	3	12	1969,1971,1972,1974,1977,1978,1980,1981,1982,	41.4
	4	9	1968,1970,1976,1979,1984,1985,1989,1991,1993	31.0
	5	4	1967,1973,1987,1990	13.8
North Equatorial Countercurrent	1	20	1968,1969,1970,1971,1972,1973,1974,1975,1976,	69.0
	2	8	1967,1981,1984,1987,1989,1990,1992,1995	27.6
	3	1	1993	3.4
Summer (July)				
Subtropical Countercurrent	2	14	1972,1975,1976,1977,1978,1980,1981,1982,1984,	60.9
	3	9	1973,1974,1979,1983,1986,1987,1991,1992,1995	39.1
North Equatorial Current	2	2	1977,1989	8.7
	3	4	1978,1980,1981,1990	17.4
	4	6	1976,1982,1985,1986,1988,1995	26.1
	5	8	1972,1974,1975,1983,1984,1987,1992,1993	34.8
	6	3	1973,1979,1991	13.0
North Equatorial Countercurrent	1	10	1973,1974,1975,1976,1980,1984,1986,1989,1991,	43.5
	2	12	1972,1978,1979,1981,1982,1983,1985,1987,1988,	52.2
	3	1	1997	4.3

2 Flow velocity and flow amount

According to the flow velocity structure of the three currents (Fig.4), the interannual difference of flow velocity and flow amount (Fig.5) and the multi-year mean statistical results (Table 2), it is found that there are something in common and differences in the flow velocity structure and flow

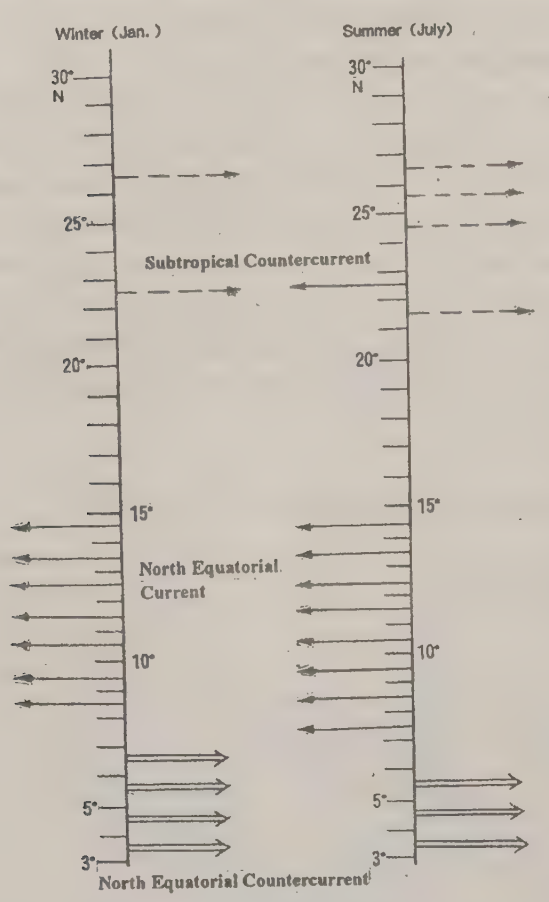

Fig.3 The zonal area of more concentrated occurrence of the three currents on the 137° E section

amount variation of the Subtropical Countercurrent, the North Equatorial Current and the North Equatorial Countercurrent. (1) On the section the flow velocity distribution for the three currents is all in a belted structure, the eastward and westward flows are mostly crisscross distributed, that is to say, there is a westward (eastward) flow between two eastward (westward) flows, with a distinct boundary. (2) For the flow velocity distribution it is dominated by the single nucleus structure, the double nucleuses for a small number or the individuals (Fig. 4 II b III b), of which there even occur three nucleuses in the North Equatorial Current (Fig.4 II a). (3) The distribution pattern of the equal flow velocity line is dominated by U-shape or V-shape, individually by W-shape. The surface flow velocity is large and the flow range is also wide, the flow velocity gradually decreases and flow width narrows with increasing of the water depth, and 10 cm/s of the equal flow velocity line is generally in 1 ~ 100m or 200m and individually about 400m. This indicates that the flow layers of the three currents are shallower, mainly occurring in surface and subsurface, and all of them belong to the surface current or subsurface current. (4) As far as the multi-year mean flow velocity is concerned (Table 2), the strongest is the North Equatorial Countercurrent, the second is the North Equatorial Current and the weakest is the Subtropical Countercurrent. From the flow velocities in winter and summer, the three currents are characterized by being strong in summer and weak in winter[8]. (5) For the multi-year mean flow amount (Table 2, Fig.5), that of the North Equatorial Current is the largest, that of the North Equatorial Countercurrent is the second and that of the Subtropical Countercurrent the minimum. In winter and summer the flow amounts of the Subtropical Countercurrent and the North Equatorial are characterized by being strong in summer and weak in winter, and that of the North Equatorial Countercurrent turns out contrary, with a trend of being strong in winter and weak in summer. This may be due to the fact that the flow width of the North Equatorial Countercurrent is narrower in summer than that in winter (Fig.3). (6) The flow velocities of the three currents are unevenly distributed with latitudes, and there are the strong flow zone and the weak flow zone (the figure omitting). The strong flow zones of the North Equatorial Current and the North Equatorial

Countercurrent are corresponding with the more occurrence section, that is to say, the flow velocity in the more occurrence section is stronger and that in the more occurrence section is stronger and that in the less occurrence section is weaker. The Subtropical Countercurrent, however, is different, the more occurrence section not identical to the strong flow zone. (7) From the interannual variation range of flow velocity and flow amount (Table 2), it can be seen that the variation range of the North Equatorial Current is minimum, more stable, and the maximum value is 1.4～1.7 times as much as the minimum value while that of the Subtropical Countercurrent and the North Equatorial Countercurrent is different, with a larger range of the interannual variation. The maximum value is 2.8～10.2 times as much as the minimum value, especially in summer when the maximum value is 8～10 times as much as the minimum value, with a more significant variation range, showing that there is a poor stability for the flow velocity and flow amount of the Subtropical Countercurrent and the North Equatorial Countercurrent. Relatively, the variation range in winter is smaller than that in summer.

Table 2 The multi-year mean results of the flow velocity and flow amount of the three currents on the 137° E section

Name of Currents	Winter(Jan.)					
	Flow velocity(cm/s)			Flow amount(10m/s)		
	Average	Variation range	Deference multiple between the Maximum and the Minimum	Average	Variation range	Deference multiple between the Maximm and the Minimum
Subtropical Countercurrent	17.1	10.3~33.0	3.2	14.3	4.7~24.7	5.2
North Equatorial Current	23.8	19.0~31.4	1.6	94.3	76.8~113.7	1.4
North Equatorial Current	54.3	29.4~82.5	2.8	53.9	25.4~85.9	3.3
	Summer(July)					
Subtropical Countercurrent	23.8	7.0~38.0	5.4	22.9	3.3~34.5	10.2
North Equatorial Current	26.2	19.5~35.0	1.7	109.2	86.4~126.1	1.4
North Equatorial Current	61.3	15.7~129.0	8.2	46.3	11.2~75.5	6.7

The statistical number of years for the numerals in the table:29 years for winter (1967～1995) and 23 years for summer (1972～1995, no surveying in 1994)

In Fig.5, E_1,E_2……E_8 marked under the curve of flow amount variation year by year indicate the number of El Nino taking place from 1967 to 1995, of which the flow amount variation of the North Equatorial Countercurrent in winter seems to be related to El Nino events. The rest 6 events all occurred during the increasing period of the flow amount of the North Equatorial Countercurrent except E_5 and E_6.

What is mentioned above is the multi-year variation and multi-year mean status of the flow path, flow velocity and flow amount of the three currents on a section. The following discusses the plane distribution of the three currents.

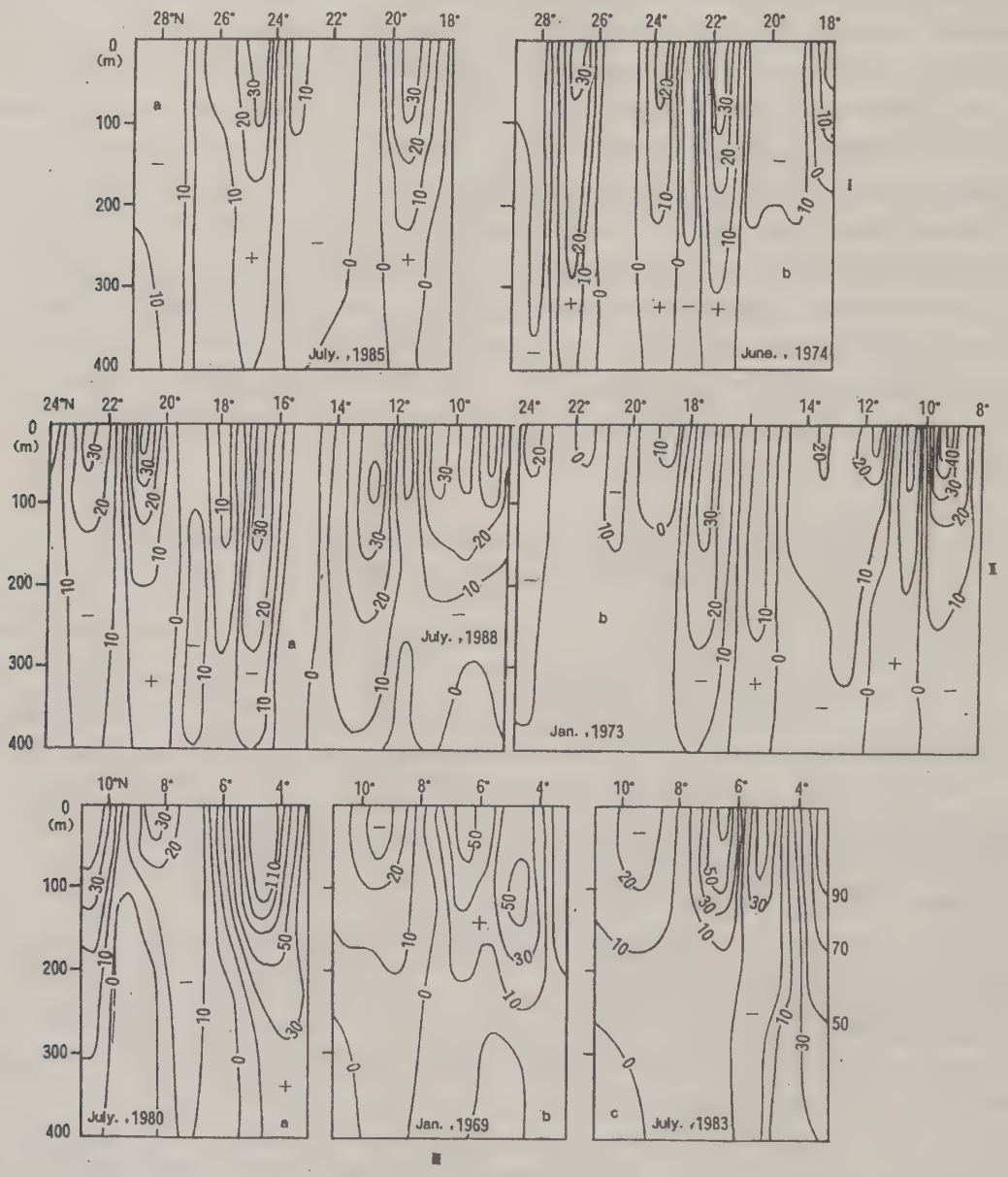

Fig.4 The flow velocity structure of the three currents on the 137° E section

I .the Subtropical Countercurrent; II . the North Equatorial Current III. the North Equatorial Countercurrent

3 The surface dynamic height distribution in winter

The survey during Dec.1965~Mar.,1966 and Jan. ~ Mar.,1967 was the most extensive one with the most complete data obtained in the winter cruises of CSK. Its corresponding surface dynamic height distribution is shown as in Fig.6.

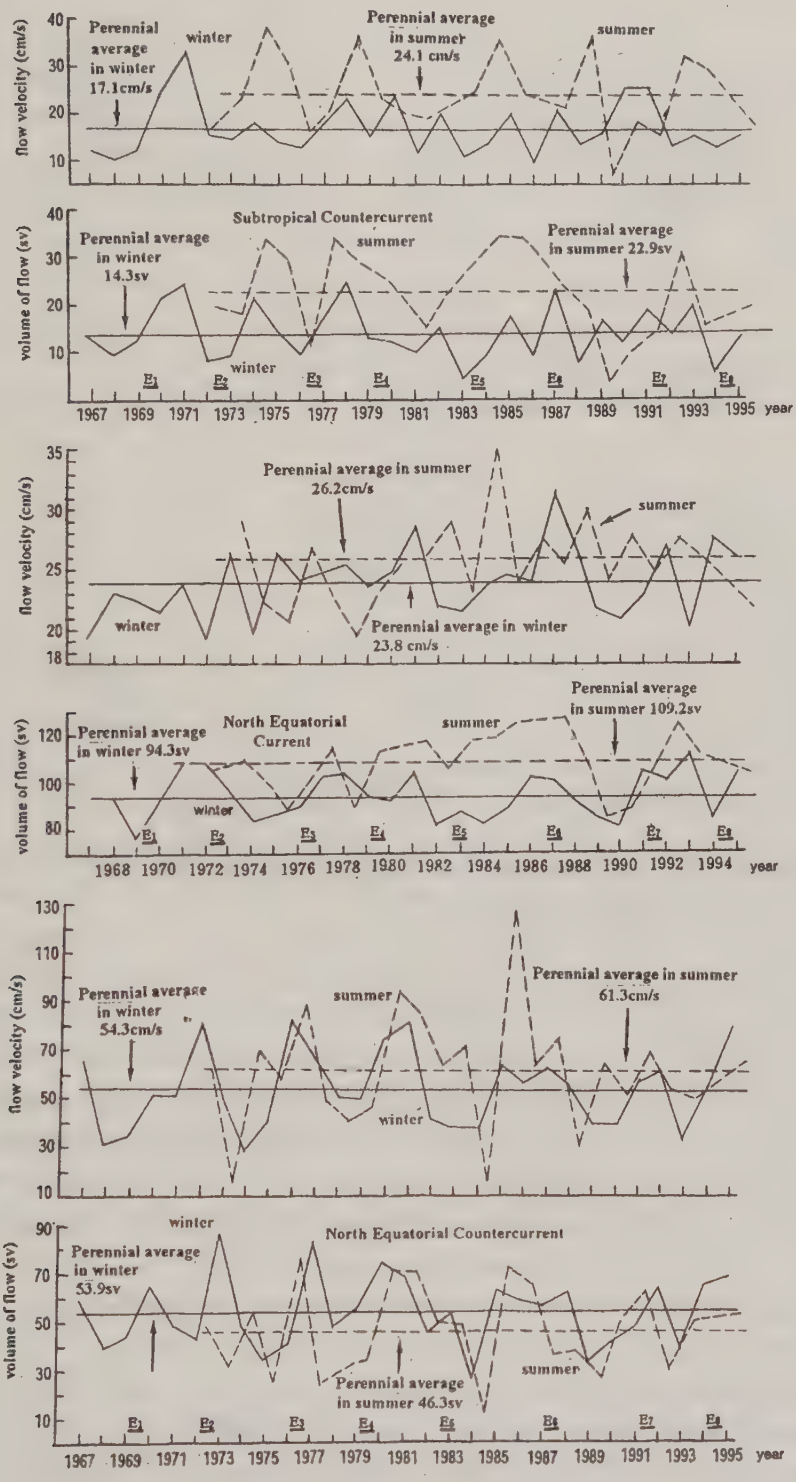
flow velocity (cm/s)
Perennial average in winter 17.1cm/s
winter
Perennial average in summer 24.1 cm/s
summer
volume of flow (sv)
Subtropical Countercurrent
Perennial average in winter 14.3sv
summer
Perennial average in summer 22.9sv
winter
E1 E2 E3 E4 E5 E6 E7 E8
1967 1969 1971 1973 1975 1977 1979 1981 1983 1985 1987 1989 1991 1993 1995 year
flow velocity (cm/s)
Perennial average in summer 26.2cm/s
summer
winter
Perennial average in winter 23.8 cm/s
volume of flow (sv)
North Equatorial Current
Perennial average in winter 94.3sv
summer
Perennial average in summer 109.2sv
winter
E1 E2 E3 E4 E5 E6 E7 E8
1968 1970 1972 1974 1976 1978 1980 1982 1984 1986 1988 1990 1992 1994 year
flow velocity (cm/s)
Perennial average in winter 54.3cm/s
summer
Perennial average in summer 61.3cm/s
winter
volume of flow (sv)
winter
North Equatorial Countercurrent
Perennial average in winter 53.9sv
summer
Perennial average in summer 46.3sv
E1 E2 E3 E4 E5 E6 E7 E8
1967 1969 1971 1973 1975 1977 1979 1981 1983 1985 1987 1989 1991 1993 1995 year

Fig.5 The flow velocity and volume variation of the three currents on the 137° E section year by year, from references[5,6]

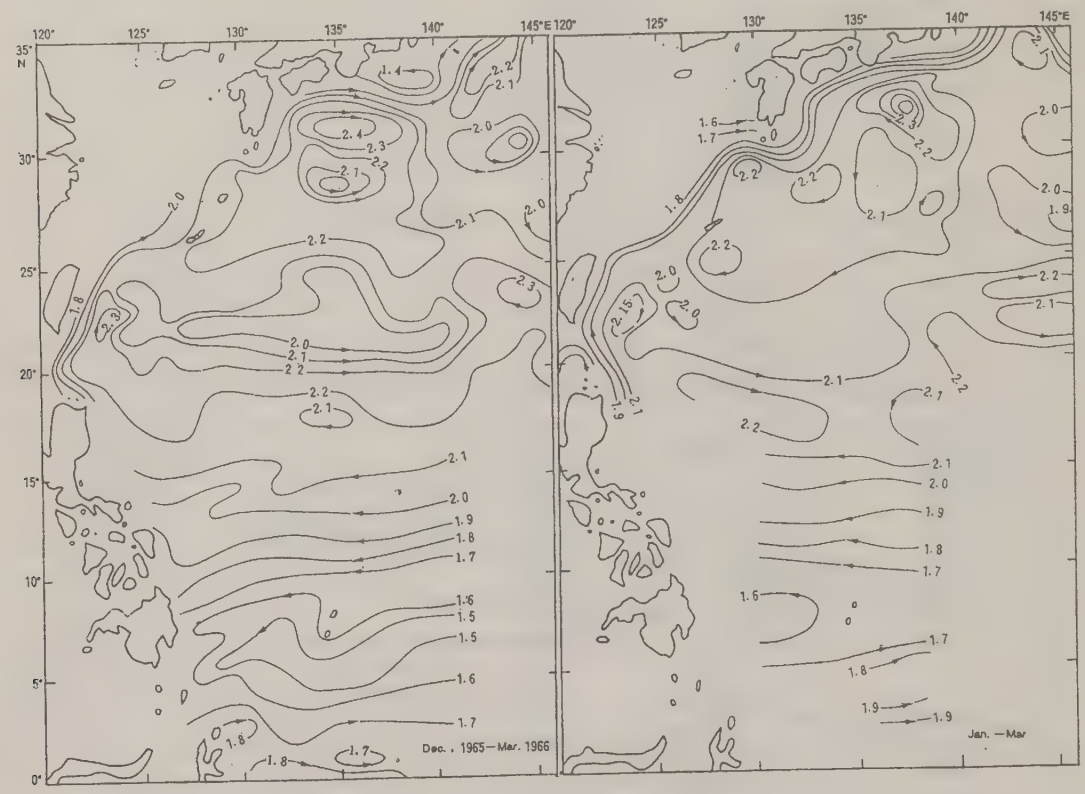

Fig.6 The surface dynamic height distribution of the northwest Pacific Ocean in winter (0/1 000 × 10^2h Pa), from reference[4]

Firstly, let us discuss the current status in the winter from 1965 to 1966 (Fig.6a). Between 0° and 7° N the geo-potential lines from 1.7 to 1.8 indicate that the sea water flows from east to west, down to the south along the Mindanao Island and turns eastward again near 2° ~5° N. They are the North Equatorial Current and the North Equatorial Countercurrent. Among them the geo-potential lines from 1.5 to 1.6 make up an almost closed ellipse-shaped anti-clockwise circulation which is the location of the cold eddy of Mindanao. Near 17° ~12° N, the North Equatorial Current from east to west starts to branch off. The geo-potential line of 1.9 up to the north together with that of 2.0 ~ 2.1, flows northward along the east coasts of Samar Island and Luzon Island, forming the "origin" of the west boundary current. The geo-potential lines of 1.7 ~ 1.8 down to the south become the Mindanao Current. The geo-potential line of 2.2 near 18° ~20° N can be regarded as the northern boundary of the North Equatorial Current, It basically flows from east to west in the latitudinal direction, turns to north to the east of the Bashi Chan. And after completing a clockwise revolving to the east of Taiwan Province, it flows eastward along the latitudinal line of 20° N. This latitudinal belted and ellipsoidal circulation (cutting across 30 longitudes) consisting of 2.2 geo-potential line is just the subtropical ridge whose central location is to the east of Taiwan and near 23° N, 145° E, with over 2.3 geo-potential of the central value. To the north of "the subtropical ridge" an anti-clock triangular circulation is constituted by the geo-potential lines of 2.0

~2.1, that is, "the subtropical trough". At the Bash Chan. and the east coast of Taiwan, the close geo-potential lines of 1.8~2.1 represent Kuroshio which flows to the north along the east coast of Taiwan and enters the East China Sea. After flowing out of the Tokara Strait, it flows to the south coast of Japan. The geo-potential lines of 2.3~2.4 in the southern Kuroshio to the south of Honshu forms a clockwise ellipsoidal circulation, that is, the Kuroshio ridge. Therefore, the structure of the subtropical eddy in this winter is characterized by two ridges (the Kuroshio ridge and the subtropical ridge) and a trough (the subtropical trough). The eastward flow along 2.2 geo-potential line on the southern side of the subtropical trough and the northern side of the subtropical ridge is just the Subtropical Countercurrent.

Now let us discuss the current condition from Jan. to Mar., 1967 (Fig.6b). The surface dynamic height of the sea area to the south of 15° N is approximately similar to that in Fig 6a, but that to the north of 15° N is different. The subtropical ridge consisting of 2.2 geo-potential line occurs between 16° ~18° N and 127° ~135° E, and its location is slightly to the south than the subtropical ridge in Fig 6a, its scope and strength are smaller and weaker than that in Fig. 6a. Although the Kuroshio ridge in this winter is still located to the south of Honshu, its location is somewhat to the east. Similarly, the 2.1 geo-potential line near 15° N can be regarded as the northern boundary of the North Equatorial Countercurrent. When the sea water flows to the offshore area to the northeast of the Luzon Island, 2.1 geo-potential line turns to the east and flows eastward along the latitudinal line of 19° N after a clockwise revolution. And it can be regarded as the Subtropical Countercurrent, which is similar to that in Fig.6a. Consequently, the current states in the two winters show that the origin of the Subtropical Countercurrent in winter seems to be in the sea area near a warm ridge center of the subtropical ridge at the east mouth of the Bash Chan. and to the east of Taiwan. The biggest difference for the current states in this two winters is the location of the "subtropical trough". "The subtropical trough" in Fig. 6b, unlike that in Fig. 6a, is not located between 127° ~141° E and 21° ~25° N, but near 25° ~27° N to the east of 142° E, that is to say, moving eastward and to the north, with a slight decrease in strength. As a whole, the structural pattern of the Subtropical Current eddy from Jan. to Mar., 1967 is still "two ridges and a trough" but is not as typical as that in the winter from 1965 to 1966(9). Nevertheless, the current states in the two winters reflect an important phenomenon, that is to say, in winter the Subtropical Countercurrent flows eastward along the margins of the warm ridge and cold trough and its origin is the same as that of Kuroshio, a branch of the eastern current to the east of Taiwan.

4 The drifting tracks of buoys in winter

In order to explain the current state in winter shown by surface height distribution map, it is proved by the drifting tracks of satellite tracking drift buoys. Although the observational times for the two kinds of data are unsynchronous and unmatched, it is still of some help to understanding the trend qualitatively. Fig.7 shows the classification results of 30 buoys on the 144° E section put by the Hydrographic Department, Maritime Safety Agency, Japan in Feb. ~ Mar. from 1984 to 1996, which is classified by the features and trends of the drifting tracks of buoys[7]. Three of the 5 track types (the westward type, northwestward type and southwestward type, the sum of these three takes

up 70% of the statistical buoy number) reflect the tracks of the North Equatorial Current and the North Equatorial Countercurrent. Now let us take the westward track type as example.

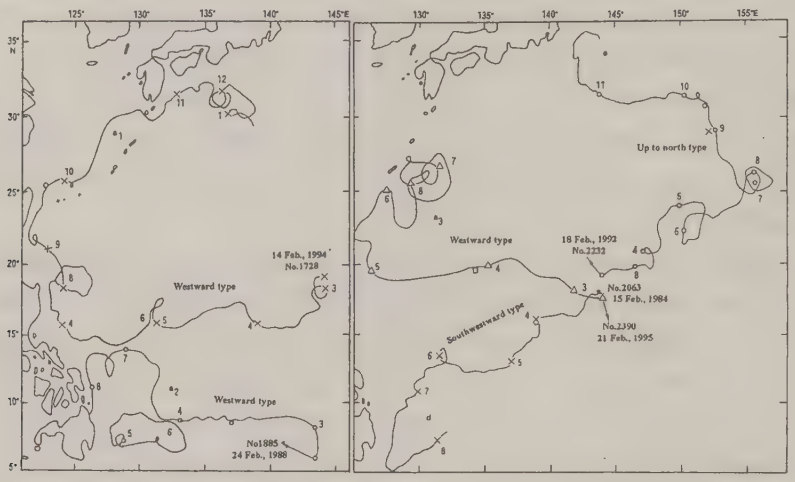

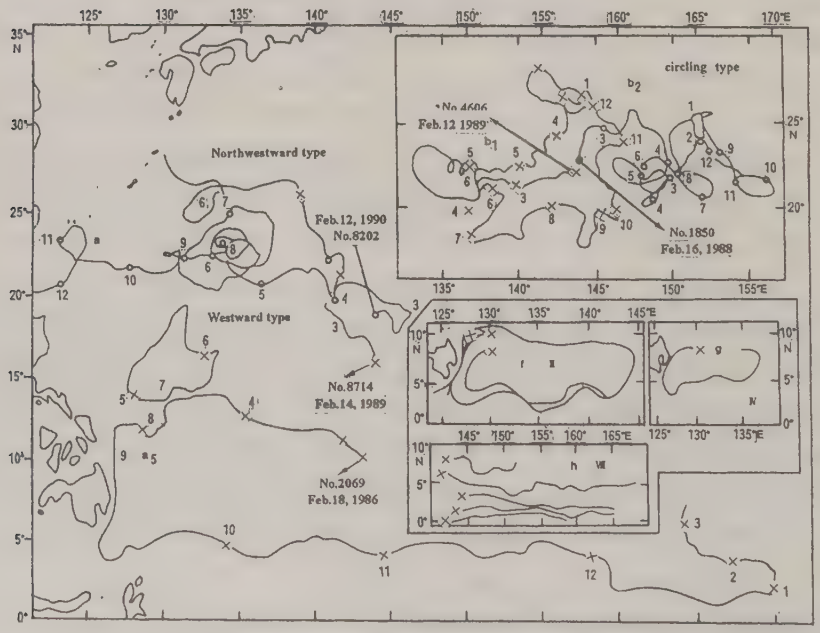

Fig.7 The types of drifting tracks of satellite tracking drift buoy[7]

The figures by X,O,△ indicate month, the number is the buoy number and the figures by the number show the time of putting the buoys.

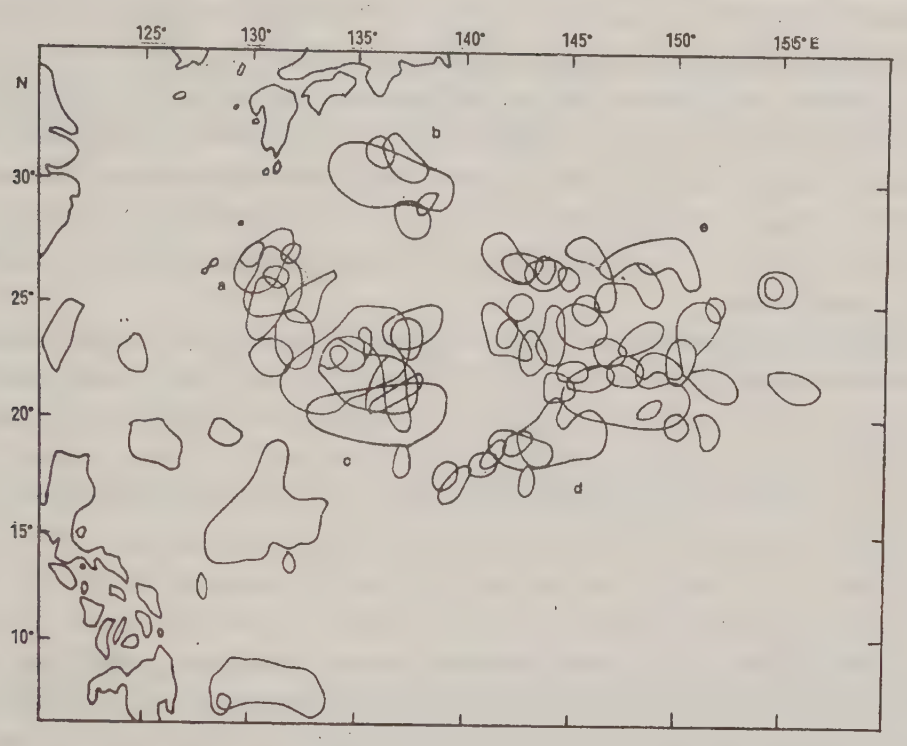

Fig.8 The eddies in the Subtropical Countercurrent area in the northwest Pacific Ocean

The westward type refers to the drifting track from the putting point to the disappearing point, from east to west, drifting to the west coast of the Pacific Ocean, then continuing to drift in branches. This type makes up 50% of the number of buoys put and most of the putting points are to the south of 20° N. For the drifting times of the buoys: 63 days for the shortest, 389 days for the longest and 253.7 days on an average. The type of the westward tracks can be approximately divided into five cases:

(1) After being put into the sea, the buoys basically drift westward in a straight line. Arriving at the offshore area to the northeast of Luzon, they turn to the north or the northeast, continuing to drift to Okinawa and then to the east of Amami Oshima, where they circle and disappear (Fig.7a). This track is approximately similar to the current state of the origin of the Subtropical Countercurrent, reflecting the partial path of the origin of the Subtropical Countercurrent.

(2) After being put into the sea the buoys move around for a small circle, then drifting westward to near the east coast of Luzon. Some circle again there, then drifting up to the north, some up to the north directly, entering the East China Sea along the east coast of Taiwan, then continuing to drift northeastward along the continental slope of the East China Sea. Returning to the Pacific Ocean through the Tokara Strait, the buoys drift to the south of Honshu along the south coast of Japan, circling and disappearing. The track reflects the origin of the North Equatorial Current and Kuroshio and the path of Kuroshio.

(3) After being put into the sea the buoys drift westward in a straight line, circling as an ellipsoid in the sea area to the east of Mindanao, then drifting northwestward, turning to the south

and disappearing near the east coast of Samar (Fig.7a). This track reflects the path of the North Equatorial Current the Mindanao cold eddy and the Mindanao Current.

(4) After being put into the sea the buoys drift westward slightly by north, to the northeast of the Samar Island, circling a large circle and then turning to the southwest, down to the south along the east coasts of Samar Island and Mindanao Island, turning eastward again near 4° N and drifting to near 165° E along the latitudinal lines of 4° ~5° N and disappearing (the track in Fig.7 a5). This track reflects the path of the North Equatorial Current, the Mindanao Current and the North Equatorial Countercurrent.

(5) After being put into the sea the buoys drift westward by north in a broken line, circling for months in the sea area of 20° ~25° N and 132° ~137° E, then drifting westward to the east of Taiwan, circling again and continuing to drift southwestward, entering the South China Sea through the Bashi Chan. (Fig.7 a4). This track still reflects the current state of the North Equatorial Current.

As to the drifting tracks of the buoys between 0° and 10° N (Fig.7f, g, h), they indicate three facts: (1) Influenced by the North Equatorial Current, the buoys drift westward after being put into the sea, turning down to the south the east coast of Mindanao, reflecting the path of the Mindanao Current. (2) The track from the putting point to the disappearing point of the buoys forms an anti-clockwise closed elliptical curve in the sea area to the east of Mindanao, which just reflects the location and scope of the Mindanao cold eddy. (3) The buoys put near 141° E, 142° E and 144° E basically drift eastward along the latitudinal lines, with a straight and stable track, reflecting the path of the North Equatorial Countercurrent.

The circling tracks of the drifting buoys (as Fig.7b1, b2) imply that there exists an unstable eddy. If the circling part of 30 drifting buoy tracks mentioned above is mapped on a map by points (Fig.8), it can be found that the Subtropical Countercurrent area is just one with frequent eddies, thus covering up the flowing of the Subtropical Countercurrent, and it is hard for the drifting tracks of the buoys to reflect the path of the Subtropical Countercurrent.

References

1. Japan Meteorological Agency, 1968~1997.*The Results of Marine Meteorological and Oceanographical Observation*, No.41~No.86
2. Maritime Safety Agency, 1986~1997.*Data Report of Hydrographic Observations*, Series of WESTPAC, Vol.1~Vol.12
3. Hydrographic Department, Maritime Safety Agency, 1987,1992,1996. WESTPAC Atlas.Vol.1~Vol.3
4. Japan oceanographic Data Center, 1967,1968,1969,1970. CSK Atlas. Vol.1~Vol.4
5. Gu Yuhe, Sun Xiangping and Xu lanying, 1999, The Subtropical Countercurrent on the 137癈 longitudinal section, *Acta Oceanologca Sinica*, to be published
6. Gu Yuhe, Sun Xiangping and Xu lanying, 1999. The Norht Equatorial Current and the North Equatorial Countercurrent on 137° E section, *Studia Marina Sinica*, to be published.
7. Gu Yuhe, Sun Xiangping and Xu lanying, 1997, Variation of salinity and analysis of buoy tracks on 144° E longitudinal section,*Oceanology and Linmology*, to be published
8. Gu Yuhe, 1996, The lantitudinal volume transport of current on 137° E section in the northwest Pacific Ocean, *Oceanology and Linmology* 27 (1): 79-85 .
9. Guan Bingxian Circulation structure and its variation in the sea area to east of Taiwan and Philippines in winter, *Oc eanology and linmology* 20 (5); 393~400.

The Basic Features of Sea Surface Wind of each Season in the Shore and Offshore Areas of Qingdao

Diao Xuexian
(*Qingdao Marine Forecast Station, SOA, Qingdao*)

Abstract Based on sorting out the data, this paper makes statistics and analysis for the basic features of sea surface wind of each season in the shore and offshore areas of Qingdao and calculates the maximum wind velocity once in a century.

Keywords sea surface wind, wind direction, mean wind velocity, maximum wind velocity

Introduction

Wind is a factor indicating the horizontal movement of air and a vector with direction and rate. The wind direction is expressed by 16 directions and the wind velocity by m/s (or by wind scale). The wind direction and wind velocity in an area are dependent on the environmental factors such as air press field and topography. Wind is closely related to the production and life of people. As far as the sea area is concerned, the departments such as those of marine communications and transportation, marine and aquaculture must understand wind variations. And the wind factors need to be grasped in the marine development, port construction and other activities. Serious disasters can be caused if the wind velocity is too large. Qingdao is one of the most important harbor cities in China, it is of the climatic and practical significance to understand the wind features in the sea area near Qingdao. Although there are some documents about the wind around Qingdao, most of them pay particular attention to the wind on land. This paper discusses the basic features of sea surface wind of each season in the shore and offshore areas of Qingdao.

Data and Treatment of Data

According to the geographic location, two marine stations, Xiaomaidao and Qianliyan are chosen represent the shore and offshore areas of Qingdao respectively (hereafter called "this area" for short), and the wind data of the two stations from 1965 to 1994 and the data such as the historical weather maps made by Beijing Meteorological Center are taken as an analysis basis. Through examining the wind data, it is necessary to make the treatment of homogeneity and comparison.

1 Homogeneity treatment

Before 1970, Virta Wind Pressure Plate was used as a wind measurement instrument, then it was

replaced by the wind direction wind gauge connected electrically. Because of the function defect of Virta Wind Pressure Plate, the indication tended to be on the high side when the wind velocity is large. Therefore there did not exist homogeneity in the wind velocity record before and after 1970. For the sake of caution the corrections of the instrument errors are made by an empirical formula for the wind velocity record $Va \geqslant 17.0$m/s (corresponding to $\geqslant 8$ scale) before 1970, then a more homogeneous wind velocity value V_b can be extracted[1]

$$V_b = 0.89V_a + 0.33 \quad (1)$$

2 Comparison treatment

The heights above sea level for the wind measurement instruments at the two stations of Xiaomaidao and Qianliyan are respectively close to 40m and 80m, with about 40m difference. As the wind velocity in a friction layer increases with height there is no comparison between the wind velocity records of the two stations because of the height difference. For this reason, correcting the formula by height

$$V_z = V_{z_1} \frac{\lg z - \lg z_0}{\lg z_1 - \lg z_0} \quad (2)$$

where z is a calculated height, 10m above sea level in this paper, z_1 represents the height of the instrument above sea level and z_0 is coarseness of sea level, 0.03m. Making the height correction, the sample data of sea surface V_z 10m above sea level are obtained.

Mean Wind Velocity and Its Plane Distribution

The mean wind velocity represents the general state of air pressure gradient in a given area, by the formula

$$\overline{V_i} = \frac{1}{N}\sum_{i=1}^{N} V_i \quad (3)$$

where, V_i is the mean velocity of the representative month*(i)* in each season over the years and N is number of years.

The mean velocity of different seasons (the representative month) can be obtained by the formula(3); the maximum is in winter, 4.6~6.8m/s, the minimum in summer, 3.1~4.8m/s and the medium is in the two seasons, spring and autumn. The mean velocity of different seasons in the offshore area is obviously larger than that in the shore area, especially in winter (Fig.1). The wind velocity distribution, therefore gradually disappears from the shore to the offshore. The wind velocity line is approximately identical to the coastline and the closest in winter(Fig.2).

The air pressure fields in this area are different in each season. In winter the continental high pressure is strong, with a large air pressure gradient and a strong air current. Influenced by the subtropical high pressure in summer, the air pressure gradient is more even and the air current is subsiding. This area is located at a place where sea and land meet. Because of the different heat characters of the sea and land, sea surface is a heat source in winter and a cold source in summer, and the horizontal difference of temperature can result in the air pressure gradient force. In winter

when the air current moves from the land to the sea surface, it speeds up. In summer when the air current moves from the land to the sea surface, it is easy for it to decrease. At the same time the sea surface is smoother than the land, so that the frictional force decreases. And the air current over the sea is larger than that over the land under the same air pressure gradient. Because of the combined action of the factors mentioned above, the mean wind velocity in this area is characterized by the obvious seasonal difference and regional difference.

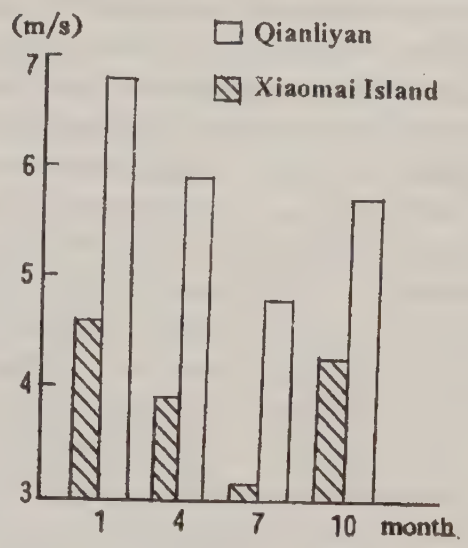

Fig.1 A histogram showing the mean wind velocity in each season(the representative month)

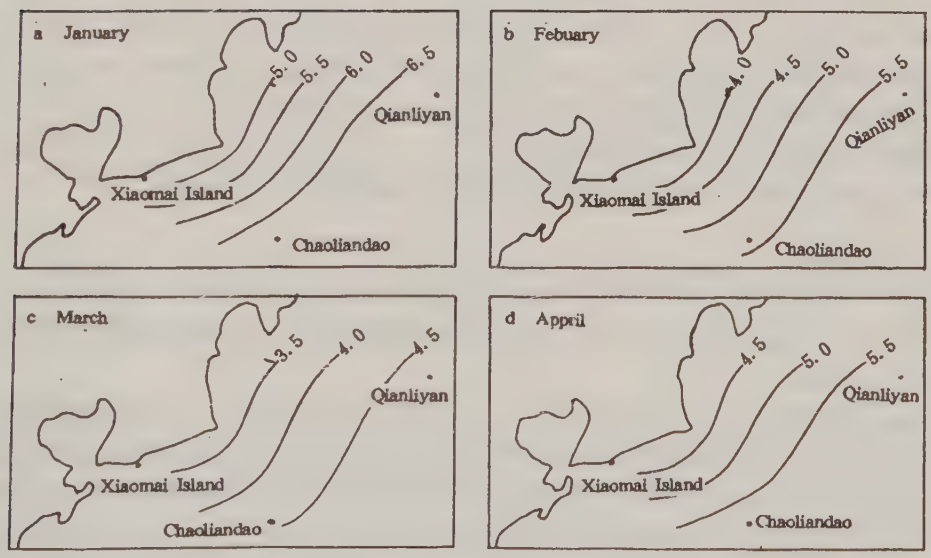

Fig.2 A map showing the mean wind velocity distribution of each season(the representative month)

Wind Direction Frequency, Mean Wind Velocity in Each Direction and Its Composition

1. Wind direction frequency

Wind direction frequency shows the distribution state of wind in each direction. Since the

continental high pressure frequently moves about in winter, the wind by north is prevailing in this area. In the shore area the leading wind direction is in WNN~N direction and its total frequency is up to 59%. In the offshore area the leading wind direction is in WNN~NE direction, with 62% of total frequency. The most wind directions in these two area are in NW direction, 24% and 18% respectively. As the subtropical high pressure is to north and to west in summer, the wind by south is prevailing in the offshore area, dominated by the wind in SSE-SSW direction. Its frequency is totally up to 61% and the most wind directions are in S direction, with 33% of frequency. In the shore area the leading wind direction is in ENE~SSE direction, with 60% of total frequency, and the most wind directions are in E direction, with 19% of frequency . In the transition season of spring and autumn there occur alternately the wind by north and the wind by south. However, in spring there is a more frequency of the wind by south in the offshore area and the wind by east in the shore area, and the frequencies of the wind in each direction are more scatter in autumn.(Fig.3).

As far as the whole year is concerned, influenced by monsoons in this area, the frequency of the monsoon direction in the offshore area is distinct, basically corresponding to the wind direction frequency in the adjacent offshore area[3]. And affected by the factors such as topography, the regional feature in the shore area is rather notable. The coastline of Qingdao bordering on the Huanghai Sea trends approximately in EW direction (see Fig.2) and there are the Lao Mountain and its rest ranges along the coast. On the bottom when the air current in SE~S direction moves toward the coast, it meets with obstruction and is easy to turn to east. This makes the frequency of wind by south in each season in the shore area less than that in the offshore area and the frequency of wind by east is more than that in the offshore area, even in summer(see Fig.3). There is totally 52% SE~S direction frequency in the offshore area, 28% more than as that in the shore area. And in the shore area ENE~ESE direction frequency is 42%,33% more than that in the offshore area.

2 Mean velocity in different directions

The mean velocity in different directions is represented by the formula

$$\overline{V_{ij}} = \frac{1}{N}\sum_{i=1}^{N} V_{ij} \qquad (4)$$

where V_{ij} is the mean velocity in different directions (j) of the representative month (i) in each season over years.

From formula(4) we can obtain the mean velocity V_{ij} in different directions in each season (the representative month) in this area. In winter the wind by north is stronger and in the offshore area the mean wind velocity in WNW~NNE direction is over 7.0m/s, the maximum being that in WNW direction the mean wind velocity up to 8.1m/s. In the shore area the mean wind velocity in NNW~NW direction is over 5.5m/s, the maximum being that in NNW direction, up to 5.7m/s. In summer the wind is relatively gentle, in the offshore area, the maximum, up to 5.8m/s, is that in NE direction, next in S direction, up to 5.6m/s. In the shore area both WNW and NNW direction winds are the maximum, all up to 4.3m/s. In the two seasons of spring and autumn wind directions change a lot, dominated by the wind by north (Fig.3).

In this area the mean wind velocity each direction has the regional features. As the shore area is located along the southern coast of the Huanghai Sea, the air current by north decreases through the continental friction, and herefore the wind by north decreases. When the air current moves from the

shore area to the sea, it gradually increases with decreasing of friction. In the first half of the year the air current by north increases rapidly because of the energy replenishd by increasing temperature and humidity on the sea, resulting in the larger wind by north in the offshore area, especially in winter. In the offshore area when the air current by south moves to the coast, its energy will decrease with obstruction or changing direction. Therefore, in the shore area the wind by south in each season is obviously smaller than that in the offshore area, and the wind by east is larger than that in the offshore area(Fig.3).

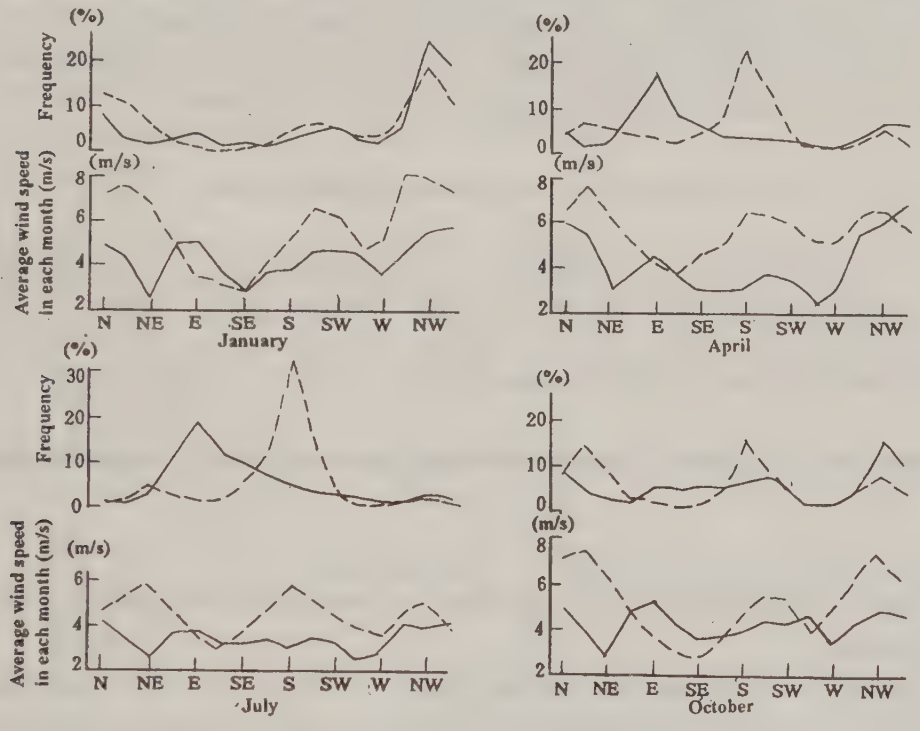

Fig.3 The wind direction frequency and the mean wind velocity curve in each direction in each season (——— Xiaomaidao, ····· Qianliyan)

3 Resultant Wind

Resultant wind is the moving distance of the air in a given area and it is used to determine the mean transport of the meteorological physical quantity(such as vapour, quantity of heat). As wind is a vector, the resultant wind can be calculated by the vector adding law to the mean wind velocity in each direction, by the formula

$$\left.\begin{aligned} V_x &= V\sin\theta \\ V_y &= V\cos\theta \end{aligned}\right\} \quad (5)$$

Projecting the mean wind velocity in each direction on the cartesian coordinate system, extracting Vx and Vy of$x$ and $y$axes respectively, and with the formula

$$\theta = \text{arctg} \frac{\sum V_x}{\sum V_y} \quad (6)$$

the resultant wind direction can be extracted and represented by 16 directions. with the formula

$$V_R = \frac{1}{N}\sqrt{(\Sigma V_x)^2 + (\Sigma V_y)^2} \quad (7)$$

the resultant wind velocity V_R can be extracted. From formulas (5)~(7) we can obtain the resultant wind of each season in this area, the resultant wind direction is corresponding to or close to the most wind directions, the maximum resultant wind velocity is in winter and the minimum in summer and that in the offshore area is larger than that in the shore area (Table 1).

Table 1 Resultant wind in each season(representative month)

	Winter(Jan.)		Spring(Apr.)		Summer(July)		Autumn(Oct.)	
	Direction	Velocity	Direction	Velocity	Direction	Velocity	Direction	Velocity
Xiaomaidao	NNW	4.6	NE	3.9	ESE	3.1	NNW	4.3
Qianliyan	NNW	6.8	S	5.9	S	4.8	N	5.7

The Maximum Wind Velocity, Number of Gale Days and Main Weather Types of Gale

1 The maximum wind velocity in each direction, the mean maximum wind velocity and number of gale days

The maximum wind velocity in each direction refers to the maximum value of wind velocities in each direction in a given period. If taking the mean to the maximum wind velocities $V(max)i$ of the representative month (i) in each season over the years, that is, using the formula

$$\overline{V}_{(\max)i} = \frac{1}{N}\sum_{i=1}^{N} V_{(\max)i} \quad (8)$$

to represent the mean maximum wind $\overline{V}_{(\max)i}$ velocities of the representative month in each season, the general conditions of the maximum wind velocity can be reflected.

Since the stronger air current by north in winter is down to south frequently, the gale days(the maximum wind velocity a day ≥ 8 scale) in the offshore area are up to 13.2 days and the mean monthly and the mean maximum wind velocity is up to 19.0m/s. The maximum wind velocities from WNW to NE directions are close to or over 20.2m/s, of which the maximum ones are in WNW and NE directions, up to 24.2m/s. Influenced by topography, the wind force in the shore area greatly decreases, with 5 days of gale monthly on the average. The mean maximum wind velocity is 15.7m/s, that from NW to N directions is >17.0m/s, of which the maximum is in NNW direction, up to 19.4m/s. The gale days in summer are only 1.2days for the shore area and 6.2 days for the offshore area, and the mean maximum wind velocity is minimum in the whole year, 14.0m/s and 16.6m/s respectively. When hit by the strong tropical cyclone, the wind force is rather strong. There occur 29.

2m/s of wind velocity in WNW direction in the offshore area and 28.2m/s in NNW direction in the shore area, both of which rank first in the maximum wind velocities in each season. In the transitional period of spring and autumn, the number of gale days ranks in the middle, about 7 and 9. 5 days in the shore and offshore areas respectively. In the offshore area the autumn wind is very strong, the mean maximum wind velocity is corresponding with that in winter, with 28.2m/s of the maximum wind velocity in WNW direction. In the shore area the strongest is spring wind, with 16. 4m/s of the mean maximum wind velocity and 25.5m/s of the maximum wind velocity in NNW direction. As the air current movement in the friction layer has displacement of different eddies, both wind direction and wind velocity are very unstable and irregular, so there occurs the phenomenon that the maximum wind velocity in the shore area is larger than that in the offshore area and the wind directions in the two areas are somewhat different (Fig.4 and 5).

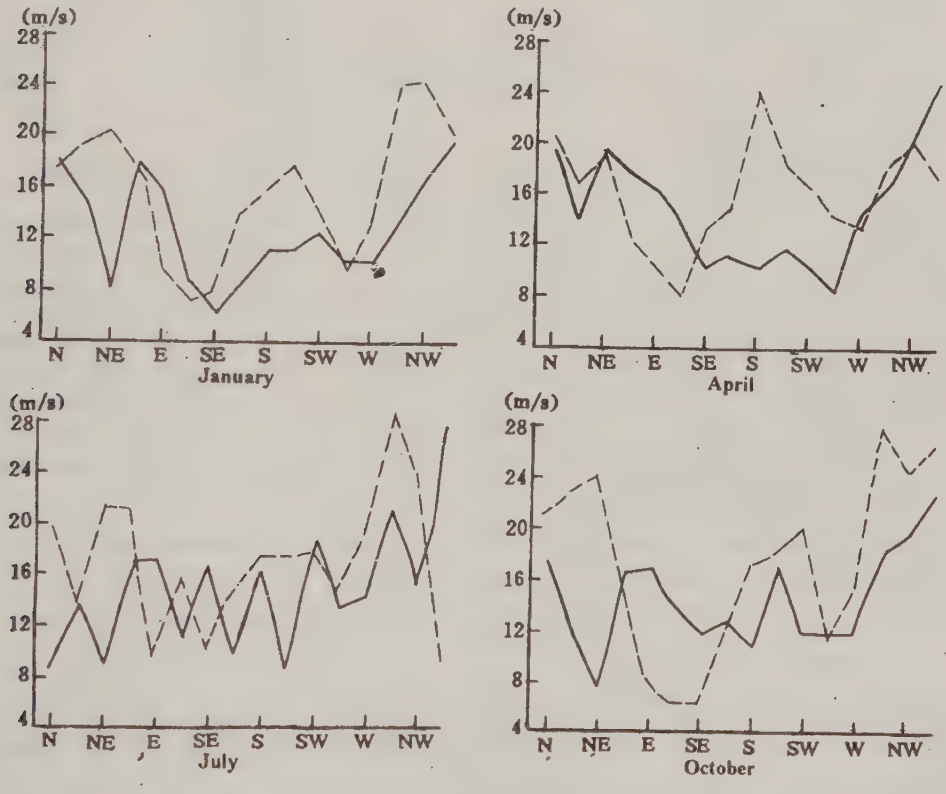

Fig.4 The curves of the maximum wind velocity in each direction in each season (the representative month) (———— Xiaomaidao ------ Qianliyan)

2 Main weather types of gales

Reconnoitering the historical weather maps, the weather situation forming a gale in this area can be induced into four main types.

(1) Cold front type

The powerful continental high pressure is the most important weather system influencing this

area in winter, early spring and the end of autumn. With 3~4 high pressure activities occurring monthly on an aveage, there occurs the gale by north where the air pressure gradient is large after the front, the wind force ranges mostly from scale 7~ 8 to scale 10 for the maximum. There are three paths, north northwest and west, for high pressure to invade into the area, mostly northwest path, about 6/10. The gale often lasts for 2~3days, sometimes the gale processes come one after another, lasting for 5~6 days, or even longer. In other seasons the strength of frontal surface decreases, the sea surface is colder comparing with the land surface, which plays a role of frontolysis, so that there occur a few gales.

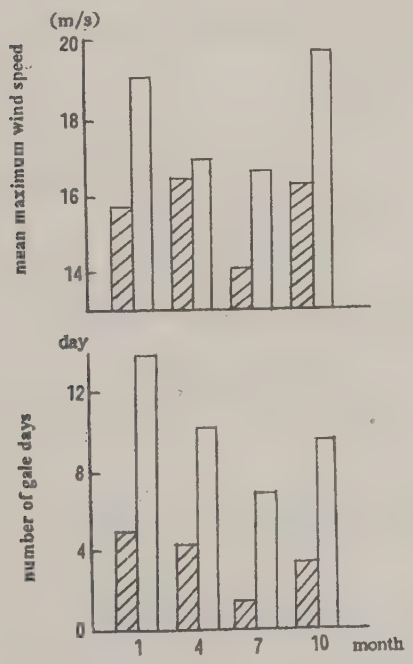

Fig.5 The histograms respectively showing the mean maximum wind velocity

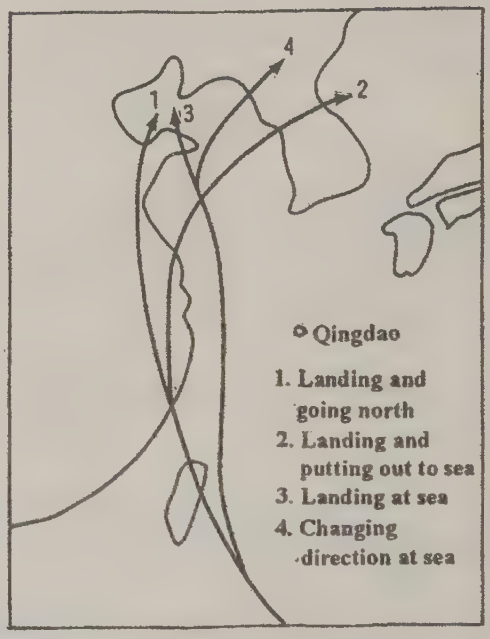

Fig.6 A sketch showing the strong tropical cyclone

(2) The back type of high pressure

It mostly occurs in spring. When the continental high pressure is down to south, if there develops a low pressure or a low pressure trough, coordination of these two systems can result in a situation of high in east and low in west. There often occurs the gale by south in this area, with about scale 7 of wind force in general, up to scale 9 for the maximum, or entering the sea of high pressure strengthens a little movement, if there occurs a low pressure which moves closely in its back part, resulting in a situation of high in south and low in north. There also occurs a gale by south, but the lasting time is shorter and the wind force mostly is not over scale 8.

(3) The temperate cyclone type

The temperate cyclone mainly refers to the cyclone of the Changjiang River and the Huaihe River and that of the Huanghe River and the Huaihe River, with a larger influence of the cyclone of the Changjiang River and the Huaihe River in the late spring and early summer. After forming in the Changjiang River valley and the Huaihe River valley, the cyclone rapidly moves to east. If the

cyclone meets with the high pressure down to south, resulting in a situation of high in north(west) and low in south(east), the gale by north of scale 7~8, or even a stronger one, can be produced between the two systems.

(4) The strong tropical cyclone type

It includes the tropical storm, the strong tropical storm and typhoon, mostly hitting this area in summer and early autumn, occurring mostly in the middle ten days of July and the first ten days of September, accounting for about 8/10 of those in the whole year. Its central paths are very complicated and roughly divided into 4 kinds of paths: landing up to north, landing out the sea, landing on the sea and changing direction in the offshore area(Fig.6), of which the first two paths account for about 7/10. In this area the wind force mostly ranges from scale 8 to 10, sometimes up scale 11. The maximum wind velocities in summer in the shore and offshore areas are produced under such circumstances, with a small frequency number of occurrence, less than 2 times yearly on the aveage.

The Maximum Wind Velocity Once in a Century

For the extreme value of the maximum wind velocity occurring possibly in a long period, usually its inherent law is revealed by using the long period distribution theory of the extreme value on the probability. At present there are many theoretical models commonly used for calculating the long period distribution of the extreme value. Gober matrix is calculated by the matrix method and Gober distribution is adopted by the least square method in this paper(As space is limited, the calculating method is omitted). Supposing the reoccurrence period is 100 years in this area, the maximum extreme value of wind velocity on the sea surface once in a century occurs in summer through calculation, 30m/s in the shore area and 32m/s in the offshore area. Both in spring in the shore area and in autumn in the offshore area are respectively close to its maximum extreme value(Table 2). The results calculated by the two methods mentioned above are very close, thus it can be concluded that the extreme value of the maximum wind velocity calculated is reliable. As to the extreme value of the maximum wind velocity in the different heights from the bottom to the sea surface, it can be calculated by the formula(2).

Table 2 The maximum wind velocities once in a century in different seasons(the representative month)

		Winter(Jan.)	Spring(Apr.)	Summer(July)	Autumn(Oct.)
Xiaomaidao	Matrix method	21.6	29.0	29.2	24.4
	Least square method	22.0	30.1	30.1	24.8
Qianliyan	Matrix method	30	27.3	31.2	30.9
	Least square method	30.8	20.0	32.2	31.2

Conclusions

1. For the wind direction in this area, in the offshore area the monsoonal wind direction is

obvious, the wind by north prevailing in winter and the wind by south in summer. The shore area is characterized by a distinctive regional style. The occurrence frequency of the wind by south in each season is less than that in the offshore area, that of the wind by east more than that in the offshore area, especially in the two seasons of spring and summer.

2. In this area the maximum mean wind velocity occurs in winter and the minimum in summer, and mostly the wind by north is relatively larger especially in winter. In general, its distribution gradually increases from the shore to the offshore, and only the wind by east in each season in the shore area is larger than that in the offshore area.

3. There occurs the gale of > scale 8 in the whole year, the most in winter and the least in summer and that in the offshore area is obviously more than that in the shore area. For the mean maximum wind velocity, that in autumn and winter is larger in the offshore area and dominated by spring and autumn in the shore area and the minimum is in summer for both areas. For the maximum wind velocity, the maximum is in summer and those in the shore and offshore areas are respectively up to 28.2m/s and 29.2m/s. The calculated values of the maximum wind velocity once in a century are up to 30m/s and 32m/s respectively.

References

Yan Junyue,etc., The offshore Climate of China, Science Press, 454~455,460~461,1993.

Sun Yiqing, Marine Engineering Environment Conditions and Its Load, The Publishing House of Shanghai Communications University 24,299~306,1989.

Lei Zongyou,etc., The Handbook of China Marine Environment, The Publishing House of Shanghai Communications University, 60~81,1988

Analysis on Features of Temperature and Salinity in the Northern Taiwan Straits During February-March, 1998

Hu Jianyu[1,2], Hong Huasheng[2], Chen Zhaozhang[1], He Zhigang[1], Hong Jiansheng[3] and Liang Hongxing[3]

1 (Institute of Subtropical Oceanography, Xiamen University, Xiamen 361005, China)
2 (College of Oceanography and Environmental Sciences, Xiamen University)
3 (Fujian Institute of Oceanology, Xiamen 361012, China)

Abstract The distributional features of temperature and salinity in the northern Taiwan Straits have been analyzed based on the CTD data during February-March, 1998. The characteristics of temperature and salinity are summarized as follows: (1) there exists a coastal water along the western coast of the Taiwan Straits, with low temperature and low salinity at the upper layer; (2) a high temperature and high salinity water tongue extends northeastward along the eastern coast of the Taiwan Strait.

Keywords: temperature, salinity, northern Taiwan Straits, distribution

A comprehensive oceanographic survey was conducted by R/V "Yanping 2" in the northern Taiwan Straits during February 20~March 8, 1998. During the investigation, there were 30 stations (locations shown in Fig.1) of CTD profile observations which were made by SBE19 Seacat Profiler of Sea Bird Electronics, INC. Based on the distributions of temperature and salinity at the surface, 10m, 20m, 30m, 50m and bottom layers, the distributional features of temperature and salinity at different layers have been analyzed in this paper.

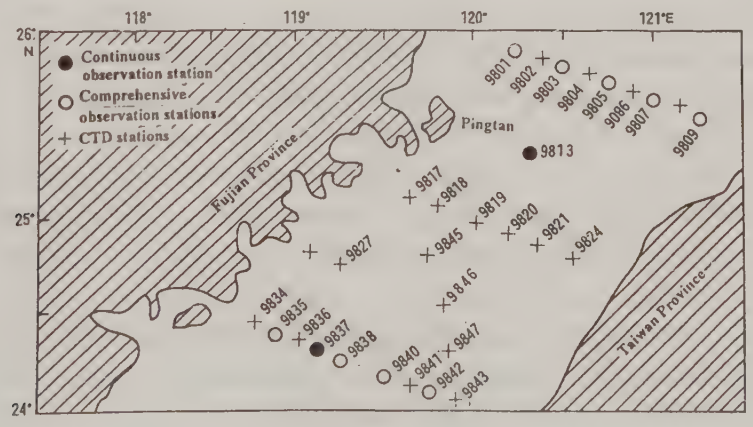

Fig.1 Locations of CTD stations during the the cruise (1998-02-20~03-08)

1 Distribution Features of Temperature and Salinity

1.1 Surface layer

Fig.2 shows that during the investigation, the surface temperature varies from 12℃ to 23℃, and there is a low temperature belt with the temperature less than 13℃ near the western coast of the Taiwan Straits, which extends southwestward and also splits a low temperature water tongue towards the middle Taiwan Straits to the southeast of Pingtan Island. However, a high temperature water tongue extends northeastward along the eastern coast of the Taiwan Straits, the front of which (i.e. the isothermal curve of 18℃) can reach 26° N. In addition, a high temperature water tongue can be seen to extend northwestward with its front reaching 119° E in the southern part of the studied area.

The distribution features of salinity at the surface layer are similar to those of temperature. A low salinity belt exists along the western coast of the Taiwan Straits, in which the salinity is less than 30, and extends southwestward while forming a low salinity water tongue towards the middle Taiwan Straits to the southeast of Pingtan Island. Meanwhile, a high salinity water tongue extends northeastward along the eastern coast of the Taiwan Straits with the front (i.e. the iso-salinity curve of 34.5) reaching 25.75° N. In the southern part of the studied area, a high salinity water tongue with the salinity greater than 34.5 extends northwestward and its front can reach 119° E.

In the middle Taiwan Straits, a front is formed between the water of low temperature and low salinity and the water of high temperature and high salinity, especially, the isothermal curves and iso-salinity curves are denser so that the strength of the front is greater in the southwestern part of the studied area. Furthermore, another relatively stronger front exists near Station 9803 in the northern Taiwan Straits. These fronts can also be seen clearly in the underway measurement of sea surface temperature and salinity during the cruise.

Generally speaking, the Minzhe Coastal Water flows southwestward along the western coast of the Taiwan Straits in winter and the water with the feature of low temperature and low salinity flows close to the coast. However, besides flowing southwestward along the coast, the Minzhe Coastal Water has a low temperature and low salinity branch which extends southeastward from the northern Taiwan Straits to the middle Taiwan Straits during this cruise. The high temperature and high salinity water along the eastern coast of the Taiwan Straits is considered to have come from the southern Taiwan Straits, and is also confirmed by the remote sensing images of the sea surface temperature which show that there is a high temperature water entering the South China Sea from the Luzon Strait and part of it flowing northeast-ward along the eastern coast of the Taiwan Straits during the cruise. Apparently, the high temperature and high salinity water can be regarded as the invaded water from Kuroshio because the salinity of the water, as shown in Fig.2, is greater than 34.0 and even greater than 34.5 in the southeastern part of the studied area.

The distributional features of temperature and salinity at the 10m and 20m layers are almost the same as those at the surface layer (shown in Fig.3 and 4). Obviously, it can be concluded that the thickness of the water mass is at least 20 meters in the studied area, which can also be confirmed by the vertical distributions of temperature and salinity at each station. During the cruise, the

temperature and salinity are almost homogeneous vertically from the surface layer to the 20m layer at each station.

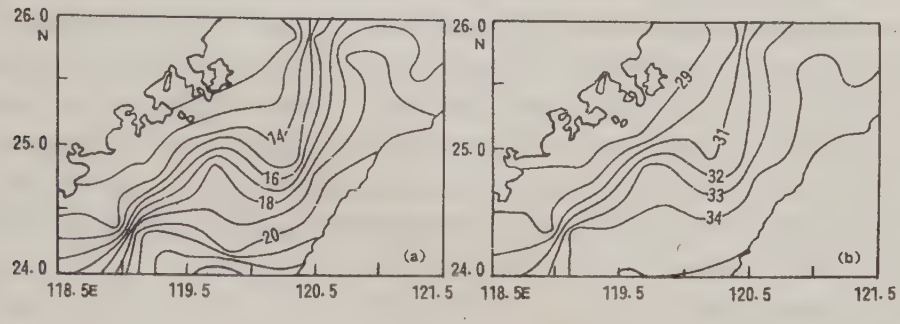

Fig.2 Distribution of temperature and salinity at the surface layer during the cruise (1998-02-20~03-08) (a)temperature (0m layer), (b) salinity (0m layer)

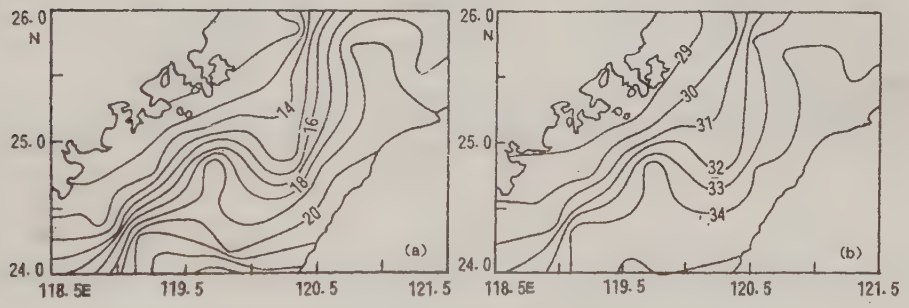

Fig.3 Distribution of temperature and salinity at the 10m layer during the cruise (1998-02-20~03-08) (a) temperature (10m layer), (b) salinity (10m layer)

1.2 Intermediate layer (30m layer)

Since the depth in the studied area is about 50m and when the vertical distributional features of temperature and salinity at all stations are considered, the 30m layer is set to present the intermediate layer in this paper.

In the whole studied area, the distributional features of temperature and salinity at the intermediate layer (shown in Fig.5) are about the same as those at the surface layer, 10m layer and 20m layer. The Minzhe Coastal Water flows southwestward along the western coast of the Taiwan Straits and still has the characteristics of low temperature and low salinity. The temperature and salinity at the 30m layer are less than 16℃ and 32.5, respectively. A branch of the coastal water extends southeastward like a tongue to the east of the Pingtan Island, which is more obvious than that at the surface layer, and tongues close to the eastern coast of the Taiwan Straits. However, the

shallow area near Stations 9826 and 9827 becomes a center of low temperature and low salinity in the western coast of the Taiwan Straits, where the temperature is less than 15℃ and the salinity less than 31.5. There still exists a high temperature and high salinity water tongue directing northward in the eastern Taiwan Straits. The isothermal curve of 19℃ and the iso-salinity curve of 34 can reach 26N. Though the high temperature and high salinity water tongue has a northwestward tendency in the southern part of the studied area, it is more obviously directing northward, with the isothermal curve of 19℃ and the iso-salinity curve of 34 being able to reach 25° N, i.e., the sea area to the northeast of the Pingtan Island. In the southern part of the studied area, the salinity is greater than 35 at the 30m layer, which is similar to that in the ocean, and the scale of high salinity area is larger than that at the surface layer. This furthermore shows that the high temperature and high salinity sea water in the eastern and southern Taiwan Strait may come from the ocean and can be regarded as the invaded water from Kuroshio.

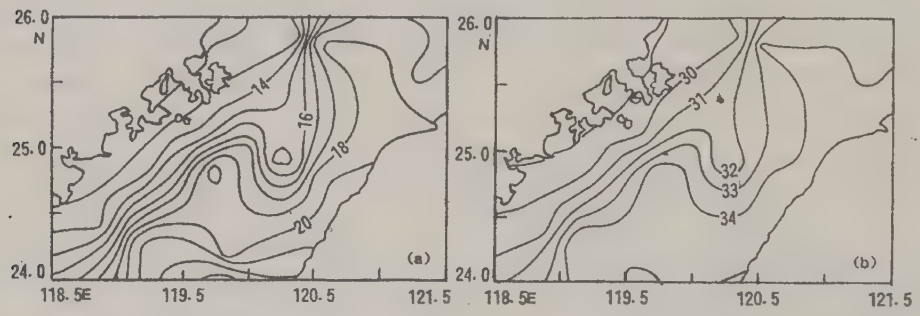

Fig.4 Distribution of temperature and salinity at the 20m layer during the cruise (1998-02-20~03-08) (a) temperature (20m layer), (b) salinity (20m layer)

In the middle Taiwan Straits, there also exist fronts between water masses at the intermediate layer, but the strength is smaller than that at the surface layer, e.g., a strong front still exists near Station 9803. It can be deduced from the temperature and salinity distributions that the low temperature and low salinity Minzhe Coastal Water tongues towards the fronts from the northwestern sea area while the high temperature and high salinity sea water flows towards the fronts from the southeastern sea area.

1.3 Bottom layer

The distribution features of temperature and salinity at the bottom layer are different from those at the upper layers, but are almost the same as those at the 50m layer. As shown in Fig.6 and 7, the whole studied area is still under the control of two water masses, one of which is the relatively low temperature and low salinity sea water in the western Taiwan Straits and the other is the high temperature and high salinity sea water in the eastern Taiwan Straits. In the western Taiwan Straits, except that the temperature at Stations 9826 and 9827 is less than 14℃ because of shallow water, the temperature at the bottom layer of the other sea area is between 16 and 17℃. Similarly, there is a

center of low salinity (less than 30) near Stations 9826 and 9827, but the salinity at the bottom layer of the other sea area is between 32.5 to 33.5. There still exists a low temperature and low salinity water tongue in the northern part of the studied area, which directs to the middle Taiwan Straits from the sea area to the north of Pingtan Island and thus results in the iso-salinity curve of 34 drawing close to the eastern coast of the Taiwan Straits. The high temperature and high salinity water tongue not only flows northeastward along the coast, but also moves northwestward towards the middle Taiwan Straits. The water tongue is narrow near Station 9824 when affected by the low temperature and low salinity sea water from the northwestern sea area. Furthermore, the temperature and salinity at the bottom layer are almost the same as those at the layers above it in the eastern and southern Taiwan Straits, which shows that the northward flowing high temperature and high salinity water is homogeneous vertically. The salinity is high in the southern part of the studied area, where the water with the salinity greater than 35 exists between 24~24.5° N and the distribution scale of the high salinity area is the largest among all layers. The isothermal curves and iso-salinity curves are dense in the southwestern part of the studied area, which are caused by the interaction between the low temperature and low salinity sea water from the northwestern sea area and the high temperature and high salinity sea water from the southeastern sea area.

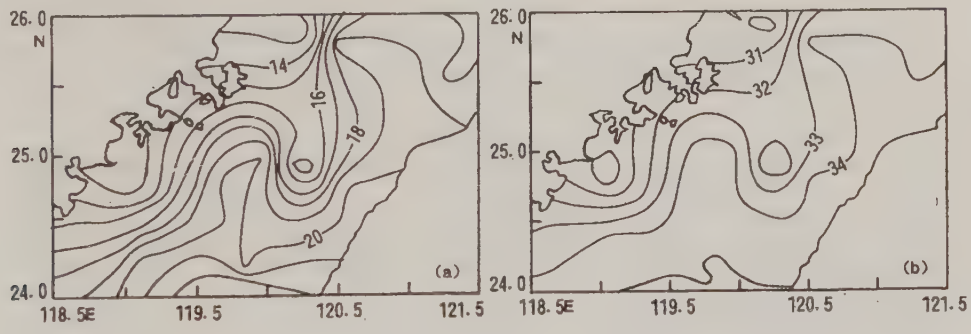

Fig.5 Distribution of temperature and salinity at the 30m layer during cruise (1998-02-20~03-08) (a)temperature (30m layer), (b) salinity (30m layer)

However, the front can not be formed at the bottom layer as at the surface layer and intermediate layer in the northern Taiwan Straits because the interaction between the water masses is not strong enough there.

2 Discussion and Conclusion

In conclusion, the distribution features of temperature and salinity in the studied area are summarized as follows:

(1) There exists a southwestward flowing water, with the feature of low temperature and low salinity at the upper layer, along the western coast of the Taiwan Straits. The surface temperature is less than 13 ℃ and the salinity is less than 30, which agrees well with the previous investigated results of the temperature and salinity in the western Taiwan Straits (Xiao and Cai, 1988). This water

should be originated from the Minzhe Coastal Water which flows southwestward and can reach the sea area near Jinmen Island in winter. The low temperature and low salinity coastal water not only flows southwestward but also splits a branch to the southeast of Pingtan Island and directs southeastward to the middle Taiwan Straits. The investigation results in January of 1984 show that the Minzhe Coastal Water has a branch directing to the middle Taiwan Straits like a tongue at the surface layer (Fujian Institute of Oceanology, 1988; Huang, 1989), and Wang and Chern(1989) also point out that the Minzhe Coastal Water has the tendency to invade the eastern Taiwan Straits.

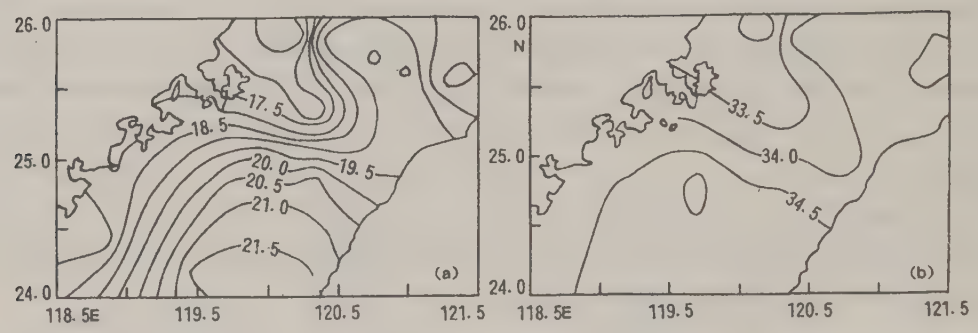

Fig.6 Distribution of temperature and salinity at the 50m layer during the cruise (1998-02-20~03-08) (a)temperature (50m layer), (b) salinity (50m layer)

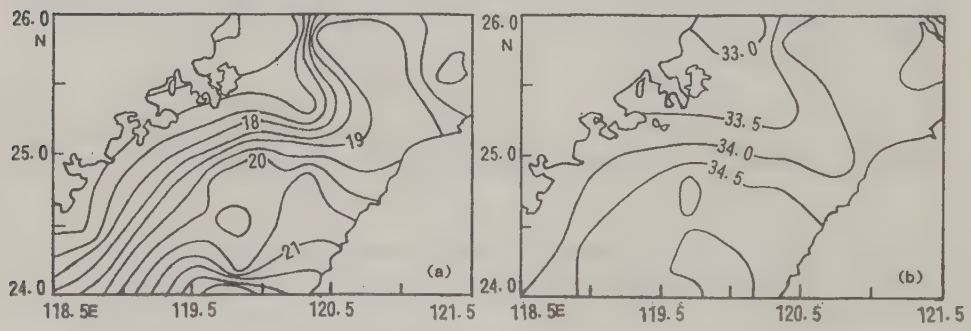

Fig.7 Distribution of temperature and salinity at the bottom layer during the cruise (1998-02-20~03-08) (a) temperature (bottom layer), (b) salinity (bottom layer)

(2) A high temperature and high salinity water appears in the eastern Taiwan Straits, which flows from southwest to northeast along the coast and can reach the sea area near 26° N. The temperature is about 19℃ and the salinity is greater than 34 from surface to bottom. The satellite remote sensing images also show that the high temperature and high salinity sea water comes from the southern Taiwan Straits during the cruise and can be considered as the invaded water from Kuroshio. According to many research findings, Hu et al (1990) concluded that Kuroshio can invade the Taiwan Straits and flow northeastward along the eastern coast of the Taiwan Straits in winter. However, the invasion is strong sometimes but weak some other times. The investigated data of this

cruise show that the invasion is strong during the investigation and the invaded water with characteristics of high temperature and high salinity can extend northeastward to the sea area of 26° N.

Reference

1. Fujian Institute of Oceanology, 1988. Research Reports on the Comprehensive Investigations in Northern and Central Taiwan Strait. Beijing: Science Press, 138-188
2. Hu, Jianyu, Z.Fu and L.Wu, 1990. Studies on the wintertime current structure and T-S fine-structure in the Taiwan Strait. Chin. J.*Oceanol. Limnol.*, 8(4): 319-327
3. Huang, Rongxiang, 1989. Characteristics of water temperature and salinity in northern and central Taiwan Strait.*Marine Science*, 6: 33-38
4. Wang, Joe and C.S.Chern, 1989. On cold water intrusions in the eastern Taiwan Strait during the cold season.*Acta Oceanographica Taiwanica*,22: 43~67
5. Xiao, Hui and S.Cai, 1988. Distribution characters of sea temperature and salinity in western Taiwan Strait.*Journal of Oceanography in Taiwan Strait*, 7(3): 32-37

Analysis on Causes for Yearly Increment of Content of the Inorganic Phosphorus in the Nearshore Sea Area of Yantai

Ji Ling, Ren Rongzhu, Liang Yuangao and Li Zheng
(*Yantai Ocean Administration Office, SOA*)

Abstract Detailed analyses of the monitored data provided by the Yantai Ocean Administration Office between 1989 and 1996 show that, the fluctuation regularities of content of the inorganic phosphorus are as follows: the content of inorganic phosphorus fluctuated near the class-1 standard line basically from 1989 to 1993, tended to increase rapidly from 1993, and increased continuously, causing water quality to be deteriorated from the class-2 to class-3 standard by 1996. Causes for increment of the content of inorganic phosphorus are also analyzed. The results show that, the flux of phosphorus entering Yantai nearshore sea area increases at an annual rate of 16.5 percent, in which the increment rates of the phosphorus contained in washing powder and in phosphate fertilizer are 12.9 and 17.5 percent respectively. Both of them kept a positive interrelationship with their fluxes into the sea. In addition, the migration and regeneration mechanism of the phosphorus within the nearshore area also lead to the inorganic phosphorus accumulating in the nearshore area of Yantai.

Keywords the nearshore area of Yantai, inorganic phosphorus, pollution

Yantai, on the Huanghai Sea and the Bohai Sea, has a tortuous coastal line of some 909 km in length. There is an area of about 6 563.28 sq. km within the bathymetric contour of 15 m, including a water area of 1 867.6 sq. km and a beach area of 306.28 sq. km that are applicable for aquatic cultivation. It's an important base for Yantai's economy to develop its nearshore area. But, the drainage of waste water into the nearshore area increases sharply along with the development of industry and agriculture, and with the increment of population. According to the results of monitoring by the Yantai Ocean Administration Office (YOAO) that, organic pollution tends to be heavier in the north offshore area of Yantai. The inorganic phosphorus becomes the leading pollutant at present, which was listed at the 3rd-position in 1993. No report was found yet on special research of fluctuated inorganic phosphorus in the northern nearshore area of Yantai. In this paper, the fluctuation regularity will be sought for, and the fluctuation causes will be probed into in order to offer the treatment measures accordingly after analyses on the supervised data in the past 9 years provided by YOAO.

1 Present Situation and Fluctuating Trends of the Inorganic Phosphorus within the Nearshore Area

1.1 Sources of the Data

Supervised data for 9 years (from 1988 to 1996), sampled in 8 spots (see Fig.1 for details) with in the nearshore area of Yantai are adopted in this paper. The data were collected three times, in May (the dry season), August (the wet season) and October (the noraml water season) respectively every year.

1.2 Conclusion and Discussion

See Table 1 for the sampled data, Table 2 for the fluctuation in different years and seasons of the inorganic phosphorus in every season (May, August and October) during the 9 years within the nearshore area of Yantai.

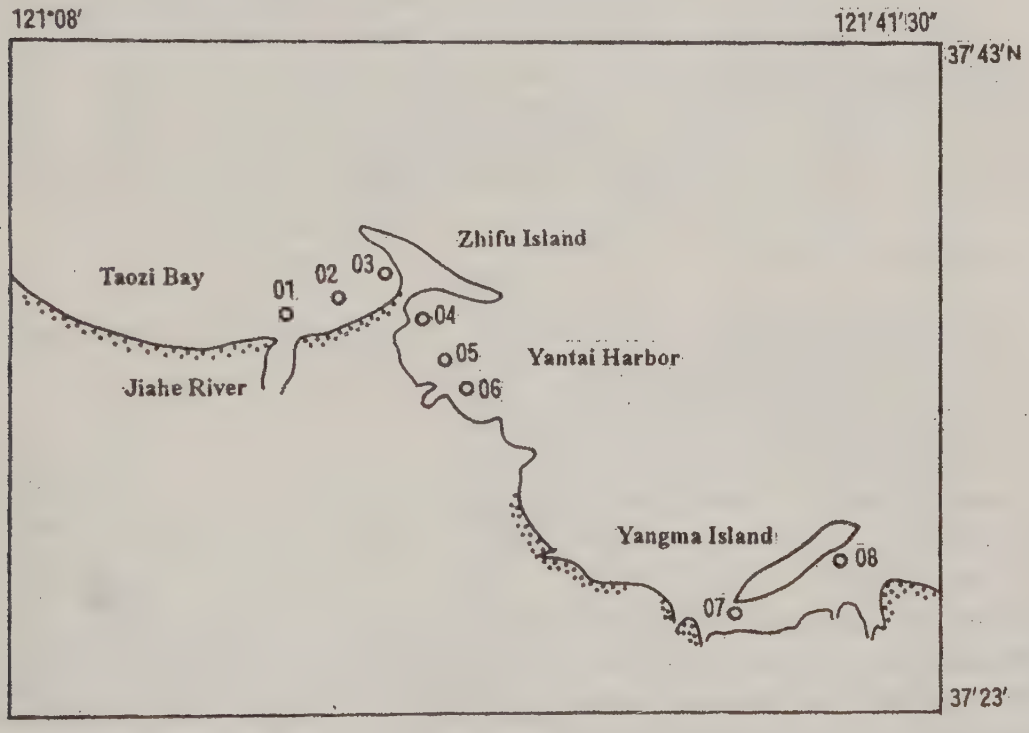

Fig.1 Positions of the Water Quality Supervision Spots

It can be seen from Fig.1 that, the average value of the content of phosphorus is 0.018 mg/L within the nearshore area of Yantai in the 9 years. The content reaches its maximum value of 0.025 mg/L, higher than standard for the Class-1 water quality in October; next, it reaches 0.015 mg/L, just the same as the standard, in May; and it reaches the min. value of 0.014 mg/L, lower than the standard in August. The average pollution index is 1.20 over the years, and the average over-standard rate is 56 percent. Periods with the over-standard rate are mostly in October, with the rate of 75 percent and the average over-standard index 1.67. It can be seen from Fig.2, the Average Fluctuation Curve over the Years, that the content of inorganic phosphorus fluctuated near the Class-1 standard line from 1988 to 1993. It tended to increase rapidly from 1993. In 1994 and 1995, the content exceeded the class-1 water quality standard line and in 1996, the class-2 water quality standard line. It can be seen from the fluctuation curve that the content is highest in the normal water season, that in the dry season comes second and that in the wet season lowest. Since 1995, the measured content of inorganic phowphorus in the sea area in every season has exceeded the class-1

seawater standard and belongs to the class-2 standard and in the normal water season, it belongs to the class-3 standard of water quality.

Table 1 Statistics of the monitoring data for the Inorganic Phosphorus in the Nearshore Area of Yantai from 1989~1996 (mg / L)

	1988	1989	1990	1991	1992	1993	1994	1995	1996	Average	Average Pollution Index
Dry Season (May)	0.012	0.012	0.015	0.016	0.009	0.016	0.010	0.023	0.024	0.015	1.00
Wet Season (August)	0.008	0.007	0.019	0.014	0.011	0.007	0.013	0.019	0.024	0.014	0.93
Normal-water Season (October)		0.023	0.010	0.015	0.026	0.022	0.034	0.025	0.047	0.025	1.67
Annual Average	0.010	0.014	0.015	0.015	0.015	0.015	0.019	0.022	0.032	0.018	1.20

2 Analyses on Causes

The phosphorus enters the soil, rivers or families due to weathering, corroding, drip washing, development and utilization of the phosphate ore. See Fig.3 for details of its circulation courses in nature. It can be seen from Fig.3 that, phosphorus contained in the sea comes from the land, including excrement of human beings and animals, domestic seweage, and loss of phosphorus from the soil on one the hand, and, from the regenerated phosphorus of the sea itself on the other hand.

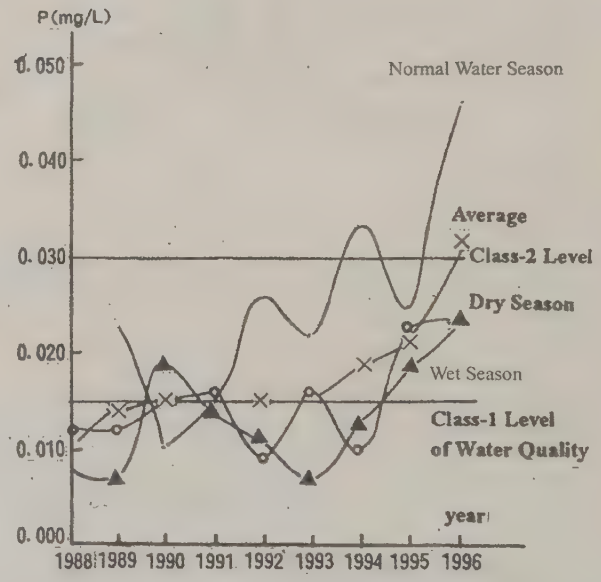

Fig.2 Interannual Fluctuation of Inorganic Phosphorus in the Offshore Area of Yantai

2.1 Influences from the Sources

As the offshore area and bays are mostly connected with rivers emptying into them and these rivers have short courses, large gradients and during the flood season, rise suddenly the pollutants from farmland and towns are easy to be carried into the sea. Furthermore, such human development activities as culture, transport in the nearshore area will also increase the drainage of pollutants within the area.

Population in the urban city of Yantai has increased at an average rate of 3.94 percent; consumption volume of washing powder and phosphate fertilizer at the rates of 12.9 and 17.5 percent in the past 9 years, according to the Yantai Annual Statistics Report. Fluctuations of population in the urban area, and the consumption of washing powder and phosphate fertilizer in Yantai in the past 9 years are shown in Fig.4. We are now going to analyze and probe into each

cause for the discharge of inorganic phosphorus into the sea .

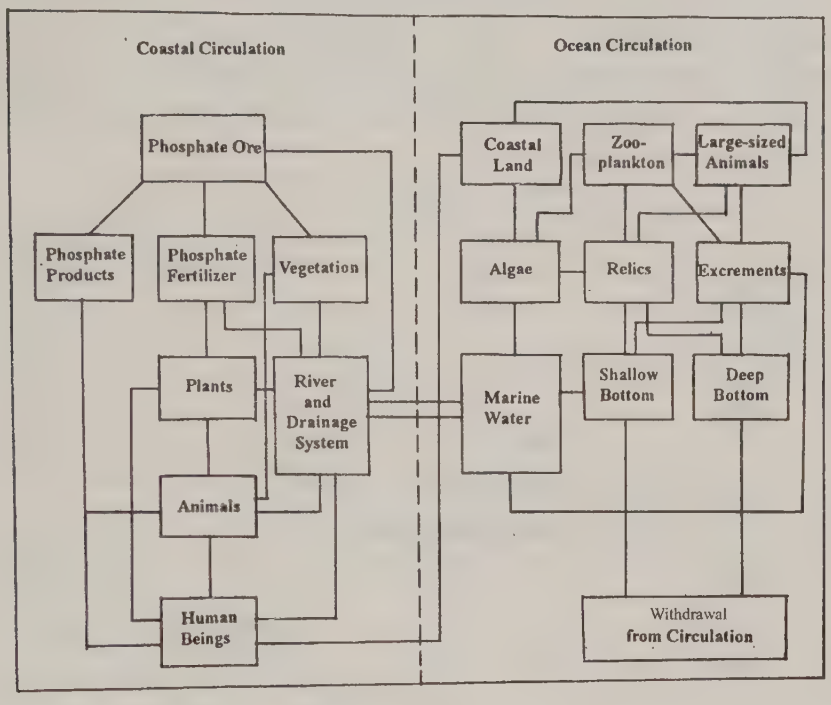

Fig.3 Circulation of Phosphorus in Nature

2.1.1 Population

It can be seen from Fig.4 that, population is increasing in Yantai year by year. It increased to 464 500 in 1996 from 353 200 in 1988, with an annual increment rate of 3.94 percent on an average. Consumption of meat, eggs, grain and vegetable is 4 times as much, at the rate of 15.8 percent as compared with the increment of population. Phosphate content in the above-mentioned foods is absorbed by the human beings, and the remained matters are drained, after being digested and absorbed by the human bodies, into the sea directly with the domestic seweage through the drainage pipelines.

2.1.2 Phosphorus-bearing detergents (Washing Powder)

Tripoly-phosphate of soda is added into the washing powder, accounting for 15 percent ofthe total in weight generally, to be used as surface active agent. Consumption volume of the washing powder has increased yearly in the past 9 years (see Fig.4), according to the Yantai Annual Statistics Report of 1988 to 1996. According to statistics, consumption of the washing powder had increased to 5,081 t in 1996 from 2,500 t in 1988 continuously, at an average increment rate of 12.9 percent a year. Total volume of the drained triple-phosphate of soda, resulted from usage of the washing powder, was 762.15 t in 1996.

2.1.3 Application of Phosphorus-bearing Fertilizer

Along with the improvement of agricultural science and technologies, chemical fertilizers have developed from nitrate fertilizer, the single type available before, into many types of compound

fertilizers of nitrogen-phosphorus, including special compound fertilizers for fruit-trees and vegetables. Content of phosphorus in the compound fertilizer ranks the second, next to nitrogen. According to information provided by Yantai Agriculture Bureau, the applied volume of the phosphate fertilizer had been fluctuating between 12,000 and 16,000 t within a narrow range before 1990. The volume increased rapidly after 1991, and reached 38,200 t in 1996 with an average increment rate of 17.5 percent annually.

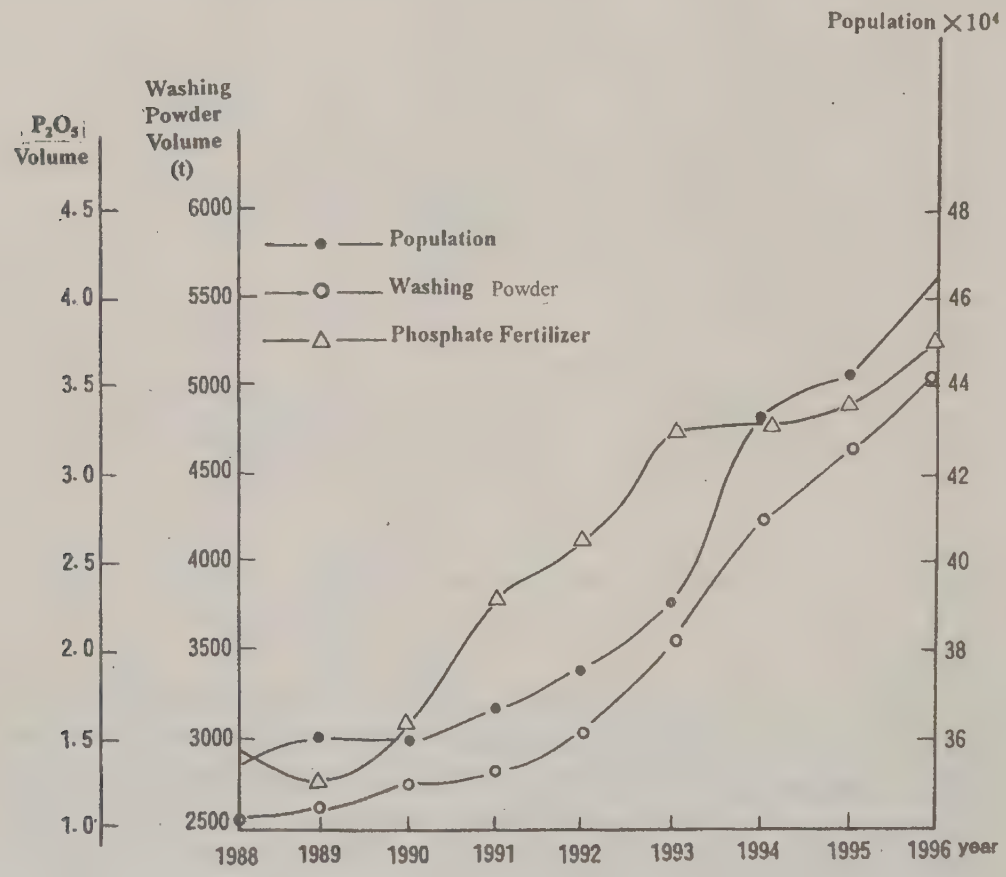

Fig.4 Fluctuations of Population, Consumption of Washing Powder and Phosphorus-Bearing Fertilizer Every Year(unit of P_2O_5: $\times 10^4$t)

Clay can absorb some inorganic phosphorus . Phosphorus-bearing fertilizer applied in the farmland will partly be absorbed by the plants, and partly remain in the soil. The surplus phosphorus-bearing fertilizer will be washed away by the rain, and finally drained into the sea when it's heavily applied.

2.1.4 Cultivation in the Coastal Land

People have paid attention to the influence of cultivation on the ocean environment. Cultivation of prawn and fishes, and feeding them with man-made feeds are the important factors contributing to the increase of the content of phosphorus in prawn ponds. According to Fishery Planning and Statistics Information of Yantai (see Table 2), it is clear that the prawn cultivation area was more

before 1992, and the area for fishes, shellfishes and algae cultivation held the major position after 1992. It may be because of the prawn diseases after 1992. Yantai has increased its total cultivation area, but the feeds thrown there have not increase. This is also because of the different requirements of feeds for fishes, shellfishes and algae cultivation. It may be concluded from this that the phosphorus excreted in the nearshore cultivation area has not changed much over years.

Table 2 Cultivation in the Northern Nearshore Area of Yantai

Time	1987	1988~ 1991	1992 ~1995
Area for Fishes, Shellfishes and Algae (sq km)	40	49	78
Area for Prawn (sq km)	60	75	50
Total Area (sq km)	100	124	128
Feed Amount (10,000 t)	1.0	1.8	1.5

2.1.5 Soil Erosion

Destruction of the vegetation will lead to soil erosion, and wash away surface phosphorus into rivers and then into the sea. Yantai has planted a large amount of trees in order to decrease soil erosion in recent years. Then, loss of phosphorus caused by soil erosion has changed slightly over the years.

2.1.6 Flux of Phosphorus into the Sea

Flux of phosphorus into the sea is referred to as the total amount of pollutant entering the sea through rivers and other drainage channels. The flux is determined by the volume of phosphorus drained to the sea from land, which will change according to different phosphorus drainage volume and forms. Then, it will be helpful to know the change of phosphorus drainage by research of the flux of that into the sea.

An annual fluctuation curve is drawn, as shown in Fig.5, on the supervised data of the flux of phosphorus entering the nearshore area of Yantai from 1988 to 1996 provided by YOAO and the Yantai Environmental Monitoring Station.

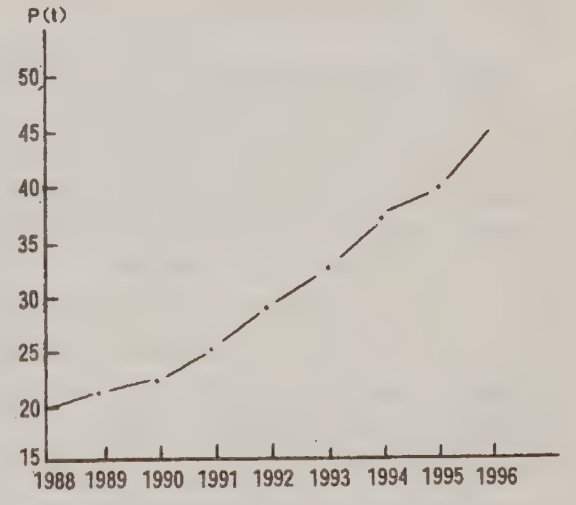

Fig.5 Changes of Flux of Phosphorus Entering the Sea Every Year

It can be seen from Fig.5 that, the flux of phosphorus entering the nearshore area of Yantai tended to increase continuously from 1988 to 1996. The increment was slow before 1990, and rapidly from 1990 to 1996, at an average rate of 16.5 percent per year. This change is just similar to the changes of human beings, consumption of washing powder and phosphate fertilizer that we have discussed in this article. Now we are going to make a quantitative analysis on the consistency.

As the drainage volume of phosphorus caused by the coastal cultivation is steady, which has little effect upon the continuous increment of flux into the sea, we do not consider it when

accounting. Three factors, the population, washing powder and phosphate fertilizer, which influence the flux's change remarkably, will be researched then.

Interrelationship between the population, the washing powder and the phosphate fertilizer and the flux of phosphorus into the sea will be accounted for in the following formula:

Population vs the flux	$Y= -54.9 + 2.17X$	$r = 0.980$
Washing powder vs the flux	$Y = -2.29 + 9.41 \times 10^{-3} X$	$r = 0.987$
Phosphoate fertilizer vs the flux	$Y= 5.92 + 9.47X$	$r = 0.956$

It can be seen from the above accounting that the population and its consumption of washing powder and phosphate fertilizer keep a good interrelationship with the flux of phosphorus into the sea. The result shows that, the annual increment rate of 15.6 percent for the flux is in conformity with the annual increment rates of 16.5 percent for population, 15.8 percent for increment of consumption of meat, eggs, grain and vegetable, 12.5 percent for washing powder and 17.5 percent for phosphate fertilizer. It is shown that the flux of phosphorus into the sea is caused by three factors including increment of phosphorus caused by man and animals and by consumption of washing powder and phosphate fertilizer.

2.2 Migration and Regeneration of Phosphorus Contained in Nearshore Sea Area of Yantai

2.2.1 Migration of Inorganic Phosphorus

In general, inorganic phosphorus migrated out from the sea by way of convection and diffusion of the sea water and use of the phytoplankton chiefly. Due to the deteriorating quality of the nearshore environment, large-sized lives within the area have decreased in varieties and in quantity. Fishing of the large-sized lives leads to decrement of the phosphorus migrating out of the area. Phosphorus contained in large amounts of the lives and their excrement remains within the nearshore area, joins in circulation, and accumulates. The reciprocating flow dominates the nearshore area of Yantai, while the residual low going out is not strong. The residual flow at the bottom is even small than that on the surface. This weakens the transport of nutrient salt in the nearshore sea srea to the outer sea, thus facilitating the accumulation of inorganic phosphorus in the nearshore sea area.

2.2.1 Regeneration of Inorganic phosphorus

Phosphate produced from excretion of zooplankton is the major way to regenerate inorganic phosphorus. One part of the phosphate excreted by animals will be directly dissolved into the water, and the other will combine in solid state with granular scraps coming from other sources. Another way for phosphorus to regenerate is decomposition of plant and animal bodies. With the effects of environment and bacteria, these organic phosphoruses are turned into inorganic phosphorus through degradation and decomposition and released into the water. Regeneration of inorganic phosphorus also plays a certain role in researches on why high content of phosphorus is maintained in the nearshore area.

Furthermore, another way of phosphorus regeneration is the inorganic phosphorus absorbed in the surface deposit releasing into the overlying waters. The higher the pH value is, the larger the releasing amount is. Phosphorus in an oxidation often releases into the water in the form of oxidized catabolism in complex types. It is shown in the monitored results of YOAO that, pH value is

basically between 7.90 and 8.28, and the average value is 8.09 in the neaarshore area of Yantai. Contents of dissolved oxygen is 7.60 to 14.40 mg/L generally, and super-saturation of the dissolved oxygen often happens in summers. They help the inorganic phosphorus contained in deposit to release into the water.

It can be seen from above that, the inorganic phosphorus contained in nearshore sea area of Yantai is strong enough at the low level of net migration out. This is the accumulation and maintenance of a high content of inorganic phosphorus in the nearshore area.

3 Prevention and Cure Measures

The high content of inorganic phosphorus in the nearshore area of Yantai constitutes a threat to the nutrient trends in the nearshore area of Yantai. The following measures are suggested in the light of such direct causes for the increment of inorganic phosphorus in the nearshore area as the excrement of humans and of animals, and larger consumption of washing powder and phosphate fertilizer:

1. To develop and use phosphorus-free washing powder, and minimize consumption of the phosphatic washing powder;

2. To develop treatment of the seweage in threesteps, set up seweage treatment plants, in order to drain domestic seweage after being treated according to standards;

3. To improve the utilizing rate of phosphate fertilizer in farmland, use fertilizer scientifically, popularize knowledge of fertilizer application, and decrease influences on the environment caused by application of phosphorus fertilizer;

4. To protect vegetation and enhance maintenance of water and soil in order to decrease the content of phosphorus in the surface runoff.

4 Conclusions

1. Content of inorganic phosphorus fluctuated basically near the Class-1 level within the neaarshore area of Yantai from 1988 to 1993. The content tends to increase sharply from 1993, and is over the Class-2 quality level by 1996;

2. Flux of phosphorus into the sea increased continuously from 1988 to 1996, at an annual increment rate of 16.5 percent. The annual increment rates for population, consumption of washing powder and phosphate fertilizer keep an just positive interrelationship with that of the flux. In addition, the weak migration ability of phosphorus and strong regeneration ability of it also contribute to the inorganic phosphorus accumulating within the nearshore area of Yantai.

References

1. J. P. Relay, Translated by Cui Qingchen, etc. (1982) *Chemi-oceanology*, published by the Ocean Press, (2) 285

2. Shangh Shaoling, (1996) Research on Phosphate within the Western Offshore Area of Xiamen, *Marine Environment Science*, 15 (1): 15 - 20

Study on Sediment Transport in the Qianjiang Bay of Guang' ao, Shantou City by Using the Element Geochemistry Method

Liu Shao, Zhao Huanting and Zhang Qiaomin

(*South China Sea Institute of Oceanology, Chinese Academy of Sciences*)

Abstract Nine samples of suspended matter at the surface or bottom and 34 elements in 20 samples of substrate sediment have been used in the neutron activation analyses. Authors study sediment and suspended matter movement by using the method of element geochemistry, and conclude through synthetic analysis and processing that the movement direction of suspended matter and substrate sediment tends to converge on the central area.

Keywords neutron activation analysis, element geochemistry, sediment transport

Introduction

Many important problems about sediment such as its source, movement direction and silting are first considered in the projects such as those of harbor planning, harbour siting, breakwater building, channel dredging and so on. Engineers and technicians need not only to know sedimentation rate but also determine movement direction. The former is a quantitative problem, the latter is a qualitative one. Several unsuccessful projects exist because of qualitative errors. Experts in geomorphology and sedimentology have made a great deal of theoretical or experimental studies and found many useful methods. For example, the artificial radioactive tracer that can estimate sediment sources and determine movement direction, successfully traced sediment for the first time in England in 1954 and made over 140 on-the-spot experiments until 1975. Li Zhangsu, a Chinese scholar, applied it too. The method cannot be extensively applied because of enormous trace dose, radioactive contamination and harmfulness to man or aquatic life. Then from the 1970s scientists began to study neutron activation analysis on tracing sediment movement. The method consists of adding trace elements or not. The artificial added trace element requires selecting suitable trace elements, moreover it must be effective and mark reliably on carriers, then it generally needs to select the stable isotope which is highly sensitive to neutron activation analysis and of very low content in the carrier. Recently ,Yin Yi etc. measured the signal element concentration in sediment by neutron activation analysis, and determined the movement rule of sediment in the light of the transport character of signal element. With the variations of geochemical environment, certain element concentration in sediment from different sections or sources is different. According to the diversity of elements in this paper, we use several activate stable isotopes as natural tracers to study sediment movement. With more than 30 measurable elements to select, we use the variations of most element concentrations as basis, processing the data to gain the element concentration coefficient and the

relationship between element concentration and each size composition , combining with the rule of the product (hereinafter called "enriched coefficien") between related coefficient and content of size composition, to study sediment transport. In addition, due to lack of source of exotic sediment or very low local sediment, the Qianjiang Bay of Guang'ao, Shantou city is good place in which to study sediment transport by element geochemistry.

1 Neutron activation analysis

Element concentration of sediment and suspended matter have been gained from neutron activation analysis. It is a method of nuclear analytical technology whose foundation is nuclear reaction. The method of using neutron with certain energy and intensity to bombard program sample, then measuring the amount of delayed radiation given out by radio nuclide decay, which is produced during nuclear reaction ,or directly measuring that of instantaneous radiation emitted by nuclear reaction, can gain the data. On the other hand, it selects appropriate radiation or decay time for the nuclide, such as Sm, La, U, Mo, W, Br, As, Ti, Na, K, Au, which have shorter half life and radiate only for 2 or 3 days, but Nd , Ce, Yb, Lu, Se, Tb, Th, Cr, Eu, Hf, Ba, Sr, Zr, Cs, Ni, Ag, Sc, Rb, Fe, Zn, Co, Ta, Sb, should be radiated for two weeks, then measuring the amount of gamma radiation with the semiconductor detector, and the multi-channel analyzer, can get the qualitative or quantitative data of element, too. The neutron activation analysis becomes a method of trace analysis and normal-analysis, and has many advantages such as high sensitivity, good accuracy, extensive adaptability and low consumption (100mg), as well as specific effectiveness and no-destruction, so it has been extensively used in many fields. At present, it is applied to the identification of source, distribution, deposition, or relative flux of sediment, analysis of water quality, and measurment of origin, distribution and diffusion of water contamination .

2 Study on suspended matter movement

The water samples at the surface, middle and bottom of 6 sites in Qianjiang Bay, are collected hour by hour during spring and neap tides in May, 1992 (Fig.1). In this paper, nine samples selected from the bottom during neap tide and surface, have been used for neutron activation analysis(Table 1). In the light of the sediment diffusive rule, if the sediment comes from the same origin, the silt content would decline from source, identically, if the number of elements in the source is stable, the element that is positive to certain size would diffuse from high to low section by its rule of diffusing from high to low concentration in sediment. The determination in this paper is more accurate and reliable because not made by individual elements but most elements with the same tendency. Certain elements in specific size vary from high to low concentration because of the difference in the nature of element geochemistry, showing that the concentration of the typical element reflects the accumulation of sediment.

Suspended matter samples of 2b-24, 3b-24 at the bottom and 2b-40, 3b-40 at the surface,

collected at 17:00, 22:00 respectively on 11th , May, 1992, and 4b-63, 5b-63, 6b-63 at the bottom and 4b-39, 5b-39 at the surface, collected at 7:00, 23:00 successively on 13th, May, 1992, have been used for by neutron activation analysis, and the data are listed in Table 1. Because the local tide is irregular semidiurnal tide, affected by topography, the direction and the pattern of transfer flow are changeable, and there occur successively eastward flow (SE) and westward flow (NW) during rising tide, westward flow (NW) and eastward flow (SE) during falling tide. Consequently, it is very difficult to determine sediment movement direction only by the samples at the bottom or surface during neap tide, in combination with the tidal direction because the number of sites is less and the regularity is not obvious. For this reason, on the basis of sediment distribution, type, as well as the data of element analysis, relationship between element concentration and size composition, we select the typical elements to study movement direction of suspended matter. The typical elements like Fe, Cr, Sc, Co, Th, Yb, are negative to sand (ϕ =2~0.125mm), but positive to silt or clay, all of the coefficients are more than -0.90, and +0.85, respectively. Most of the suspended matter is silty clay by the data of analysis.

Table 1 Data of analysis of suspended matter

Site	Tide	Silt content	Collecting time		Element concentration $\times 10^{-6}$						
		Kg/m^3	y-m-d	time	Fe(%)	Cr	Sc	Co	Cs	Th	Yb
2b-24 (bottom)	Foold	0.838	1992-05-11	17:00	5.769	83	17.73	18.2	12.2	29.06	4.27
3b-24 (bottom)	Foold	0.0257	1992-05-11	17:00	5.568	69	16.77	14.5	11.9	28.30	3.69
2b-40 (surface)	Ebb	0.0364	1992-05-11	23:00	5.999	58	15.83	17.0	10.8	28.48	3.33
3b-40 (surface)	Ebb	0.084	1992-05-11	23:00	5.505	80	17.68	17.2	13.2	32.04	4.50
4b-63 (bottom)	Foold	0.06	1992-05-13	7:00	5.150	72	16.17	15.6	12.0	29.35	4.08
5b-63 (bottom)	Foold	0.084	1992-05-13	7:00	5.368	74	16.97	16.4	12.9	29.91	4.01
6b-63 (bottom)	Foold	0.0821	1992-05-13	7:00	5.519	86	17.97	16.4	13.4	32.0	4.21
4b-39 (bottom)	Ebb	0.0304	1992-05-13	23:00	4.607	53	13.76	13.02	3.12	24.91	3.55
5b-39 (bottom)	Ebb	0.02	1992-05-13	23:00	5.375	54	15.70	15.90	10.9	27.40	4.61
Accuracy					200 ($\times 10^{-6}$)	8	0.01	0.3	0.1	0.01	0.01

In Table 1, from 3b-24 (Site 3) to site 2, the silt content increases from 0.0257 kg/m^3 to 0.838kg/m^3, and the element concentration of Fe(%), Cr ($\times 10^{-6}$, fellowing identity), Sc, Co, Cs, Th, Yb from 5.568, 69.0, 6.77, 14.5, 11.9, 28.3, 3.69 to 5.769, 83.0, 17.73, 18.2, 12.2, 29.06, 4.27, respectively. But 4b-63, 5b-63 in the west of Site 2, besides the silt content is equal or less than that

of Site 2, all of the above element concentration are less than those of Site 2 (both during the rising and falling tides). Moreover, the flood tide towards SEE indicates that the sand moves to Site 2, because the lasting time of flood tide is longer than that of falling tide. Consequently, the direction of sediment movement is the same as that of increasing element concentration. That is to say, the grain size of main silt or clay sediment declines during movement, but the extent of element enrichment increases. This feature is determined by the nature of element geochemistry. For example, Fe concentration in the sediment increases with the declining of grain size, and also is higher in silt rock in series of marine sedimentary rock and reaches maximum in clay rock. The other element is Cs, which is easily absorbed by colloid clay mineral with negative charge because of its larger ionic radius, and it is the best of alkali metal in the sequence absorbed by colloid clay mineral, namely Cs>Rb>K>Na >li.

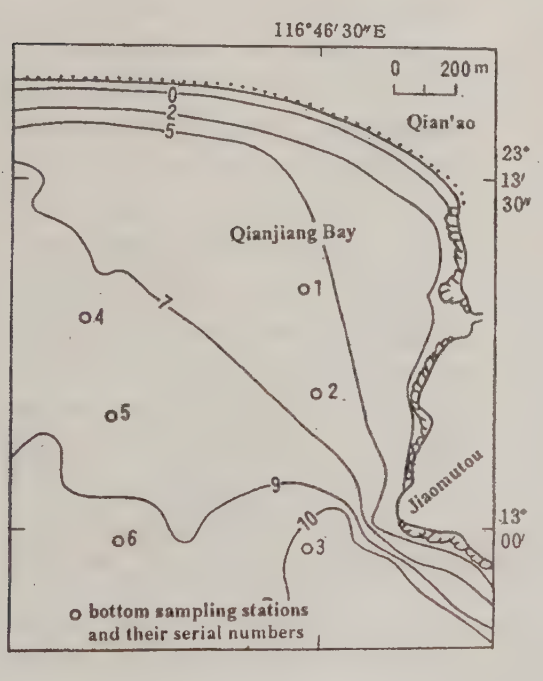

Fig.1 Suspended Matter Sampling Stations in the Qianjiang Bay, Guang'ao, Shantou in 1992 (The unit of the isobath is m; Numbers 1~6 are hydrological- suspended matter sampling stations)

Table 1 also shows that the element concentration from Site 4 to 5 increases whether during the flood or falling tide (except for Cr concentration in some sites within the detection limit, others are all out of the detection limit), and the increasing direction of element concentration is the same as that of silt content, displaying a positive correlation. The increasing of element concentration during the rising tide is still the same as that of the falling tide, but the silt content of Site 4 is slightly less than that of Site 5, and it is possible that the amount of suspended matter reduces when the neap tide residuel current toward SE exchanges in Site 5 with the falling tide toward NW .

From the above analysis of element concentration and slit content of suspended matter of 5 sites at bottom, it is concluded that both the element and silt move towards Site 2.

3 Submarine sediment transport

20 samples in submarine sediment have been used for neutron activation analysis, the data are listed in Table 2, and each sample consists of 34 element concentrations. On the basis of the data listed in Table 3 as the standard of high concentration, we count the sites where the element concentration is larger than that of standard. The results show that site A_{64} has 27 elements belonging

to high concentration ones and the numbers of Site A_{60}, A_{48}, A_3, A_{45}, A_7 are 26, 24, 24, 22, 21 respectively. The sites, where the number of high element concentration is less than half of 34, are A_{25}, A_{66}, A_{52}, A_{67}, A_{70}, A_{33}, A_{73}, A_0, A_{69} and A_{73}, the number is 10, 8, 6, 4, 4, 3, 3, 2, 1, successively.

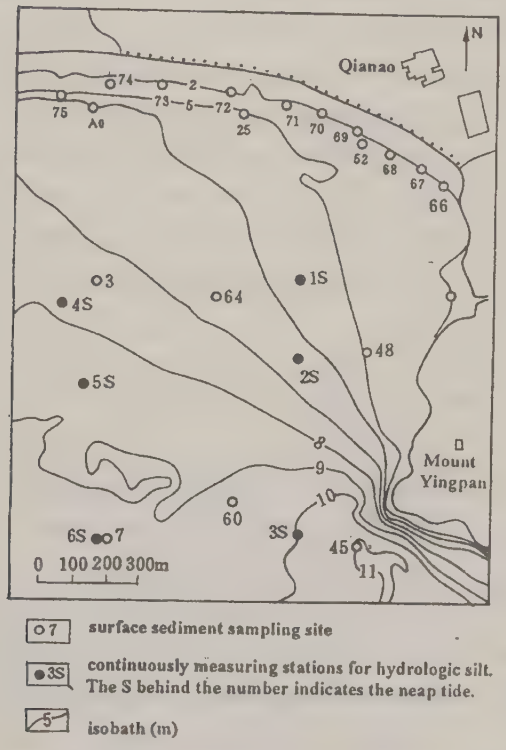

Fig.2 Part of the Sampling Stations for Bottom Surface Sediments in the Qianjiang Bay

Table 4 lists the data of K, namely K= C/C', where K is concentration coefficient, C is element concentration in certain sites and C' is average concentration in the whole area. In Table 4, the sites,where the number of element with $K < 1$ is less, for example within 8, are A_7, A_{60}, A_{64}, A_{45}, A_3 and A_{48}, and the number is 2, 3, 5, 7, 8, respectively. $K<1$ shows that the element is low concentration, which is coincident with meristic diffusibility of geochemistry, but $K>1$, $K>2$ and $K>3$, are high, higher, the highest concentration respectively. In the area only K of Ni in A_{64} is 3.1 and that of Au in A_{25} is 4.4, then Ni or Au possibly concentrates in sandy size to form a sandy mine. The sites, where the number of element is coincident with meristic diffusibility of geochemistry with $K>1$ exceed 20 or the typical elements with $K>2$ are Sc, Cr, Cs, mainly focusing on the sites A_{64}, A_3, A_{48}, A_{45}, which is in keeping with the results of simple element concentration analysis.

To show further the relationship between the nature of element geochemistry and size, a correlation analysis is made of the size composition and element concentration in each site conducted correlation analysis, and the data are listed in Table 5. In the area, statistics shows that the number of elements, whose concentration is negative to sand and all of coefficients are less than -0.80, is 20, and that whose concentration is positive to silt and coefficients are over +0.80, is 21, while that which is positive to clay and all of coefficient are over +0.80, is 19, and with 5 elements whose coefficient is more than +0.60, the total number is 24. Then it is considered that the sediment size of sites that focus the most majority of elements with high element concentration or where most of the elements accord with meristic concentration of element geochemistry, is silty or clay size, being identical to the sediment type diagram (Fig.3). Consequently, determined by the above conclusion, the sediment in the sites where the number of high element concentrations is more than that of half of analyzed elements, or where the number of elements with $K>1$ is the same as that of high concentrations, can be determined as silt or clay sediment, and belongs to the accumulation area

Table 2 Data of neutron activation analysis

	A_0	A_3	A_7	A_{25}	A_{33}	A_{45}	A_{48}	A_{52}	A_{60}	A_{64}	A_{66}	A_{67}	A_{68}	A_{69}	A_{70}	A_{71}	A_{72}	A_{73}	A_{74}	A_{75}
Fe (%)	2.033	4.786	3.626	2.824	1.740	3.844	4.275	1.463	4.246	4.722	1.362	1.430	1.259	1.323	1.303	1.136	0.99	1.174	0.815	0.560
Na (%)	0.568	1.495	1.095	0.760	0.539	1.131	1.394	0.644	1.382	1.499	0.612	0.657	0.559	0.584	0.606	0.588	0.480	0.459	0.476	0.394
K (%)	1.784	2.017	2.381	2.286	1.682	2.765	2.006	2.547	2.539	2.173	2.523	2.689	2.098	2.249	2.595	2.011	1.915	1.506	1.712	1.657
Ca (%)	2.340	0.638	1.693	0.990	2.055	0.983	1.682	1.359	1.802	1.112	0.576	1.117	0.232	1.390	1.551	<0.001	1.126	1.247	<0.001	0.191
Ti (%)	0.12	0.09	0.06	0.10	0.06	0.04	0.15	0.06	0.05	0.06	0.02	0.11	<0.01	0.08	0.11	0.06	0.03	<0.01	0.05	0.06
Sc	5.46	15.73	11.14	7.83	4.02	12.37	13.58	3.02	14.08	15.49	2.82	2.99	2.41	2.59	2.83	2.42	2.26	2.68	1.89	1.09
Cr	28	73	47	35	12	54	58	10	65	70	8	8	<8(7)	8	9	8	<8(7)	8	<8(5)	<8(4)
Co	5.6	14.9	10.5	9.2	5.2	11.4	13.6	4.2	13.2	15.2	3.8	4.3	3.6	4.1	4.1	3.7	2.7	3.5	2.4	1.7
Ni	<6(2)	<6(1)	11	8	<6(1)	12	11	6	13	25	12	<6	8	13	<6(5)	7	<6(3)	7	6	<6(3)
Zn	28	71	50	47	23	52	68	<20 (10)	61	63	<20 (15)	24	21	20	<20 (17)	<20 (17)	<20 (10)	<20 (14)	<20 (19)	<20 (10)
Rb	98	150	143	124	74	155	148	99	151	156	102	111	93	103	103	80	70	70	65	51
Sr	77	88	63	101	48	65	50	120	90	172	132	126	87	141	79	49	91	66	<40 (31)	<40 (33)
Cs	3.8	10.8	8.3	5.8	2.5	9.2	9.7	2.6	10.0	11.3	1.6	2.3	2.1	2.3	2.4	2.0	1.4	1.9	1.4	1.0
Ba	244	253	290	250	202	333	254	353	299	305	505	338	293	293	295	248	277	193	242	277
Zr	195	134	156	276	125	216	147	283	152	144	189	121	70	118	49	68	183	192	70	53
Hf	6.5	4.4	9.5	13.4	5.9	8.1	4.5	10.2	6.5	4.1	6.7	3.6	3.8	3.1	2.6	2.8	5.5	8.5	3.4	1.3
Ta	1.08	1.43	1.71	1.09	0.90	1.74	1.59	0.87	1.88	1.67	0.87	0.71	0.70	1.10	0.63	0.56	0.70	1.01	0.57	0.40
Th	9.90	25.86	21.45	21.37	7.75	22.19	23.15	13.15	23.44	25.75	16.30	6.21	5.02	8.05	5.30	4.30	5.23	7.71	3.88	2.91
U	1.96	3.21	3.18	3.24	1.44	3.33	2.86	2.15	3.89	3.01	1.84	1.43	1.67	1.07	1.07	1.13	1.22	1.24	1.17	0.73
Mo	<0.1	2.9	<0.1	<0.1	5.2	8.7	5.6	<0.1	3.2	9.2	0.5	<0.1	1.6	2.2	0.8	<0.1	<0.1	0.1	<0.1	<0.1
W	2.4	5.2	3.1	2.8	1.7	4.9	2.2	1.8	3.9	5.6	0.9	1.3	1.0	1.7	1.4	0.9	2.2	2.4	1.1	1.0
As	6.8	13.4	11.6	8.7	7.4	12.1	13.5	5.4	11.3	14.6	5.2	6.6	5.7	6.3	5.4	4.6	4.6	4.9	4.3	3.8
Sb	0.4	0.7	0.6	0.8	0.3	0.7	1.0	0.2	1.0	0.8	0.4	0.4	0.4	0.3	0.1	0.3	0.3	0.2	0.3	0.1
Ag	0.5	1.3	0.7	1.2	1.1	0.5	1.0	0.3	0.9	0.3	0.1	0.7	<0.1	0.9	1.0	0.2	0.1	1.2	<0.1	0.1
Au*	2.2	9.5	12.9	24.5	3.1	3.0	1.9	0.7	<0.1	11.0	3.1	1.6	6.0	3.2	9.2	<0.1	3.2	10.5	5.3	1.7
Se	0.04	0.07	0.07	0.04	0.04	0.03	0.03	<0.1	0.04	0.04	0.02	0.04	0.04	0.03	0.02	0.02	0.03	0.03	0.02	0.03
La	29.31	62.21	50.76	43.08	23.72	53.04	57.79	25.01	56.48	62.47	76.77	21.18	16.60	18.83	21.03	17.09	15.08	20.47	13.09	9.02
Ce	54.75	122.25	96.17	81.68	41.49	97.74	109.37	41.81	107.69	120.19	145.72	38.57	28.22	32.86	37.79	28.90	26.44	37.21	22.73	19.84
Nd	21.12	57.93	37.24	40.34	20.01	47.05	59.50	23.02	49.17	42.67	54.16	6.91	14.88	18.30	16.02	14.20	13.33	16.82	8.39	7.53
Sm	4.34	9.34	7.59	6.49	3.77	7.83	8.52	3.79	8.36	9.15	8.71	3.39	2.73	3.14	3.27	2.73	2.47	3.29	1.98	1.48
Eu	0.55	1.24	1.18	0.76	0.60	1.02	1.18	0.48	1.11	1.23	0.85	0.54	0.42	0.50	0.56	0.44	0.38	0.40	0.35	0.24
Tb	0.54	0.87	1.00	0.70	0.41	0.84	1.03	0.34	0.82	0.98	0.93	0.36	0.38	0.41	0.38	0.34	0.40	0.46	0.31	0.20
Yb	0.20	3.57	3.55	2.91	1.74	3.22	3.31	1.51	3.38	3.26	2.41	1.44	1.18	1.17	1.15	0.98	1.32	1.98	0.81	0.54
Lu	0.35	0.57	0.57	0.50	0.26	0.48	0.53	0.23	0.53	0.55	0.38	0.23	0.19	0.19	0.18	0.15	0.19	0.35	0.13	0.08

unit: ppm; *Au unit: ppb

Table 3 Data of high concent standard of element concentration

element	Concentration (%)	element	Concentration $\times 10^{-6}$	element	Concentration $\times 10^{-6}$	element	Concentration $\times 10^{-6}$	element	Concentration $\times 10^{-6}$
Fe	>3	Ti	>0.01	Hf	>10	Au	>10	Ce	>100
Na	>1	Sc	>10	Ta	>1.4			Nd	>50
K	>2.5	Cr	>50	Th	>20			Sm	>9
Ca	>1	Co	>10	U	>3			Eu	>1
Ti	>0.01	Ni	>10	Mo	>2			Tb	>0.8
		Zn	>50	W	>10			Yb	>3
		Rb	>140	As	>10			Lu	>0.5
		Sr	>100	Sb	>0.7				
		Cs	>10	Ag	>1				
		Ba	>300	Se	>=0.05				
		Zr	>140	La	>50				

by the differential theory of mechanical sediment.

To help explain the problem of sediment source, besides the analysis by the above rule, the data are processed further, namely, the related coefficient between element concentration and size multiplied by the percentage of size composition is the enriched coefficient (Table 6). Its importance is to supply scientific judgement for finding out typochemical element and element movement direction. The larger enriched coefficient reflects the higher concentration of element in certain size, and the negative enriched coefficient shows that the element is dispersed in specific sizes, and the larger the negative number is, the greater the dispersion degree is. From Table 6, it can be seen that the number of elements with silty sand enriched coefficient more than 30 in sites A_{66}, A_3 is 22, and that of each A_{64}, A_{48}, A_{45} is 21,and that of A_7 is 20. While the number of elements with clay size enriched coefficient more than 30 in Site A_{64} is at most 24, and that of sites A_3, A_{48}, A_{60}, A_{45}, A_7 is 23,22,19,15,10 respectively. The sites whose products occupy the first three places are all in the silty clay section in sediment type diagram, the others are in the clay-silt section, then it is clear that the processed data approach the real character of sediment. It is clear from element concentration coefficient, element high concentration, and enriched coefficient of data in each site, that the sediment type reflected by the site where the

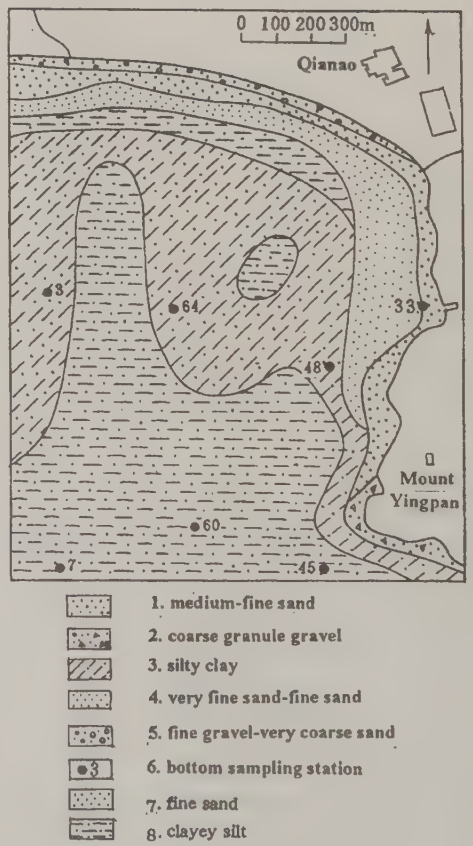

Fig.3 Types of Bottom Sediments in the Qianjiang Bay

number of element concentrations is large or by the enriched coefficient is more than 30, and is more identical. From the enriched coefficient, it can be seen that Site A_{64} is the accumulation center, where the number of elements with clay enriched coefficient more than 30 is at most 24, while on the east-west line, Sites A_3 and A_{48} with 23 and 22 respectively are bilateral the towo flanks of the accumulation, and they transport towards the center at the same time, but the extent of movement is slightly greater from east to west. Similarly, the extent of transporting to the centre from south to north is greater than that from north to south.

On the other hand, the statistics of the sites where the number of high element concentrations is less than 17 shows that, according to the differential theory of sediment, the sediment becomes from cough to fine with the hydro-dynamic decreasing. The number of high element concentrations in Sites A_{25} and A_{52} is 10, 6 respectively, and compared with the number of 27 at Site A_{27}, it clearly shows that the sediment moves to south. Moreover, the concentrated element and the dispersed coefficient reflect the same rule. For example, the numbers at the Sites A_{25} and A_{52} are 25,8 respectively, compared with the number of 29 at site A_{64}, showing a sediment tendency to the south, too. The tendency of several sites in the north alongshore isn't clear because of effect of wave and alongshore current, but from the number of high element concentration and enriched coefficient, for example the number in site A_{66} is 8 and the coefficient is 15, while the Sites A_{74}, A_{75} in the north section by west have no high element concentrations and the coefficient is 0, the sediment still moves mainly toward east or south.

From the local flow field, the tide is a regular semidiurnel one, and the flood tide points to SE, whose duration is long and velocity is great, and the falling tide points to NW. The residual current points to SEE (direction of flood tide), the direction of net output of sediment is also to the east. The flow always forms circle current during exchanging in the center of the bay where the deposition is mainly chemical action and the size is finer and the sediment is silty clay.

Analyzing the relationship between element concentration and size of sediment, it is found that Zr, Hf are positive to sand and their coefficients are +0.53, +0.49 respectively, but they are negative to silt and clay, which may associated with the formatioon of the sand mine of ziron.

Secondly, Sc and Cs are negative to sand and their coefficient is -0.99, while they are positive to silt and clay and their coefficients are both up to +0.98. Sc is a typical dispersive element in the crust and is also dispersed in the hypergenesis environment. It is probable that Sc exists, in a form of isonorphism mixture, in the main rock-forming minerals such as pyroxene, amphibole, olivine. In the hypergenesis environment, Sc is unstable and easily destructible, then it is isolated partially or totally, or absorbed by clayey minerals in the weathering-crust.Next, Sc is a hydrolytic element, consequently it deposits in the hydrolytic-sediment (like clay or bauxite). Cs is a typical lithophile rare alkaline dispersion element and doesn't form independent minerals because of large ionic radius, but Cs is absorbed and enriched by mud, clay or organisms of sediment on the river or marine bottoms. Sc and Cs have one isotope like ^{45}Sc, ^{133}Cs, and both are unalternating-charge lithophile dispersion elements like Sc^{3+}, Cs^{+1}, and absorbed by clay. From the present data of this section, it is preliminarily determined that the sediment, where Sc concentration is over 15×10^{-6}, and Cs is over 10×10^{-6} (Table 7), belongs to silty clay. Whether the method of determining the sediment type by the range of the two elements' concentration is applicable to other sea area has yet to be further

Table 4 Element concentration or dispersion coefficient

	A0	A3	A7	A25	A33	A45	A48	A52	A60	A64	A6	A6	A	A	A	A7	A7	A7	A74	A75
Fe		2.1	△	△		△	△		△	2.1										
Na		△	△			△	△		△	△										
K			△	△		△		△	△	△	△	△		△	△					
Ca		△	△		△		△	△	△					△						
Ti																				
Sc		2.5	△			△	2.1		2.2	2.5										
Cr	△	2.8	△			2.1	2.2		2.5	2.7										
Co	△	2.1	△	△		△	△		△	2.2		△								
Ni	△	△	△			△	△		△	3.1	△	△								
Zn	△	2.3	△	△		△	2.2		△	2.0										
Rb		△	△	△		△	△		△	△										
Sr		△		△				△	△	2.0	△	△	△	△			△			
Cs		2.3	△	△		2.0	2.1		2.2	2.4										
Ba			△	△		△		△	△	△	△	△	△	△	△					
Zr	△		△			△		△	△		△						△	△		
Hf			△	2.3		△		△	△		△							△		
Ta		△	△	△		△	△		△	△				△						
Th		2.0	△			△	△	△	△	△	△									
U		△	△			△	△	△	△	△										
Mo			△	△	△	2.4	△			2.5										
W	△	2.1	△			2.0			△	2.3								△		
As		△	△	△		△	△		△	△										
Sb		△	△	△		△	2.2		2.2	△										
Ag		2.1	△	△	△		△		△			△		△	△			△		
Au	△	△	2.3	4.4			△			△			△		△			△		
Se	△	△	△	△	△				△	△		△	△							
La		△	△	△		△	△		△	△	2.2									
Ce		△	△	△		△	△		△	△	2.2									
Nd		2.0	△	△		△	2.1		△	△	△									
Sm		△	△	△		△	△		△	△	△									
Eu		△	△	△		△	△		△	△	△									
Tb		△	△	△		△	△		△	△	△									
Yb	△	△	△	△		△	△		△	△	△									
Lu	△	△	△	△		△	△		△	△	△									

Remarks: △ represents k>1, Blank represents k<1, k>2 is represented by numerals

studied.

4 Conclusions

The concentration of 34 elements in marine sediment samples (100mg) is gained from neutron activation analysis. On the basis of variations of element concentration, size composition at each site, and synthetically processed magnitude, combining with character of local hydro-dynamics, it is concluded that suspended matter and sediment move to the center of the area.

(a) Elements in the suspended matter transports from low to high concentration, from north to

Table 5 Related coefficient between sediment size content and element concentration

Element	Sand	Silt	Clay
Fe	-0.98(20)	+0.97(20)	+0.97(9)
Na	-0.97(20)	-0.38(20)	+0.97(9)
K	-0.25(20)	+0.27(20)	+0.44(9)
Ca	-0.21(18)	-0.43(10)	-0.56(9)
Ti	+0.21(10)	-0.13(10)	-0.07(10)
Sc	-0.99(10)	+0.98(20)	+0.977(10)
Cr	-0.98(10)	+0.95(10)	+0.96(9)
Co	-0.97(10)	+0.92(10)	+0.97(9)
Ni	-0.58(10)	+0.47(10)	+0.70(9)
Zn	-0.94(10)	+0.90(10)	+0.92(9)
Rb	-0.945(10)	+0.93(10)	+0.92(9)
Sr	-0.14(10)	+0.02(10)	+0.53(9)
Cs	-0.99(10)	+0.98(20)	+0.98(9)
Ba	-0.20(10)	+0.22(10)	+0.66(9)
Zr	+0.53(10)	-0.53(10)	-0.29(9)
Hf	+0.49(10)	-0.43(10)	-0.43(9)
Ta	-0.91(10)	+0.92(10)	+0.81(9)
Th	-0.90(10)	+0.87(10)	+0.90(9)
U	-0.78(10)	+0.80(10)	+0.69(9)
Mo	-0.67(11)	+0.28(10)	+0.21(6)
W	-0.80(10)	+0.77(10)	+0.76(9)
As	-0.96(10)	+0.92(10)	+0.96(9)
Sb	-0.79(10)	+0.74(10)	+0.74(9)
Ag	-0.24(18)	+0.28(18)	-0.25(9)
Au	-0.28(18)	+0.26	+0.35(7)
Se	-0.57(19)	+0.61(19)	+0.11(9)
La	-0.98(10)	+0.95(10)	+0.97(9)
Ce	-0.98(10)	+0.94(10)	+0.96(9)
Nd	-0.87(10)	+0.86(10)	+0.80(9)
Sm	-0.98(10)	+0.95(10)	+0.96(9)
Eu	-0.98(10)	+0.96(10)	+0.93(9)
Tb	-0.92(10)	+0.88(10)	+0.89(9)
Yb	-0.93(10)	+0.93(10)	+0.85(9)
Lu	-0.91(10)	+0.88(10)	+0.85(9)

Remrks: Number in brackets is the number of samle

south i.e. from Site 4 to Site 5 with the transverse from the Sites 5 to 2 as axial hub, and then from south to north or Site 3 to Site 2.

(b) Sediment takes the Sites A_3, A_{64}, A_{48} as axial hub, matter moves from rough to fine and the elements converge from low to high. Speciafically, sediment in the north moves toward south to the axial hub, while the sediment in the south moves toward north to the axial hub, but on east-west line the movement from Sites A_3 to A_{64} is slightly greater than that from Sites A_{48} to A_{54}.

(c) In this section, 20 elements are negative to sand and their correlation coefficients are above -0.80 and 21. 19 elements are positive to silt and silty clay respectively, and the correlation coefficients are more than +0.80. The sediment type determined by the element concentration is in accordance with the actual situation .

Table 6 Statistics data of element concentration coefficient

Site	Sand		Silt		Clay	
	Enriched coefficient	Munber of Element	Enriched coefficient	Munber of element	Enriched coefficient	Munber of element
A0	<-50	22	>8	5	>10	18
A3	<-1.4	11	>30	22	>30	23
A7	<-23	12	>30	20	>30	10
A25	<-65	13	>12	14	>17	10
A33	<-90	12	>3.5	14	>2.1	10
A45	<-<-19	13	>30	21	>30	15
A48	<-15	13	>30	21	>30	22
A52	<-95	11	>1.5	4		
A60	<-11	11	>30	22	>30	19
A64	<-1.1	12	>30	21	<30	24
A67	<-50	12	>0.85	9		
A66	<-40	14	>0.8	9		
A68	<-50	12	>0.85	9		
A69	<-50	12	>0.8	12		
A70	<-50	12	>0.85	9		
A71	<-50	12	>0.80	9		
A72	<-50	12	>0.4	9		
A73	<-50	12	>0.70	9		
A74	<-50	12	>0.65	9		
A75	<-50	12	>0.5	9		

Table 7 Element concentration and correlation coefficients

Sample	Concentrtation		Coefficiency		
	Site	Concent	Sand	Silt	Clay
Sc	A_3	15.73	-099	+0.98(20)	+0.98(9)
	A_{64}	15.49			
Cs	A_3	10.8	-0.99	+0.98(20)	+0.98(9)
	A_{64}	11.3			

(d) The concentration of Sc element is larger than 15×10^{-6},and that of Cs is larger than 10×10^{-6}, the sediment type determined by Sc and Cs is silty clay. But whether the method is applicable to other areas has yet to be tested.

References

1 Mao Zhixiang, Yan Peilan, Huang Jianwei. Tracing Sediment Movement by neutron activation analysis and preliminary use in Shantou harbour. Research of hydraulic and water transport, Nanjng Hydraulic Research Institute. 1988 , (4): 87~95

2 Mao Zhixiang, Yan Peilan, Dai Xiankai et al. Study on bed-load movement by neutron activation analysis along north bank of hangzhou bay.*The Ocean Engineering,* 1991,(2): 63~71

3 Yi Yi, Chang Naihuang, Zhong Weini et al. Study of neutron activation technology in tracing sand.*Science in China (Series A)*, 1992, (7): 781~784

4 Department of geology, Nanjing university (editor).*Geochemistry*. Beijing: Science Press, 1960: 123~305

5 Liu Yingjun, Cao Liming, Li zhaolin.*Geochemistry of Element*. Beijing: Science Press, 1984: 1~360

A Regime of Inequality Requires Compensation

Li Linghua
(*National Marine Data & Information Service, SOA*)

"… As was argued by many disadvantaged states during UNCLOS III:
The establishment of an economic zone benefiting a limited number of coastal states would lead to inequality de jure and de facto .
…The institution of a regime of a right to participate directly or indirectly in the exploration and exploration … and a disregard for that right would only further widen the economic disparities … '
—Barbara Kwiatkowska: The 200 EEZ in the New Law of the Sea, 1989.

Compared with the open coastal configurations of USA, Russia, Canada, Australia and Japan ect. China, to a great extent, is a geographically disadvantaged state (GDS) surrounded by two or more states. Actually, the East and South China Seas are semi-enclosed seas. On the other hand, China has the largest population in the world, accounting for about 1/4 of the world total population. Its population is about 6 times that of the United States. However, reportedly, the USA has the world' s largest EEZ—more than 2 200 000 square nautical miles. It is estimated that the EEZ apportioned on the basis of terrestrial geography of China would be quite small, even if it has equitably delimited its boundaries with all its littoral neighboring states. According to calculation, the per capita sea area in China is quite limited, only accounting for about 1/15 that of the USA.What a great different!

The ocean is the common heritage of mankind, and belongs to all mankind. therefore, everyone in the world should share the same sea areas or the same resources, at least, roughly. As Prof.W.S Ball put it, there is no reason why a landlocked (LL) country cannot possess an EEZ. In the same sense, geographically disadvantaged states should be given more equitable access to the ocean's resources. There are some areas of the world where a joint EEZ may be appropriate, and alienating EEZ and noncontiguous EEZ may be tried.

It should be noted that the equity of maritime boundary should take into account not only the coastal geography, but also the demography. Only considering the coastal geography is not enough. An obvious shortcoming of the 1982 UNCLOS is that it dose not describe any factors that may crop up when some neighboring states have overlapped sea areas or when one state has a larger population but smaller sea areas.

An equitable boundary in one context may be inequitable in another. New debates on the needs and direction of the future ocean law may take place!

Reference

Wayne S. Ball, 1996, National Enclosure of the Oceans, Ocean Development & International Law, Vol.27 (l~2) 97-124.

Marine Science Bulletin

Marine Science Bulletin publishes papers on marine science and technology including physical oceanography, chemical oceanography, marine biology, marine geology, environmental oceanography, estuarine & coastal sciences, marine technology, digital ocean, coastal zone management, ocean engineering, marine economics, etc., and aims to promote international academic exchange.

Editor-in-Chief: Hou Wenfeng (侯文峰)
Deputy Editor-in-Chief: Lin Baofa (林宝法) Yang Ying (杨 鹰)
Executive Editor: Lu Mingsheng (卢明生)

Marine Science Bulletin (Vol.1 No.2 October 1999)

Responsible Institution:
State Oceanic Administration of China
Edited and Published Semi-annually by:
National Marine Data and Information Service
Address: 93 Liuwei Road, Hedong District, Tianjin 300171, China
E-mail: msb@netra.nmdis.gov.cn

ISSN1000-9620
CN12-1182/N

Price: $30.00 per year